Numerical method for coupled analysis of Navier-Stokes and Darcy flows

2018

Shinichi ARIMOTO

Acknowledgments

This thesis represents the results of the study I conducted in the Laboratory of Agricultural Facilities Engineering at Kyoto University over a period of six years. I would like to firstly express my sincere thanks to Professor Akira Murakami for all the advice he has given me. He enthusiastically guided me for four years at Okayama University and then six years at Kyoto University. Through his guidance, I learned the fun of numerical analysis.

I would also like to thank the members of the Dissertation Committee, Professor Shigeto Kawashima and Professor Masayuki Fujihara, for their constructive suggestions and beneficial advice.

My great appreciation is also extended to Associate Professor Kazunori Fujisawa for the abundance of advice he offered me during this study. Much of the present work is due to his thoughtful and helpful support. I would also like to express my gratitude to Dr. Tsuyoshi Yasuki, Dr. Yuichi Kitagawa, and Mr. Kosho Kawahara of the Toyota Motor Corporation. I was able to continue this work because of their powerful encouragement.

Finally, I am deeply grateful to my family, Takako and Eiki, for their support.

Shinichi Arimoto

January, 2018

Nomenclature

A : Area of cell

Da : Darcy number

g : Gravitational acceleration

k : Hydraulic conductivity

l : Length of cell face

m : Time step

n : Outward-normal unit vector on cell face

p : Piezometric pressure

p_f : Pressure at interface

Re : Reynolds number

t : Time

t^+ : Nondimensional time

u : Cartesian velocity

u^+ : Nondimensional Cartesian velocity

$\hat{u}_i$: Intermediate velocity

u^* : Intermediate velocity

u_i' : Intermediate velocity

u_f : Velocity at interface

U : Normal velocity on cell face

U_{ave} : Average bulk velocity in fluid domain

$(u)_{\text{face}}$: Cartesian velocity on cell face

x : Cartesian coordinate

x^+ : Nondimensional Cartesian coordinate

ρ : Density of water

ν : Kinematic viscosity of water

λ : Porosity

Δt : Computational time step

δ : Distance from cell center to interface

TABLE OF CONTENTS

LIST OF FIGURES

LIST OF TABLES

1 Introduction

1.1 Motivation

The simultaneous computation of the seepage flow in porous media and the regular flow in the fluid domain has a variety of applications to practical problems related to the prevention of natural disasters, such as the erosion of soil structures, piping flows within natural slopes, and the stability of embankments subjected to tidal waves. For example, the erosion of soils is affected by surface flows as well as by subsurface flows, i.e., seepage flows, and these two flow fields need to be grasped in order to predict how the erosion develops. The present thesis focuses on the water flows through these two domains, and a numerical method to compute the two flow fields simultaneously is proposed.

Studies on the interaction of the Navier-Stokes and the seepage flows in the fluid domain can be traced to the velocity on the boundary between the fluid and the Darcy domains. Beavers and Joseph (1967) conducted experiments under the condition that the Hagen-Poiseuille seepage flow occurs along a wall, and discussed the boundary conditions of the fluid domain. Based on the experimental results, they suggested that it was desirable to give the slip condition to the boundary between the fluid and the Darcy domains. After that, the components of the flow velocity along the boundary between the fluid and the Darcy domains were discussed several times. Saffman (1971) improved the model which was proposed by Beavers and Joseph (1967). Moreover, Neale and Nader (1974) explained the velocity and stress on the boundary between the fluid and the Darcy domains using the continuous model. In addition, Bars and Worster (2006) and Ochoa-Tapia and Whitaker (1995a, 1995b) also discussed this topic. Although a great deal of effort has been made to clarify this issue, the best model has not yet been obtained. Thus far, there have been several numerical studies dealing with the coupled analysis of the Navier-Stokes and the Darcy flows (e.g., Çeşmelioğlu and Rivière, 2012; Chidyagwai and Rivière, 2009, 2011; Badea et al., 2010; Girault and Rivière, 2009; Cai et al., 2009; Urquiza et al., 2008; Mu and Xu, 2007). They adopted different governing equations

between the fluid and the Darcy domains, as shown in Equations (1.1) and (1.2).

$$\frac{\partial u_i}{\partial x_i} = 0 \tag{1.1a}$$

$$\frac{\partial u_i}{\partial t} + \frac{\partial u_i u_j}{\partial x_j} = -\frac{1}{\rho}\frac{\partial p}{\partial x_i} + \nu \frac{\partial^2 u_i}{\partial x_j \partial x_j} \tag{1.1b}$$

$$\frac{\partial}{\partial x_i}\left(\frac{k}{\rho g}\frac{\partial p}{\partial x_i}\right) = 0 \tag{1.2}$$

where u_i, p, ρ, ν, k, and g denote the flow velocity, the piezometric pressure, the density of water, the kinematic viscosity of water, the hydraulic conductivity, and the gravitational acceleration, respectively, and t and x_i are time and the Cartesian coordinates. Girault and Rivière (2009) numerically analyzed steady solutions for Equations (1.1) and (1.2) by the discontinuous Galerkin scheme, and Chidyagwai and Rivière (2009) discussed the existence and uniqueness of the numerical solutions which are discontinuous at the interface between the fluid and the Darcy domains. Badea et al.(2010) implemented the coupling of the fluid and the Darcy domains using the iterative method, and Chidyagwai and Rivière (2011), Cai et al.(2009), and Mu and Xu (2007) proposed numerical schemes to solve Equations (1.1) and (1.2) using a two-grid method, which can reduce the computational costs with the aid of coarse and fine grids. Çeşmelioğlu and Rivière (2012) initiated studies on the existence of solutions for a problem which was coupled with an advection-diffusion equation in addition to Equations (1.1) and (1.2). Their interest was mainly in the mathematical treatment used to connect the numerical solutions in the two different domains and in the numerical procedure for satisfying the conservation of mass and momentum at the interface.

There are two objectives in the thesis. The first objective is to propose a simple numerical method to simultaneously solve the Navier-Stokes and the Darcy flows which is uncomplicated and applicable to practical problems. The second objective is to investigate the influence of the Darcy flow in porous media on the Navier-Stokes flow in the fluid domain by using the numerical method proposed in the thesis.

1.2 Thesis outline

This thesis consists of seven chapters as summarized below.

Chapter 1 is the present introduction which describes the motivation of the thesis and a review of the studies related to the thesis.

In **Chapter 2**, a numerical method for simulating the Navier-Stokes and the Darcy flows is described. The Darcy-Brinkman equations have been employed as the governing equations. At first, they are discretized by the finite volume method. They include the Navier-Stokes equations and can approximately describe the Darcy flow by changing the values of porosity and hydraulic conductivity. The solutions to the Darcy-Brinkman equations are affected by two dimensionless quantities, namely, the Reynolds number and the Darcy number.

In **Chapter 3**, the proposed numerical method is validated by means of several problems. First, the lid-driven cavity flow and the backward-facing step flow are computed in order to validate the Navier-Stokes flow in the fluid domain since the computational domain in these problems is occupied by the fluid domain. Next, the one-dimensional uniform flow in the water channel and the lid-driven cavity flow with porous media are computed in order to validate the Darcy flow in the Darcy domain and the interpolation of velocity and pressure on the interface between the fluid and the Darcy domains.

In **Chapter 4**, the backward-facing step flow with a porous step is computed to investigate the influence of the Reynolds and the Darcy numbers on the flow in the fluid and the Darcy domains. It is well-known that the distance from the step to the reattachment point depends on the Reynolds number. Various Reynolds and Darcy numbers are computed, and the distance from the porous step to the reattachment point is evaluated.

In **Chapter 5**, the influence of the void shape on the Reynolds and the Darcy numbers is investigated. A rectangular porous domain, whose void is filled only with water, is assumed. Three shapes are computed for the void. The relationship between the shape of the void and the maximum velocity in the void is discussed.

In **Chapter 6**, the conclusions described in each chapter are summarized and the future prospects of this study are discussed.

2 Coupled analysis of Navier-Stokes and Darcy flows

Governing equations are needed for a coupled analysis of the Navier-Stokes and the Darcy flows. In this thesis, we propose a numerical method for these two flows using one set of governing equations. When the Navier-Stokes and the Darcy flows are simulated using one set of governing equations, the simple linear interpolation method cannot be used at the interface between the fluid and the Darcy domains. Thus, we also propose an interpolation method which can connect the pressure and the flow velocity of the fluid and the Darcy domains. In this chapter, focus is placed on the Darcy-Brinkman equations which can express both of the flows. The governing equations and the numerical method are herein described.

2.1 Introduction

The seepage flow in porous media and the regular flow in the fluid domain have different characteristics. The Navier-Stokes equations are widely used to predict the regular flow in the fluid domain. And several models have been proposed to predict the seepage flow in porous media, for example, Darcy's law, Darcy's law with Brinkman's extension (Brinkman, 1947), Ergun's equations (Ergun, 1952), and Forchheimer's equation (Forchheimer, 1901). Predicting both of these flows at the same time has a variety of applications to practical problems. Thus, over the past few decades, a considerable number of studies have been conducted. Çeşmelioğlu and Rivière (2012), Chidyagwai and Rivière (2009, 2011), Badea et al. (2010), Girault and Rivière (2009), Cai et al. (2009), Urquiza et al. (2008), and Mu and Xu (2007) are taken as recent examples of these studies. There are three common points among all these studies. The first point is that they use the Navier-Stokes equations, as described by Equation (1.1) (or the Stokes equations which ignore the advective term), in the fluid domain. The second point is that they use Equation (1.2) which can be obtained by applying Darcy's law to the equation of continuity in porous media. The third point is that the governing equations

can be solved by satisfying the velocity at the interface between the fluid and the Darcy domains in addition to the conservation of mass and momentum. However, it is not easy to solve Equations (1.1) and (1.2) simultaneously as several requirements must be satisfied. A large part of the previous studies dealt with how well the solutions for the two partial differential equations, which have different characteristics, are connected. Such practical problems remain unsolved.

In the present study, a numerical method to simultaneously solve the Navier-Stokes and the Darcy flows is proposed. Governing equations which can express the Navier-Stokes and the Darcy flows are needed. Herein, focus is placed on the Darcy-Brinkman equations; they are used as the governing equations for the coupled analysis of the Navier-Stokes and the Darcy flows. This approach for the Navier-Stokes and the Darcy flows is called the two-domain approach. As another approach, the single-domain approach is also used (e.g., Mercier et al., 2002; Jue, 2004). In the two-domain approach, the computational domain is divided into two domains, the fluid domain and the Darcy domain. The interface between the fluid and the Darcy domains is defined, and the conditions on the interface are important. Thus, various conditions have been proposed in several researches (e.g., Saffman, 1971; Vafai and Kim, 1990; Salinger et al., 1994; Ochoa-Tapia and Whitaker, 1995a, 1995b; Chandesris and Jamet, 2006).

Numerical studies which use a combination of the Navier-Stokes equations (or the Stokes equations) and Darcy's equation have been widely done (e.g., Mu and Xu, 2007; Girault and Rivière, 2009; Cai et al., 2009; Chidyagwai and Rivière, 2009, 2011; Cesmelioglu et al., 2013; Si et al., 2014). When Darcy's equation is used to predict the seepage flow in porous media, the conditions on the interface between the fluid and the Darcy domains are important. This is because the orders of the velocity in the Navier-Stokes equations and Darcy's equation are different. In order to avoid this problem, adding the Brinkman term to Darcy's equation is effective. Hence, the approach which uses the Brinkman term has been adopted here.

In this chapter, the governing equations and the numerical method for simultaneously solving them are described. First, the Darcy-Brinkman equations used as the governing equations, along with their nondimensionalization, are presented. Next, the discretization of the governing equations using the finite volume method is explained.

2.2 Governing equations

The following partial differential equations, called Darcy-Brinkman equations, are employed for the coupled analysis of the Navier-Stokes flow in the fluid domain and the Darcy flow in porous media.

$$\frac{\partial \langle u_i \rangle}{\partial x_i} = 0 \tag{2.1a}$$

$$\frac{\partial \langle u_i \rangle}{\partial t} + \frac{\partial}{\partial x_j}\left(\frac{\langle u_i \rangle \langle u_j \rangle}{\lambda} \right) = -\frac{\lambda}{\rho}\frac{\partial \langle p \rangle^*}{\partial x_i} + \nu \frac{\partial^2 \langle u_i \rangle}{\partial x_j \partial x_j} - \frac{\lambda \nu}{K}\langle u_i \rangle \tag{2.1b}$$

where λ denotes the porosity, and $\langle u_i \rangle$ and $\langle p \rangle^*$ denote the volume-averaged velocity and the averaged piezometric pressure, respectively. The operation to average the velocity and pressure of the Navier-Stokes equations in the porous media is summarized in Anderson and Jackson (1967). The derivation of the Darcy-Brinkman equations is seen in Bars and Worster (2006) and Dukhan (2012). The averaging theorems are explained in Howes and Whitaker (1985) and Whitaker (1999). Permeability K, seen in Equation (2.1b), is replaced with hydraulic conductivity k using the following form:

$$K = \frac{k\nu}{g} \tag{2.2}$$

Equation (2.1b) is rewritten into the following form:

$$\frac{\partial \langle u_i \rangle}{\partial t} + \frac{\partial}{\partial x_j}\left(\frac{\langle u_i \rangle \langle u_j \rangle}{\lambda} \right) = -\frac{\lambda}{\rho}\frac{\partial \langle p \rangle^*}{\partial x_i} + \nu \frac{\partial^2 \langle u_i \rangle}{\partial x_j \partial x_j} - \frac{\lambda g}{k}\langle u_i \rangle \tag{2.3}$$

Equations (2.1a) and (2.3) look like the Navier-Stokes equations shown as Equation (1.1), when λ =1.0 and 1/k=0 are given. Therefore, the following partial differential equations can describe the Darcy and the Navier-Stokes flows. The following partial differential equations are employed as the governing equations for the coupled analysis of the Navier-Stokes flow in the fluid domain and the Darcy flow in porous media.

$$\frac{\partial u_i}{\partial x_i} = 0 \tag{2.4a}$$

$$\frac{\partial u_i}{\partial t}+\frac{\partial}{\partial x_j}\left(\frac{u_i u_j}{\lambda}\right)=-\frac{\lambda}{\rho}\frac{\partial p}{\partial x_i}+\nu\frac{\partial^2 u_i}{\partial x_j \partial x_j}-\frac{\lambda g}{k} \tag{2.4b}$$

Flow velocity u_i in Equation (2.4) means the usual flow velocity in the fluid domain and the Darcy velocity in porous media. It can be easily understood that Equation (2.4b) becomes the Navier-Stokes equations when λ =1.0 and 1/k=0 are given.

The nondimensionalization of Equation (2.4) reveals that two types of dimensionless parameters, namely, the Reynolds and the Darcy numbers, affect its solutions. The nondimensional quantities of u_i^+, x_i^+, and t^+ are introduced as follows:

$$u_i = V u_i^+ \ , \ x_i = L x_i^+ \ , \ t=\frac{L}{V}t^+ \tag{2.5}$$

By substituting Equation (2.5) into Equation (2.4a), a reduction into the following form can be made:

$$\frac{\partial u_i^+}{\partial x_i^+}=0 \tag{2.6a}$$

$$\mathrm{Re}\left[\frac{\partial u_i^+}{\partial t^+}+\frac{\partial}{\partial x_j^+}\left(\frac{u_i^+ u_j^+}{\lambda}\right)\right]=-\lambda\frac{L}{\rho\nu V}\frac{\partial p}{\partial x_i^+}+\frac{\partial^2 u_i^+}{\partial x_j^+ \partial x_j^+}-\lambda \mathrm{Da}^{-1}u_i^+ \tag{2.6b}$$

where Re and Da denote the Reynolds and the Darcy numbers, respectively. The dimensionless numbers are defined as follows:

$$\mathrm{Re}=\frac{VL}{\nu} \ , \ \mathrm{Da}=\frac{k\nu}{gL^2} \tag{2.7}$$

The first term on the right-hand side of Equation (2.6b) is not fully nondimensionalized, because the nondimensionalization of the pressure depends on whether or not the fluid domain or the porous media are taken into consideration. In the fluid domain, the pressure can be nondimensionalized by following form for p:

$$p=\rho V^2 p^+ \tag{2.8}$$

because the pressure depends on the change in the velocity head. Substituting Equation

(2.8) into Equation (2.6b), it is reduced into the following form:

$$\mathrm{Re}\left[\frac{\partial u_i^+}{\partial t^+}+\frac{\partial}{\partial x_j^+}\left(\frac{u_i^+ u_j^+}{\lambda}\right)\right]=-\lambda\,\mathrm{Re}\frac{\partial p^+}{\partial x_i^+}+\frac{\partial^2 u_i^+}{\partial x_j^+ \partial x_j^+}-\lambda\mathrm{Da}^{-1}u_i^+ \tag{2.9}$$

In the fluid domain, λ =1.0 and $1/k$=0 (Da^{-1}=0) hold true; Equation (2.9) becomes the nondimensional Navier-Stokes equations. On the other hand, the pressure changes with the loss of hydraulic head in the porous media. Hence, the pressure can be nondimensionalized by the following form:

$$p=\frac{\rho\, gLV}{k}\,p^+ \tag{2.10}$$

noting that V/k means the representative hydraulic gradient. Substituting Equation (2.10) into Equation (2.6b), the following form is obtained:

$$\mathrm{Re}\left[\frac{\partial u_i^+}{\partial t^+}+\frac{\partial}{\partial x_j^+}\left(\frac{u_i^+ u_j^+}{\lambda}\right)\right]=-\lambda\mathrm{Da}^{-1}\frac{\partial p^+}{\partial x_i^+}+\frac{\partial^2 u_i^+}{\partial x_j^+ \partial x_j^+}-\lambda\mathrm{Da}^{-1}u_i^+ \tag{2.11}$$

when the hydraulic conductivity is sufficiently small and the inverse of the Darcy number, Da^{-1}, is even larger than the Reynolds number, namely, $\mathrm{Da}^{-1} \gg \mathrm{Re}$ and $\mathrm{Da}^{-1} \gg 1$, and the left-hand side and the second term on the right-hand side of Equation (2.11) become negligible. Then, Equation (2.11) can be transformed into the following form:

$$\frac{\partial p^+}{\partial x_i^+}+u_i^+=0 \tag{2.12}$$

Equation (2.12) is identical to the well-known Darcy's law, which implies that Darcy's law is approximately described by the Darcy-Brinkman equations when the hydraulic conductivity is sufficiently small. Equation (2.4) can describe the Navier-Stokes equations in the fluid domain by giving λ=1.0 and $1/k$=0, and it can approximate Darcy's law in porous media. Therefore, the Darcy-Brinkman equations allow us to simulate the Darcy and the Navier-Stokes flows without employing different governing equations in the fluid domain and porous media. It should be noted that the solutions for the Darcy-Brinkman equations depend on both the Reynolds number and the Darcy number. The above nondimensionalization is summarized in Figure 2.1.

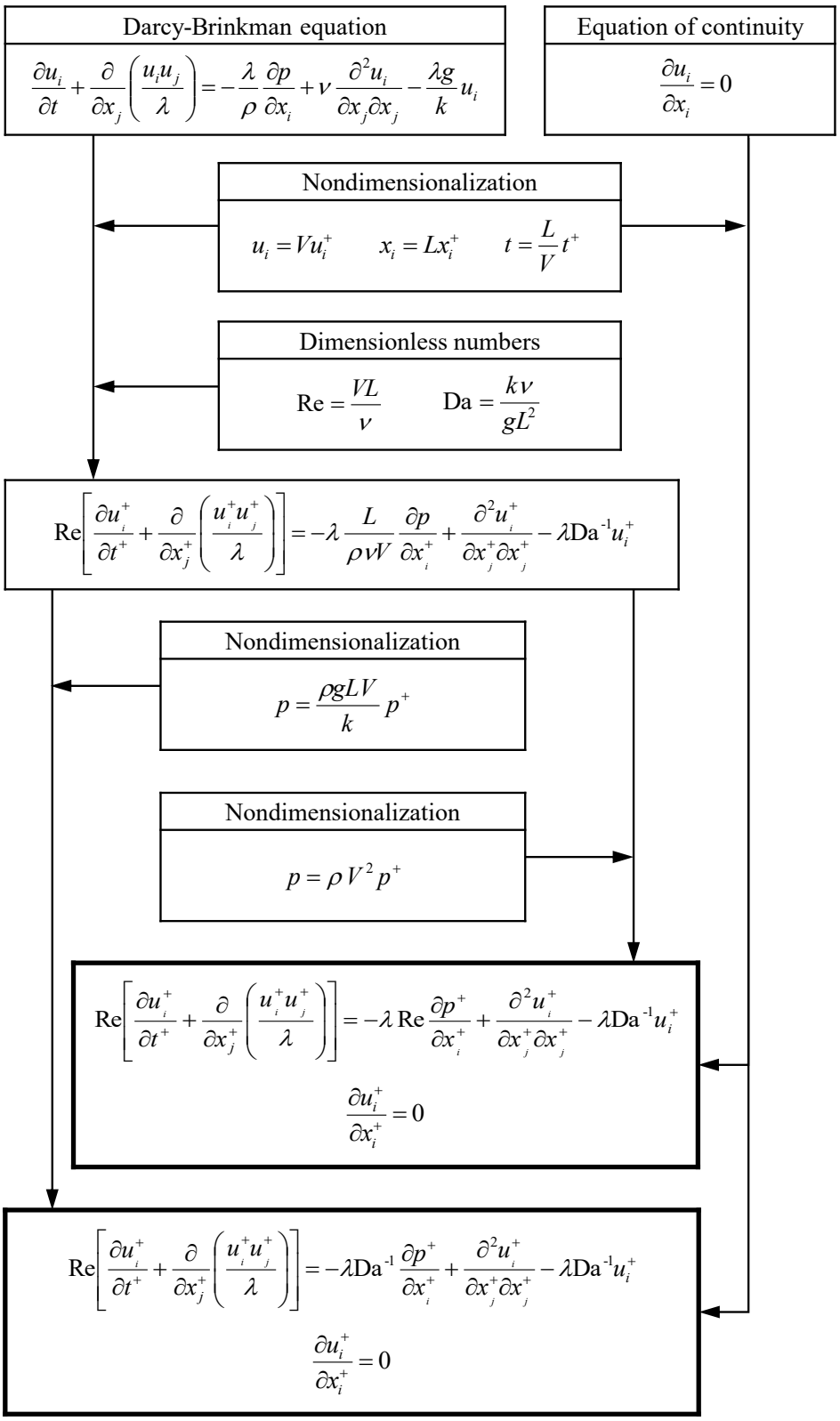

Figure 2.1 Nondimensionalization of governing equations.

2.3 Numerical method

2.3.1 Characteristics

The method presented herein is based on Kim and Choi (2000); it can be used to solve the Navier-Stokes equations for incompressible fluids by the finite volume method with unstructured grids. The finite volume method is widely used on unstructured grids (e.g., Davidson, 1996; Mathur and Murthy, 1997; Lai, 1997; Thomadakis and Leschziner, 1996; Taniguchi and Kobayashi, 1991; Hwang, 1995, 1997; Kobayashi et al., 1999). Research works on the application of the finite volume method to incompressible flows are briefly summarized in Kim and Choi (2000). The method is characterized by the grid system shown in Figure 2.2. The velocity and the pressure are stored at the centroids of the finite volume cells and flux U is additionally computed at the mid-point of each cell face, which has the following definition:

$$U = (u_i)_{\text{face}} n_i \tag{2.13}$$

where $(u_i)_{\text{face}}$ and n_i denote the flow velocity and the outward-normal unit vector on the cell face, respectively.

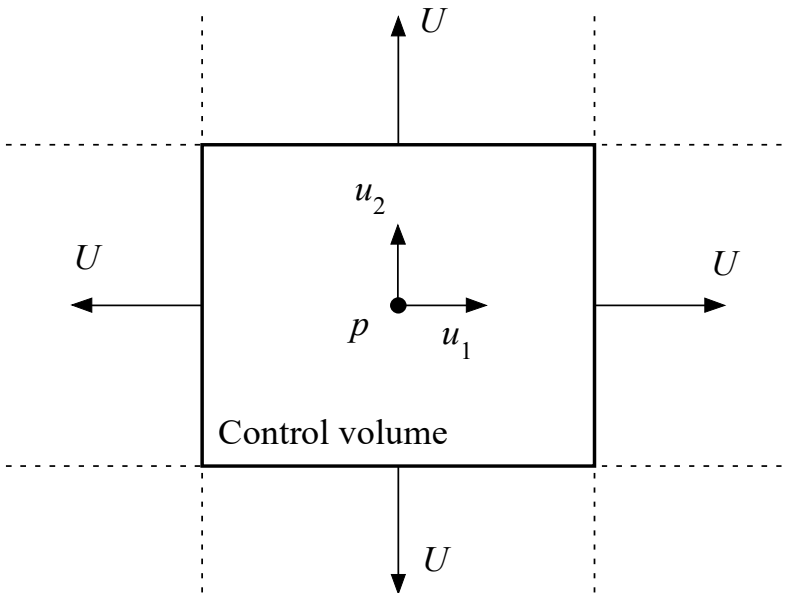

Figure 2.2 Finite volume cells and variables.

The advantages of the method for the simultaneous analysis of the Navier-Stokes and the Darcy flows are summarized in the following.

1. Unlike the finite difference method, the finite volume discretization can definitely divide the Darcy domain and the fluid domain.
2. The usage of flux U, defined at the cell faces, enables the conservation of mass and momentum to be satisfied at the interface between the fluid domain and porous media.
3. Unlike the common finite element method, the finite volume method allows the variables at the cell faces to be freely constructed. This is advantageous for extending the numerical method. For example, the discontinuous tangential flow velocity at the interface between the two different domains (e.g., Beavers and Joseph, 1967) can be easily introduced, although the flow velocity is continuously interpolated herein for simplicity.

The method proposed by Kim and Choi (2000) for numerically solving the Navier-Stokes equations can accept unstructured grids. However, the usage of unstructured grids is not straightforward when two different domains exist, namely, the fluid and the porous domains. Hence, a structured grid is employed in the following formulations and numerical simulations.

2.3.2 Numerical procedures

The numerical procedures for the rectangular finite volume cells, shown in Figure 2.2, are presented in this section. A fractional step method (e.g., Kim and Moin, 1985; Le and Moin, 1991; Choi, and Moin, 1994) is applied to Equation (2.4), namely, the flow velocity is predicted by Equation (2.4b) and then the predicted flow velocity is corrected so as to satisfy the continuity equation of Equation (2.4a). When the flow velocity is predicted by Equation (2.4b), Equation (2.4b) is divided into the following two steps:

$$\frac{\partial u_i}{\partial t} = -\frac{\lambda g}{k} u_i \tag{2.14}$$

$$\frac{\partial u_i}{\partial t} = -\frac{\partial}{\partial x_j}\left(\frac{u_i u_j}{\lambda}\right) - \frac{\lambda}{\rho}\frac{\partial p}{\partial x_i} + \nu\frac{\partial^2 u_i}{\partial x_j \partial x_j} \tag{2.15}$$

Applying the fractional step method and the Crank-Nicolson method to the time integration of Equations (2.14) and (2.15), Equations (2.16) to (2.20) can be derived.

$$\frac{u_i' - u_i^m}{\Delta t} = -\frac{\lambda g}{2k}\left(u_i' + u_i^m\right) \tag{2.16}$$

$$\frac{\hat{u}_i - u_i'}{\Delta t} = -\frac{1}{2}\frac{\partial}{\partial x_j}\left(\frac{\hat{u}_i u_j^m + u_i^m \hat{u}_j}{\lambda}\right) - \frac{\lambda}{\rho}\frac{\partial p^m}{\partial x_i} + \frac{\nu}{2}\frac{\partial^2}{\partial x_j \partial x_i}\left(\hat{u}_i + u_i^m\right) \tag{2.17}$$

$$\frac{u_i^* - \hat{u}_i}{\Delta t} = \frac{\lambda}{\rho}\frac{\partial p^m}{\partial x_i} \tag{2.18}$$

$$\frac{\partial}{\partial x_j}\left(\frac{\lambda}{\rho}\frac{\partial p^{m+1}}{\partial x_j}\right) = \frac{1}{\Delta t}\frac{\partial u_j^*}{\partial x_j} \tag{2.19}$$

$$\frac{u_i^{m+1} - u_i^*}{\Delta t} = -\frac{\lambda}{\rho}\frac{\partial p^{m+1}}{\partial x_i} \tag{2.20}$$

where u_i', $\hat{u}_i$, and u_i^* denote the intermediate velocities between u_i^m and u_i^{m+1}, respectively, and Δt is the time step. Superscript m implies the iteration for the time steps. u_i' is the intermediate velocity calculated by Equation (2.14), and $\hat{u}_i$ is obtained from the integration of Equation (2.15) using u_i' for the initial value. Equations (2.16) and (2.17) correspond to the prediction step of the flow velocity, and Equations (2.18) to (2.20) are used to calculate the pressure and the correction of the predicted flow velocity to satisfy the continuity equation. Integrating Equations (2.16) to (2.20) over the finite volume cells, and applying the Gauss divergence theorem, Equations (2.16) to (2.20) are transformed into

$$\frac{u_i' - u_i^m}{\Delta t} = -\frac{\lambda g}{2k}\left(u_i' + u_i^m\right) \tag{2.21}$$

$$\frac{\hat{u}_i - u_i'}{\Delta t} = -\frac{1}{A}\oint_l \frac{1}{2\lambda}\left(\hat{u}_i U^m + u_i^m \hat{u}_j n_j\right) dl - \frac{1}{A}\cdot\frac{\lambda}{\rho}\oint_l p^m n_i dl + \frac{1}{A}\cdot\frac{\nu}{2}\oint_l \frac{\partial}{\partial n}\left(\hat{u}_i + u_i^m\right) dl \tag{2.22}$$

$$\frac{u_i^* - \hat{u}_i}{\Delta t} = \frac{1}{A}\cdot\frac{\lambda}{\rho}\oint_l p^m n_i dl \tag{2.23}$$

$$\oint_l \frac{\lambda}{\rho}\frac{\partial p^{m+1}}{\partial n} dl = \frac{1}{\Delta t}\oint_l U^* dl \tag{2.24}$$

$$\frac{u_i^{m+1} - u_i^*}{\Delta t} = -\frac{1}{A}\cdot\frac{\lambda}{\rho}\oint_l p^{m+1} n_i dl \tag{2.25}$$

$$\frac{U^{m+1} - U^*}{\Delta t} = -\frac{\lambda}{\rho}\frac{\partial p^{m+1}}{\partial n} \tag{2.26}$$

where A, l, and n_i denote the area of the cell, the length of the cell faces, and the outward normal unit vector at the cell faces, respectively, and $\partial / \partial n$ implies the directional derivative for the outward normal direction. Porosity λ is constant in each finite volume cell. U is the flux defined at each cell face, and Equation (2.26) is derived by multiplying n_i with Equation (2.20). U^* ($=u_i^* n_i$) is the intermediate flux; it is calculated using Equation (2.13) and interpolating intermediate velocity u_i^* at the centroids of each cell to the cell faces. The method for the interpolation of the velocity and the pressure to the cell faces is explained in the following section. Substituting Equation (2.26) into Equation (2.24), the following equality is obtained:

$$\oint_l U^{m+1} dl = 0 \tag{2.27}$$

Equation (2.27) means that the velocity at each finite volume cell satisfies the continuity equation.

2.3.3 Interpolation of velocity and pressure

In order to compute the integrals appearing in Equations (2.22) to (2.25) and to discretize these equations, the velocities, the pressure, and their directional derivatives need to be evaluated at the mid-point of each cell face. In the computation, the integrals are calculated by the following equation:

$$\oint \Phi dl = \sum_i \Phi_i \Delta l_i \tag{2.28}$$

where Φ is an arbitrary flow variable, namely, the velocities, the pressure, and their directional derivatives, and l is the length of the cell boundary, and Φ_i and Δl_i denote the value of Φ at the mid-point of the ith cell face and its length, respectively. The values for the velocity and the pressure, except for flux U, are stored at the centroids of the finite volume cells (See Figure 2.2), and they need to be interpolated at each cell face from those at the centroids of the neighboring cells. Thus, the manner in which these variables are interpolated plays an important role in the stable computation at the interface between the fluid and the Darcy domains. This section introduces an interpolation scheme, as shown in Figures 2.3 and 2.4, for achieving a stable and physically-natural computation of the Darcy-Brinkman equations.

For simplicity, rectangular finite volume cells are considered herein. As will be explained in the next chapter, the simple linear interpolation of the variables may induce physically unrealistic oscillations at the interface of the two different domains. In order to avoid the oscillations, the interpolation method described by the following equations is useful:

$$p_f = \begin{cases} \dfrac{\delta_b p_a + \delta_a p_b}{\delta_a + \delta_b} & \text{if both are the same domain} \\ p_a & \text{if left is fluid domain and right is Darcy domain} \\ p_b & \text{if left is Darcy domain and right is fluid domain} \end{cases} \tag{2.29}$$

$$u_{i,f} = \begin{cases} \dfrac{\delta_b u_{i,a} + \delta_a u_{i,b}}{\delta_a + \delta_b} & \text{if both are the same domain} \\ u_{i,b} & \text{if left is fluid domain and right is Darcy domain} \\ u_{i,a} & \text{if left is Darcy domain and right is fluid domain} \end{cases} \tag{2.30}$$

$$\left.\frac{\partial p}{\partial n}\right|_a = \begin{cases} \dfrac{p_b - p_a}{\delta_a + \delta_b} & \text{if both are the same domain} \\ \dfrac{p_b - p_a}{\delta_b} & \text{if left is fluid domain and right is Darcy domain} \\ \dfrac{p_b - p_a}{\delta_a} & \text{if left is Darcy domain and right is fluid domain} \end{cases} \tag{2.31a}$$

$$\left.\frac{\partial p}{\partial n}\right|_b = \begin{cases} \dfrac{p_a - p_b}{\delta_a + \delta_b} & \text{if both are the same domain} \\ \dfrac{p_a - p_b}{\delta_b} & \text{if left is fluid domain and right is Darcy domain} \\ \dfrac{p_a - p_b}{\delta_a} & \text{if left is Darcy domain and right is fluid domain} \end{cases} \tag{2.31b}$$

$$\left.\frac{\partial u_i}{\partial n}\right|_a = \frac{u_{i,f} - u_{i,a}}{\delta_a} \tag{2.32a}$$

$$\left.\frac{\partial u_i}{\partial n}\right|_b = \frac{u_{i,f} - u_{i,b}}{\delta_b} \tag{2.32b}$$

where p_f and $u_{i,f}$ denote the values of the pressure and the velocity at the interface, respectively, and δ is the distance from the cell center to the interface. Subscripts a and b indicate that the values are related to the left and right cells, respectively, as seen in Figures 2.3 and 2.4. Equation (2.30) is also applied to the interpolation of intermediate velocities u_i', $\hat{u}_i$, and u_i^*.

Figures 2.3 and 2.4 illustrate the interpolation of the pressure and the velocity, respectively, when the left is the Darcy domain and the right is the fluid domain. Equation (2.29) implies that the pressure is linearly interpolated if the neighboring cells are within the same domain, but that the pressure of the fluid domain is extended to the interface if the domains of the two cells are different. On the other hand, the velocity of the Darcy domain is extended to the interface if it is shared by the different domains, as described

by Equation (2.30). Since Equations (2.29) to (2.32) represent the interpolation method, taking the interface between the horizontally-placed left and right cells as an example, these equations are obviously applicable to any interface, such as the one between the vertically-placed upper and lower cells.

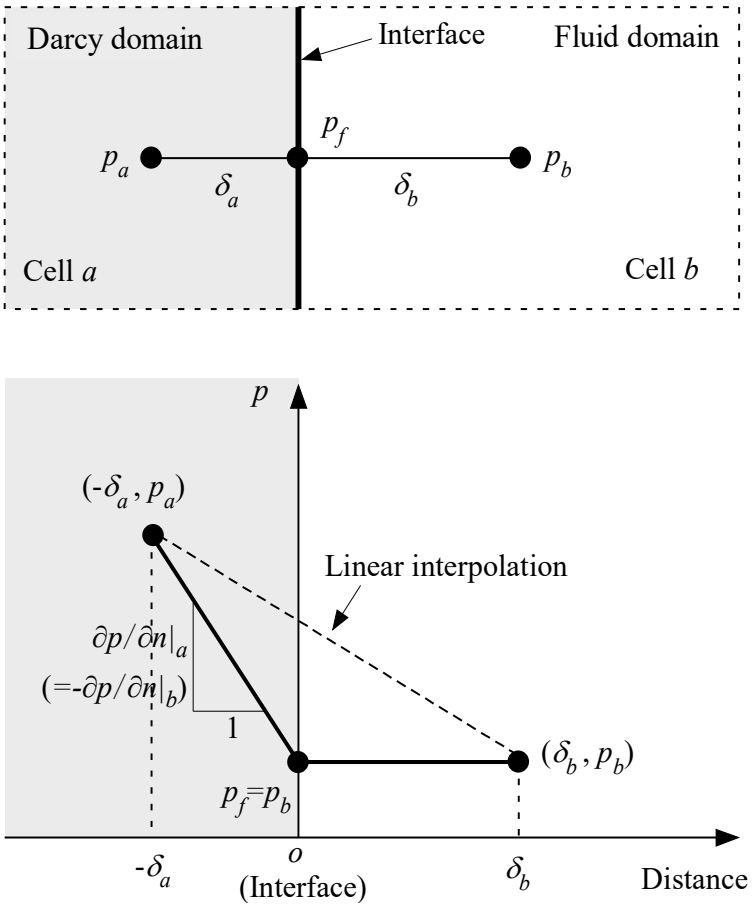

Figure 2.3 Interpolation of pressure at interface between fluid and Darcy domains.

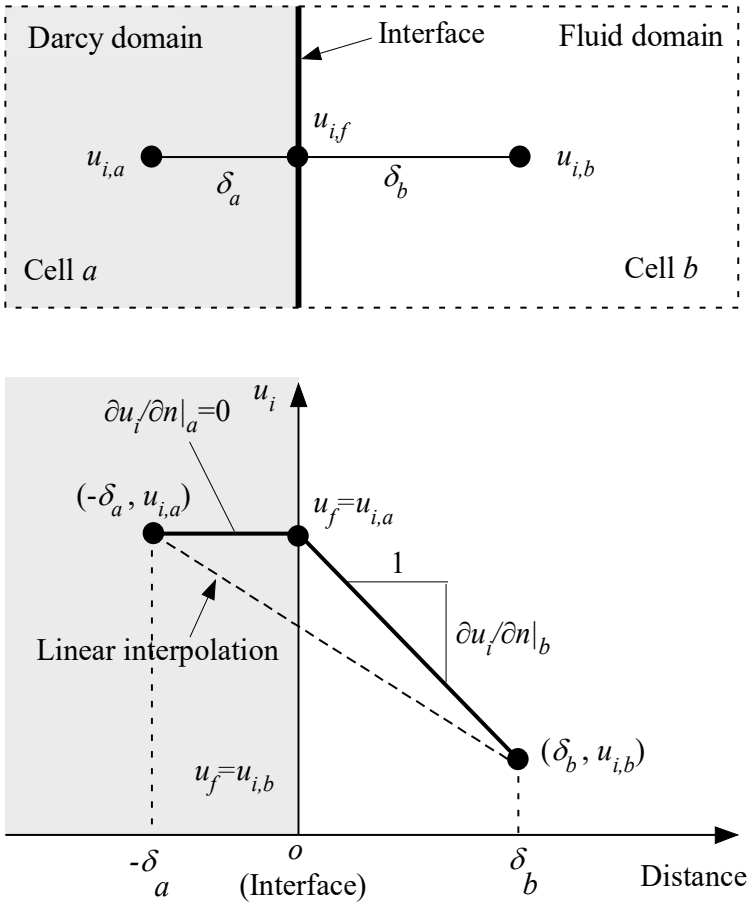

Figure 2.4 Interpolation of velocity at interface between fluid and Darcy domains.

2.3.4 Linear solvers

Equations (2.22) and (2.24) become the systems of linear equations for velocity $\hat{u}_i$ and pressure p^{m+1}, respectively. Letting N_c be the total number of finite volume cells, Equation (2.22) produces a $2N_c \times 2N_c$ matrix, while Equation (2.24) produces a $N_c \times N_c$ matrix. Generally, these matrixes are asymmetric and sparse. The Gauss-Seidel method is used for Equation (2.22), and the QMRCGSTAB method (Chan et al., 1994), which is a variant of the BiCG method, is applied to Equation (2.24).

2.4 Conclusions

In this chapter, a numerical method has been proposed to achieve the simultaneous analysis of the Darcy and the Navier-Stokes flows using the Darcy-Brinkman equations as the governing equations. The results are summarized as follows.

1. The governing equations nondimensionalized with the Reynolds and the Darcy numbers can be transformed to Darcy's law when the hydraulic conductivity is sufficiently small and the inverse of the Darcy number is even larger than the Reynolds number.

2. The pressure gradient in the Darcy domain is usually even greater than that in the fluid domain, such that the linear interpolation of the pressure induces unrealistically high gradients for the water pressure in the fluid domain neighboring the interface.

3. The flow velocity in the fluid domain is usually even greater than that in the Darcy domain, such that the linear interpolation of the velocity overestimates the inward or outward flux at the interface.

4. The key to obtaining stable and physically natural solutions lies in the interpolation of variables onto the interface between the porous and fluid domains.

3 Validation of numerical method for Navier-Stokes and Darcy flows

A numerical method for the coupled analysis of the Navier-Stokes and the Darcy flows was proposed in the previous chapter. In this chapter, the numerical method is validated through the use of several problems.

3.1 Introduction

In the previous chapter, a numerical method was proposed to realize the simultaneous analysis of the Darcy and the Navier-Stokes flows using the Darcy-Brinkman equations as the governing equations. The Darcy-Brinkman equations are identical to the Navier-Stokes equations when the porosity of 1.0 and the infinite hydraulic conductivity are given, and it has been shown that the Darcy-Brinkman equations can approximately satisfy Darcy's law for porous media.

The proposed numerical method is applied to three problems. First, the lid-driven cavity flow and the backward-facing step flow are computed in order to validate the Navier-Stokes flow in the fluid domain since the computational domain in these problems is occupied by the fluid domain. The computed results are compared with the results of previous studies, which were obtained by solving the Navier-Stokes equations. Second, the one-dimensional uniform flow in the water channel and the lid-driven cavity flow with porous media are computed in order to validate the Darcy flow in the Darcy domain and the interpolation of the velocity and the pressure on the interface between the fluid and the Darcy domains. The computed water pressure in the one-dimensional uniform flow is compared with the analytical solution calculated by Darcy's law. Two different layouts for the Darcy domain are computed in the lid-driven cavity flow with porous media. In this problem, the interpolation of velocity and pressure on the interface between the fluid domain and the Darcy domain is mainly discussed.

3.2 Lid-driven cavity flow

The lid-driven cavity flow is well known as a problem which has a non-uniform flow. A square domain filled with water is assumed, as shown in Figure 3.1. The left, right, and bottom walls of the domain are fixed, while the top wall is movable. When the top wall is moved to the right with constant velocity, the water around the top wall is dragged along with the wall. The dragged water goes to the right wall. Then, the water turns downward because it cannot pass through the right wall. The turned water goes to the bottom wall, and then turns to the left again. On the other hand, the water flows into the top left corner from the lower side in order to fill the shortage of the water which goes to the right wall. By repeating these steps, the vortex appears in the domain. Ghia et al. (1982) reported that the vortex is obtained in the analysis using the Navier-Stokes equations.

Figure 3.1 shows the geometry and the boundary conditions for the lid-driven cavity flow. The height and the width of the computational domain are L. As the boundary conditions, the horizontal velocity of V is given to the top surface and the non-slip condition is imposed on the side and bottom walls. The Reynolds number in this problem, Re, is defined as follows:

$$\mathrm{Re} = \frac{VL}{\nu} \tag{3.1}$$

The computation is performed with Re=1000. The inverse of the Darcy number is set to zero in the fluid domain. After the initial flow velocity and the initial water pressure are set to zero, the numerical computation is carried out until the steady state is realized. Figure 3.2 shows the finite volume cells for the computation. The computational domain is divided into 50 cells in the horizontal and vertical directions. A total 2500 cells are used to compute the problem.

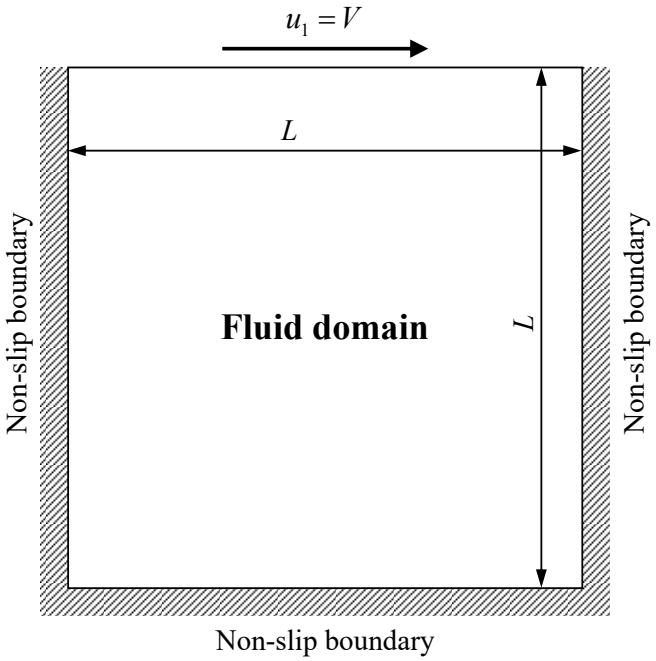

Figure 3.1 Geometry and boundary conditions of lid-driven cavity flow.

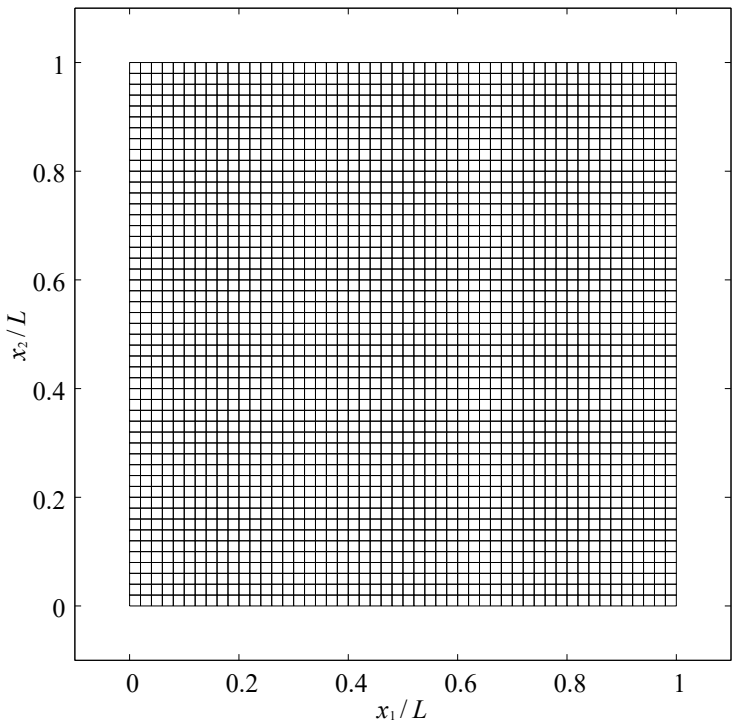

Figure 3.2 Finite volume cells for lid-driven cavity flow.

The velocity distributions at the steady state are shown in Figure 3.3. The flow exhibits the vortex as is usually seen in the lid-driven cavity flow. Figures 3.4 and 3.5 show the distributions of the horizontal and vertical flow velocities at the central cross section of the domain, respectively. The computed flow velocity is in good agreement with the results by Ghia et al. (1982). The proposed numerical method can simulate the Navier-Stokes flow in the fluid domain when λ =1.0 and Da^{-1}=0 are given.

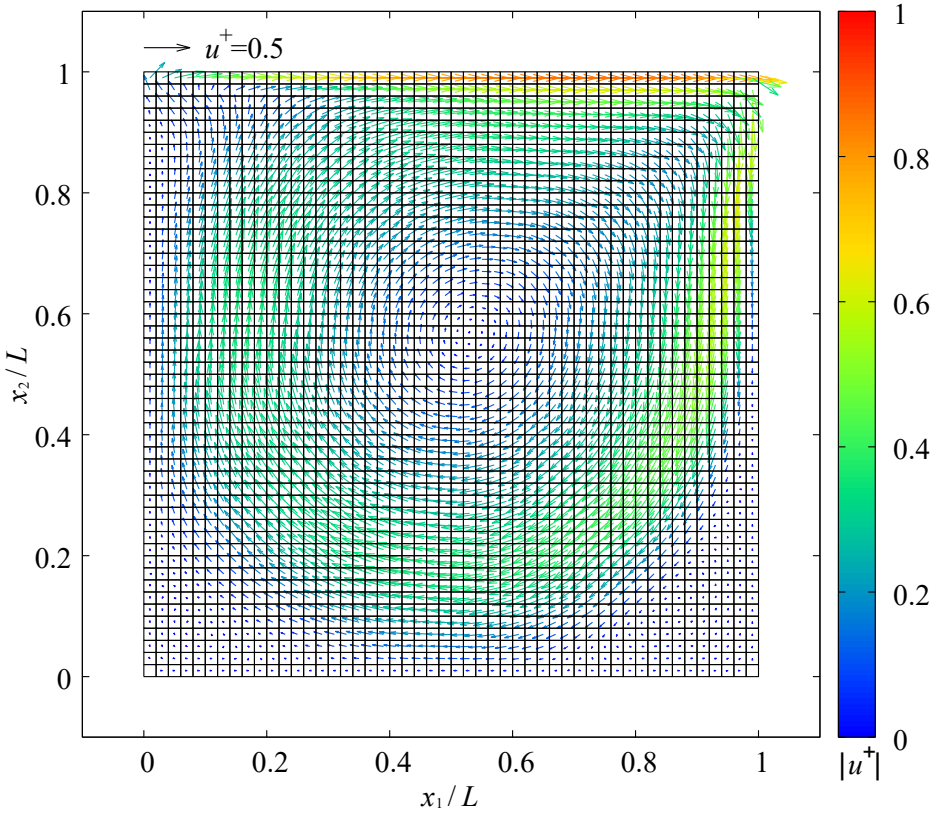

Figure 3.3 Computed velocity vector of flow (Re=1000).

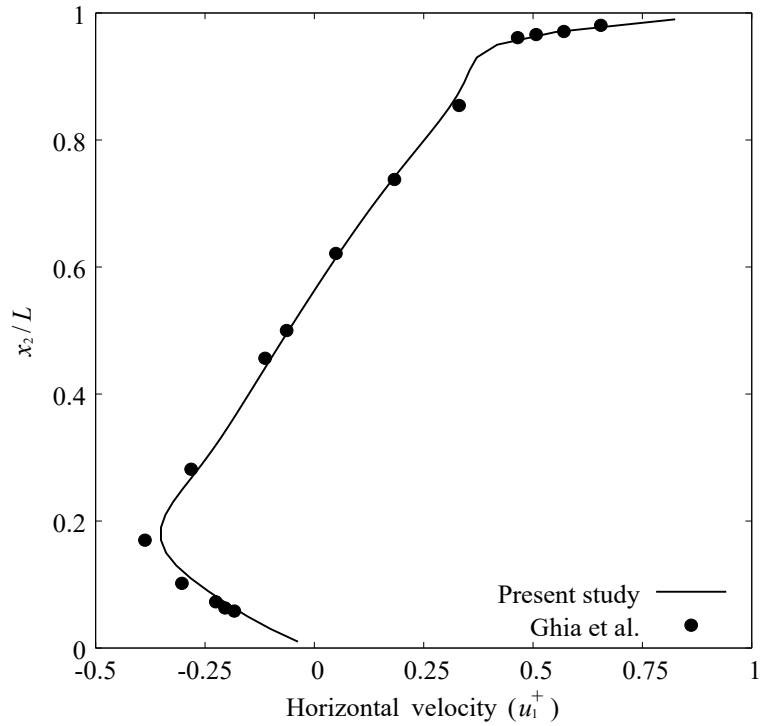

Figure 3.4 Distribution of horizontal velocity at central cross section.

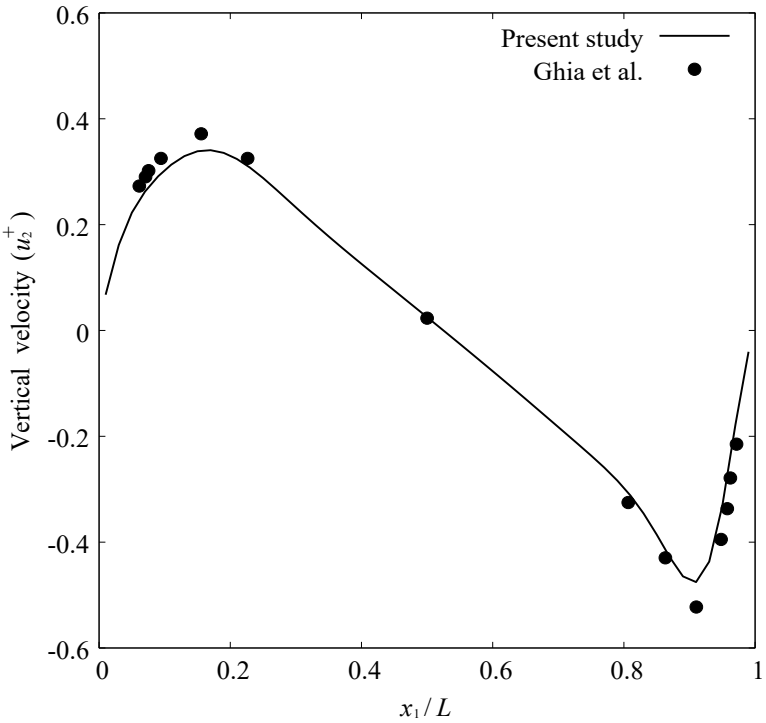

Figure 3.5 Distribution of vertical velocity at central cross section.

3.3 Backward-facing step flow

The backward-facing step flow is well known as a basic flow field which involves separation and reattachment. The flow field in the backward-facing step flow has a step on the downstream side, as shown in Figure 3.6. The inflow comes into the domain from the left side of the domain, and goes along the top and bottom walls. Then, the flow separates from the wall at the step. After the separation, the water flows for a while and reattaches to the wall again. The distance from the step to the reattachment point has been addressed in studies on the backward-facing step flow. In this study, the reattachment point is defined as the point where the velocity along the bottom wall changes from a positive value to a negative one. The distance from the step to the reattachment point is normalized by the following equation:

$$\overline{X} = \frac{X}{h} \tag{3.2}$$

where $\overline{X}$ denotes the normalized distance between the step and the reattachment point, X denotes the distance between the step and the reattachment point, and h denotes the height of the step. Many experimental and numerical analyses have been conducted all around the world. The first experimental study on the backward-facing step flow goes back to Armaly et al. (1983). They showed that the position of the reattachment point depends on the changing of the Reynolds number from within the range of the laminar to the turbulent flow.

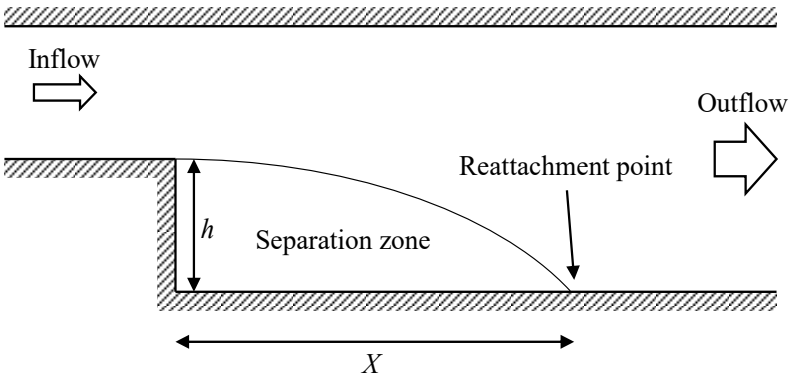

Figure 3.6 Backward-facing step flow.

The geometry and the boundary conditions for the problem are shown in Figure 3.7. The parabolic profile of the flow velocity is given on the left boundary of the fluid domain and the right side has the free outflow condition where the pressure and the gradient of the velocity are zero. The non-slip condition is imposed on the top and bottom sides. The flow velocity and the pressure are initially set to zero in all of the computational domain. The finite volume cells are shown in Figure 4.3. A total of 15,200 finite volume cells are used. The computation is carried out until the flow field becomes steady.

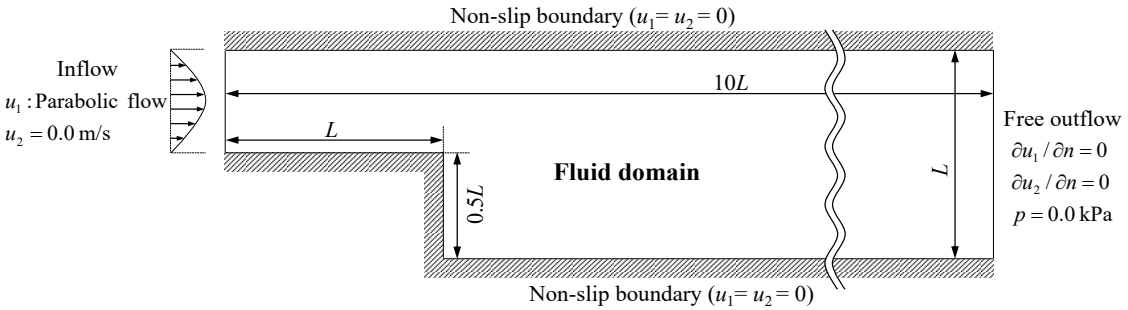

Figure 3.7 Geometry and boundary conditions of backward-facing step flow.

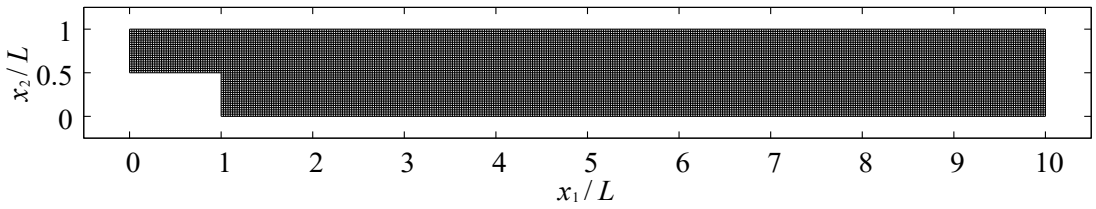

Figure 3.8 Finite volume cells for backward-facing step flow.

Three different Reynolds numbers, namely, 264, 396, and 528, are computed. The Reynolds number, Re, in this problem is defined as follows:

$$\mathrm{Re} = \frac{U_{\mathrm{ave}} L}{\nu} \tag{3.3}$$

where U_{ave} is the bulk velocity in the fluid domain and L is the height of the channel (See Figure 3.7).These values are placed in the range of those given in previous studies on the backward-facing step flow (e.g., Kim and Moin, 1985; Kim and Choi, 2000).

The velocity distributions at the steady state for all the Reynolds numbers are shown in Figure 3.9. The flows in all cases exhibit separation bubbles after the step as is usually seen in the backward-facing step flow. Then, the separated flow reattaches to the bottom wall around the center of the computational domain. The flow along the top wall also separates from the wall and reattaches. This is because the width of the duct has expanded to the lower side. After the reattachment to the top and bottom walls, the flow goes along the top and bottom walls. Finally, the distribution of horizontal velocity forms a parabola at the outflow boundary.

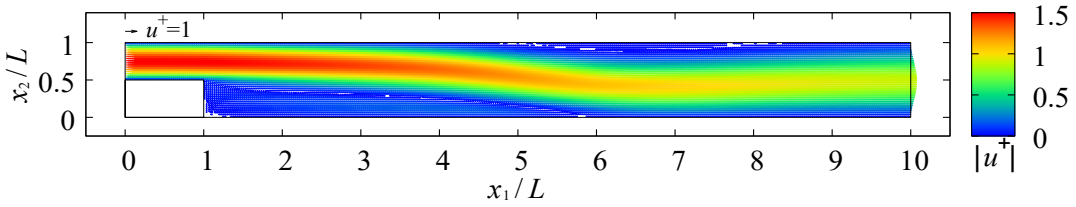

(a) Re=528

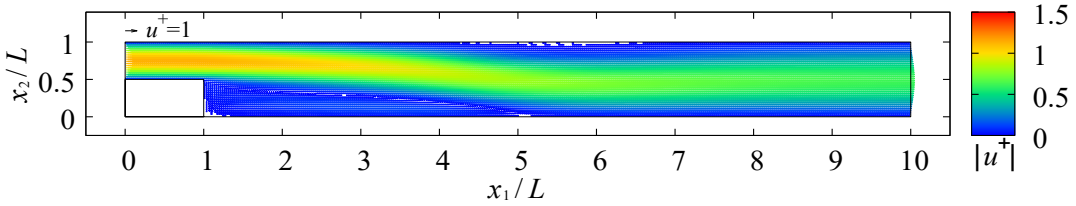

(b) Re=396

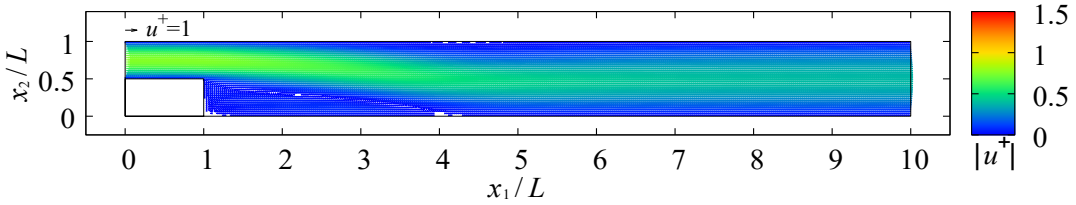

(c) Re=264

Figure 3.9 Computed velocity vector of flow.

Figure 3.10 shows the relationship between the Reynolds number and the position of the reattachment point. The computed reattachment points are in good agreement with the computational results by Kim and Moin (1985). These results indicate that the proposed numerical method can simulate the flow in the fluid domain when λ =1.0 and Da^{-1}=0 are given.

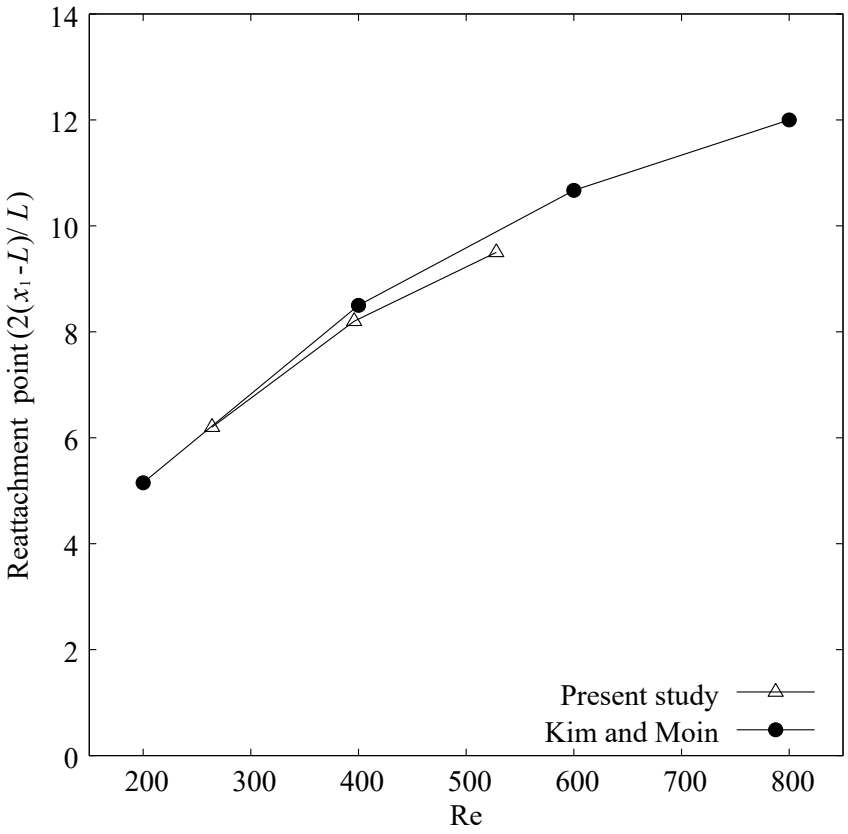

Figure 3.10 Plot of reattachment point using Reynolds number.

3.4 One-dimensional uniform flow in water channel

The one-dimensional flow problem is assumed to validate the numerical method presented in the previous chapter. The seepage water flows from the high pressure side to the low pressure side in a water channel filled with porous media and seepage water when the different levels of pressure are given to both sides of the water channel (See Figure 3.11). The relationship between the velocity of seepage flow u and the pressure on both sides is described by the following equation:

$$u = \frac{k}{\rho g}\frac{p_1 - p_2}{\delta} \tag{3.4}$$

Equation (3.4) is the well-known Darcy's law. In the one-dimensional uniform flow problem, the analytical solution can be obtained by this equation.

In this section, the water channel, including the fluid and the Darcy domains, is computed. The obtained velocity and pressure are compared to the analytical solution obtained by Darcy's law in order to validate the proposed numerical method. And the oscillation of the flow velocity and pressure is measured in order to evaluate the stability of the computed solution.

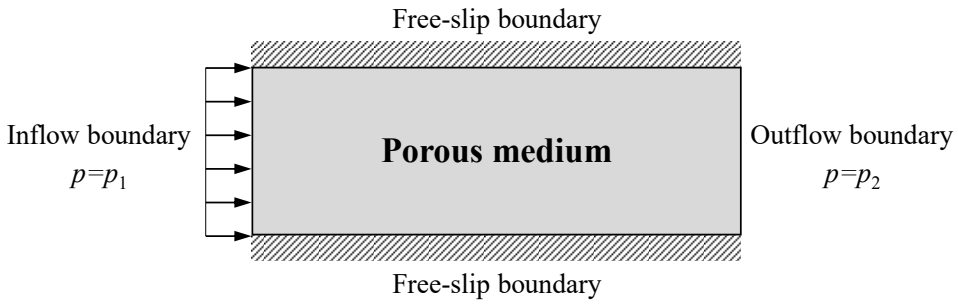

Figure 3.11 Water channel filled with porous media.

The geometry and the boundary conditions of the water channel are shown in Figure 3.12. The channel is 15L long and L wide. It includes the porous media ($5L<x_1<10L$) and is divided into two domains. Each domain possesses a different Darcy number and a different porosity, as shown in Table 3.1. As the boundary conditions, the inflow velocity is given on the left side of the channel, and the water pressure on the right side is kept at 0 kPa. The free-slip condition is imposed on the upper and lower sides. After the initial flow velocity and water pressure are both set to zero, the flow field is computed up to the steady state. Figure 3.13 shows the finite volume cells discretizing the water channel. The computational domain is divided into 150 cells in the horizontal direction and 10 cells in the vertical direction. A total of 1500 cells are used to compute the problem.

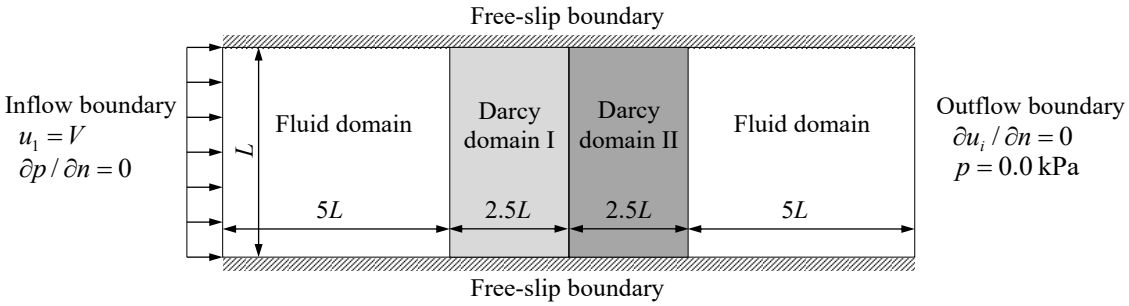

Figure 3.12 Geometry and boundary conditions of one-dimensional flow.

Table 3.1 Properties of Darcy domains.

	Darcy domain I ($5 < x_1/L < 7.5$)	Darcy domain II ($7.5 < x_1/L < 10$)
Darcy number	1.63×10^{-8}	6.52×10^{-8}
Porosity	0.4	0.5

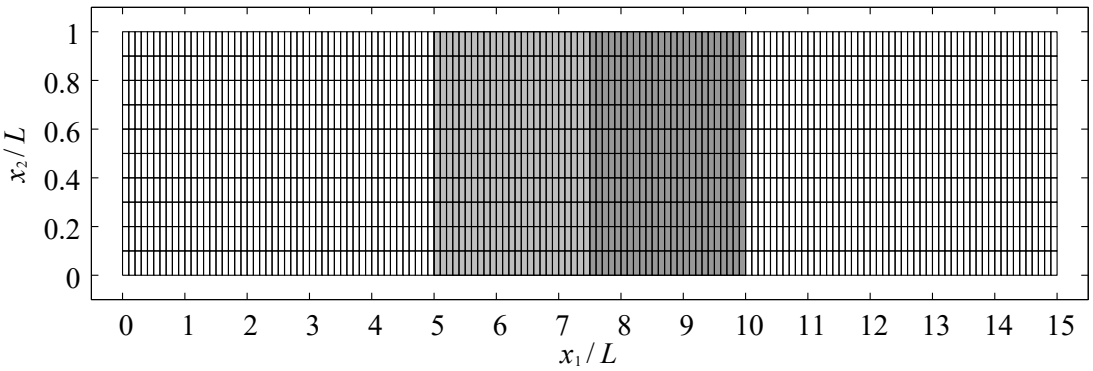

Figure 3.13 Finite volume cells for one-dimensional flow.

Figures 3.14 and 3.15 show the computed water pressure and horizontal flow velocity at the steady state, respectively. The water pressure in both the fluid and the Darcy domains is nondimensionalized by Equation (2.10). The distribution of the computed pressure is almost identical to the analytical solution calculated from Darcy's law. As seen in Figure 3.15, the flow velocity is kept at the constant value of the inflow velocity along the channel, although slight oscillations can be seen at the interfaces between the different domains.

Here, focus shall be placed on the effect of interpolating the pressure by Equation (2.29). Figure 3.16 shows the velocity calculated using the simple linear interpolation on all cells. The other conditions are the same as in the above-described problem. When Equation (2.29) is not used for the interpolation of the water pressure and the simple linear interpolation is employed, the strong oscillation of the flow velocity is observed at the interface between the porous media and the fluid domain, as shown in Figure 3.16. The figure shows the numerical results of the computed flow velocity at numerous time steps, namely, 50, 500, and 2000. The oscillation appears at the interfaces located on the left- and the right-hand sides of the porous media and it is amplified with the time steps. When the pressure is linearly interpolated at the interface, the pressure gradient in the fluid domain becomes unrealistic, as seen in Figure 3.17, because the pressure gradient in the porous media is usually even greater than that in the fluid domain. As seen in Figure 3.17, if the pressure is interpolated linearly at the interface where the hydraulic conductivity changes sharply, the pressure in the cells of the fluid domain is overestimated due to the

influence of the decrease in pressure in the domain where the hydraulic conductivity is small. Thus, at the interface of the fluid domain, the velocity calculated by Equations (2.22) and (2.25) becomes large locally, and this causes the oscillation. Therefore, Equation (2.29) interpolates the pressure by ignoring the influence of the pressure in the cells with small hydraulic conductivity. Equation (2.29) is made equivalent to the following equation in order to obtain a steady-state solution for the Darcy equations:

$$\frac{k_a}{\rho g}\frac{p_f - p_a}{\delta_a} = \frac{k_b}{\rho g}\frac{p_b - p_f}{\delta_b} \tag{3.5}$$

Equation (3.5) denotes 'when the flow velocity is constant, the pressure gradient becomes small (large) in the region with the large (small) hydraulic conductivity'. Moreover, interpolating the pressure based on Equation (3.5) enables the computation of the steady-state analysis close to the analytical solution.

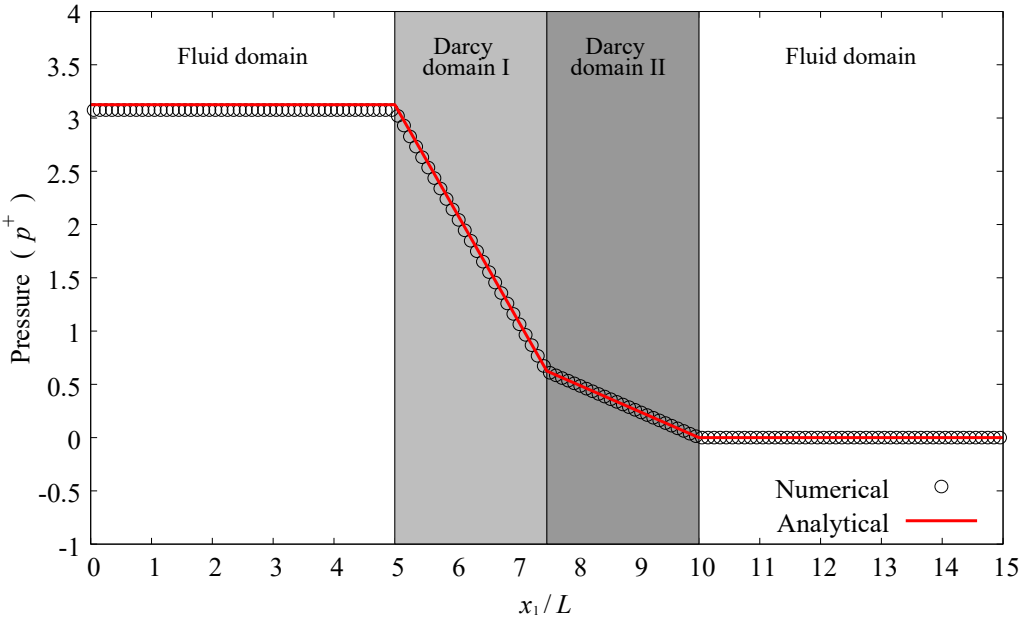

Figure 3.14 Computed pressure along horizontal axis.

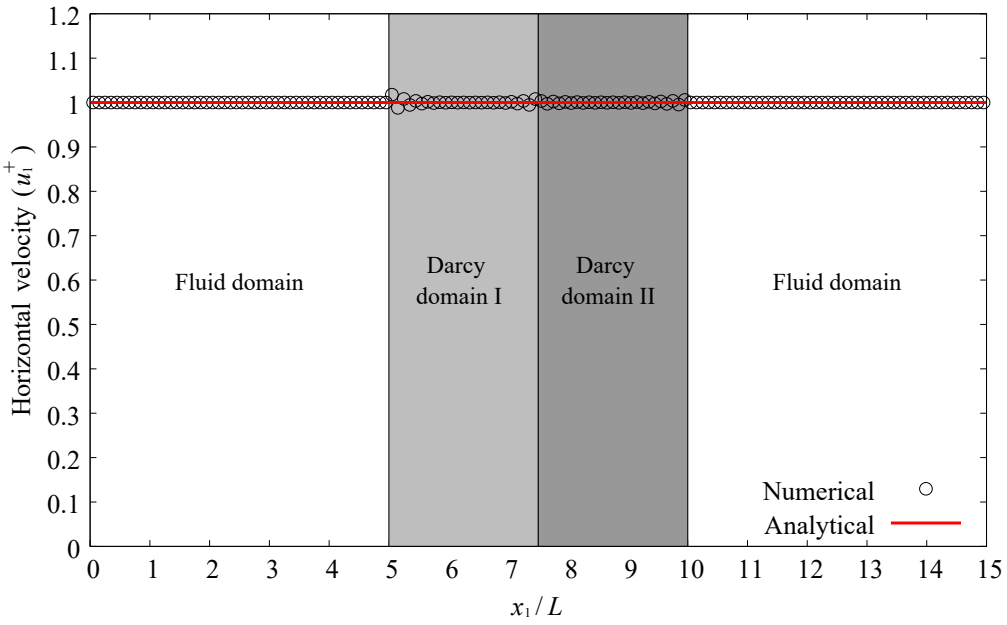

Figure 3.15 Computed flow velocity along horizontal axis.

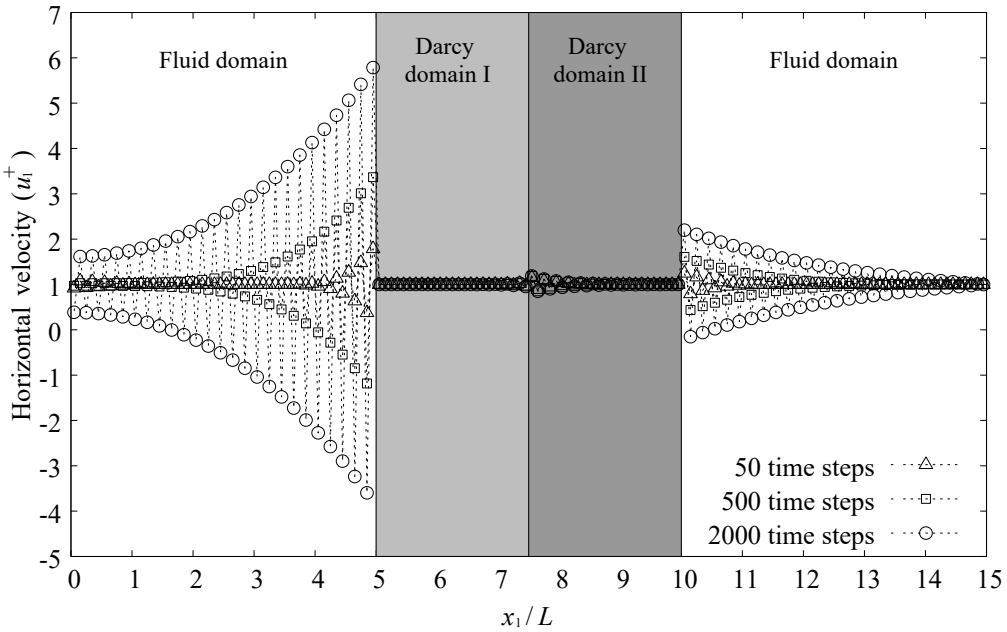

Figure 3.16 Oscillation of flow velocity at interface.

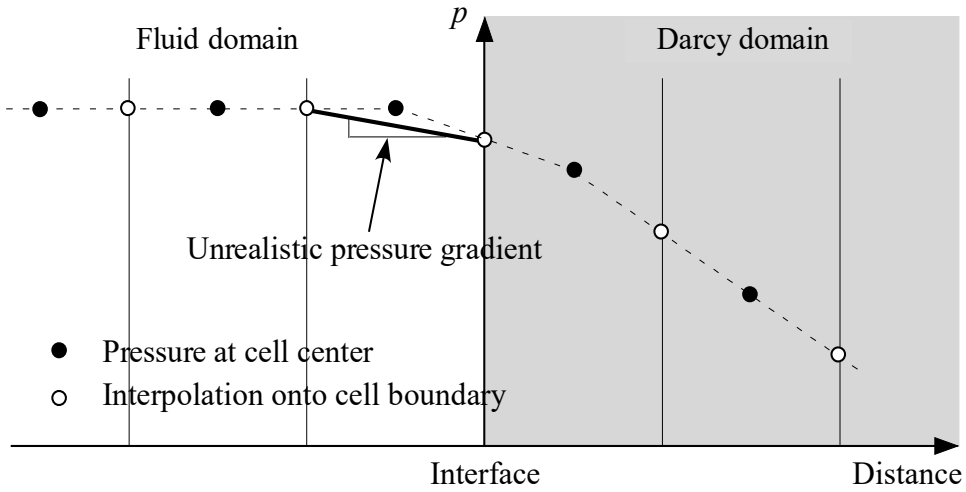

Figure 3.17 Linear interpolation of pressure around interface between water and Darcy domain.

3.5 Lid-driven cavity flow over porous media

The regular lid-driven cavity flow is calculated in Section 3.2. The computed flow velocity is in good agreement with the results by Ghia et al. (1982). In this section, the lid-driven cavity flow problem, which has porous media in the computational domain, is computed in order to validate the interpolation of the velocity and the pressure between the fluid and the Darcy domains.

Figure 3.18 shows the geometry and the boundary conditions for the lid-driven cavity flow. The height and the width of computational domain are L. The Darcy domain is installed in the bottom quarter of the square domain, while the rest of the region is occupied by the fluid domain. As for the boundary conditions, horizontal velocity V is given to the top surface and the non-slip condition is imposed on the side and bottom walls. The Darcy number and the porosity of the Darcy domain are assumed to be 1.0×10^{-8} and 0.4, respectively. After the initial flow velocity and the initial water pressure are set to zero, the numerical computation is carried out until the steady state is realized. Figure 3.19 shows the finite volume cells for the computation. The computational domain is divided into 40 cells in the horizontal and vertical directions. A total of 1600 cells are used to compute the problem.

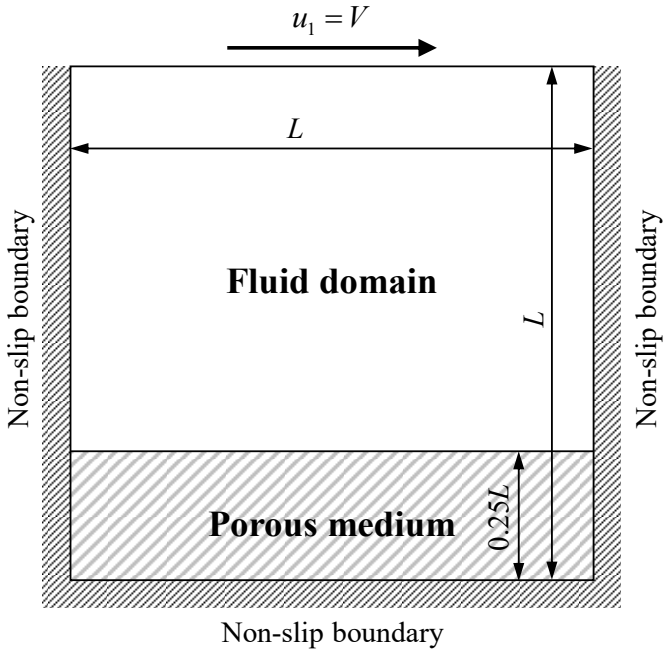

Figure 3.18 Geometry and boundary conditions of cavity flow with Darcy domain at bottom.

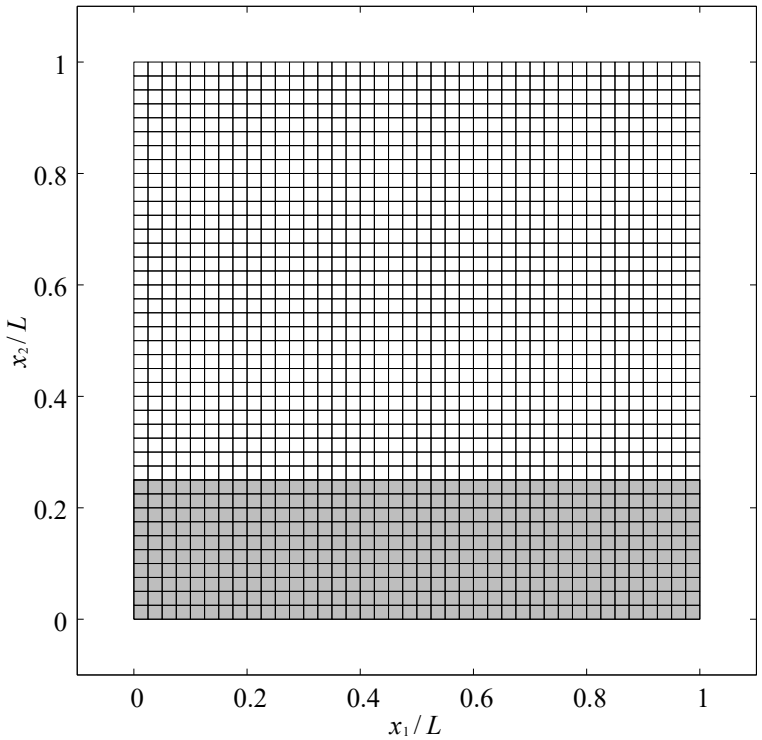

Figure 3.19 Finite volume cells for cavity flow with Darcy domain at bottom.

Figure 3.20 shows the computed flow velocity field. As seen in the figure, a large vortex is induced in the fluid domain by the given boundary velocity at the top. Figure 3.21 highlights the velocity field in the Darcy domain because the flow velocity in the Darcy domain is even smaller than that in the fluid domain, and the detailed velocity profile cannot be recognized in Figure 3.20. Figure 3.21 reveals that the upward seepage flow, heading to the vortex created in the fluid domain, occurs in the central region of the Darcy domain, which results from the lower pressure at the vortex. Figure 3.22 shows the distribution of the computed water pressure at the steady state. The water pressure in both the fluid and the Darcy domains is nondimensionalized by Equation (2.10). It is seen from the figure that the pressure at the center of the vortex is smaller and is continuously computed at the interface between the fluid and the Darcy domains. Furthermore, the vortex formed in the fluid domain moves slightly to the right as the porous medium is placed at the bottom of the computational domain.

Let us now take a more careful look at the effect of the interpolation of pressure by Equation (2.29). Figure 3.23 shows the pressure distribution computed using the linear interpolation which does not consider the hydraulic conductivity. The other conditions are the same as for the above problem. The pressure in Figure 3.23 exhibits discontinuity on the surface between the fluid and the Darcy domains. The unrealistic and large pressure is calculated, especially on the surface where water flows out from the fluid domain and into the Darcy domain. On the other hand, the pressure decreases unrealistically around the surface where water flows out from the Darcy domain and into the fluid domain. This is caused by the difference between the magnitude of velocities in the fluid and the Darcy domains. Figure 3.24 presents a schematic of the situation whereby the velocity is interpolated linearly on the surface between the fluid and the Darcy domains. In two-dimensional flow problems, the velocity in the fluid domain is generally calculated more excessively than the velocity in the Darcy domain. Thus, the velocity of the flow which flows out from the surface is overestimated if a linear interpolation is used for the velocity. As a result, the pressure increases unrealistically in the area where the inflow is overestimated when Equation (2.25) is solved. In order to avoid this unrealistic pressure, the velocity should be interpolated by giving large weight in the area where the hydraulic conductivity is small. Equation (2.30) embodies these ideas. Equations (2.29) and (2.30)

mean that the velocity in the Darcy domain is adopted and the gradient of pressure in the fluid domain becomes zero on the interface between the fluid and the Darcy domains.

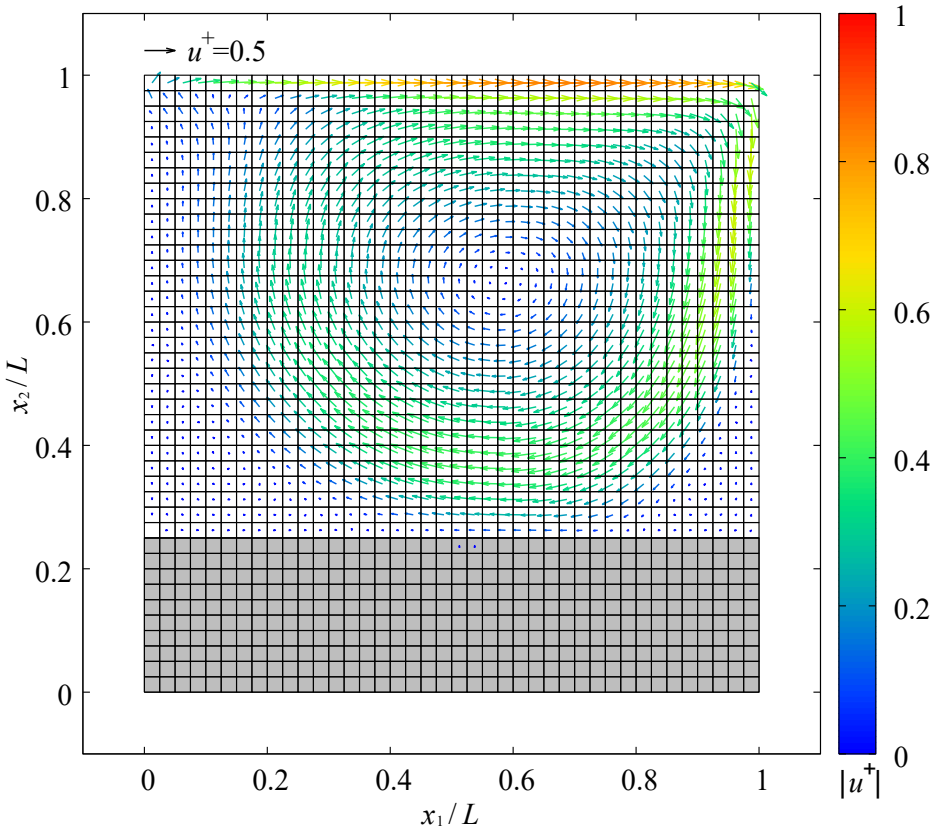

Figure 3.20 Computed velocity vector of flow.

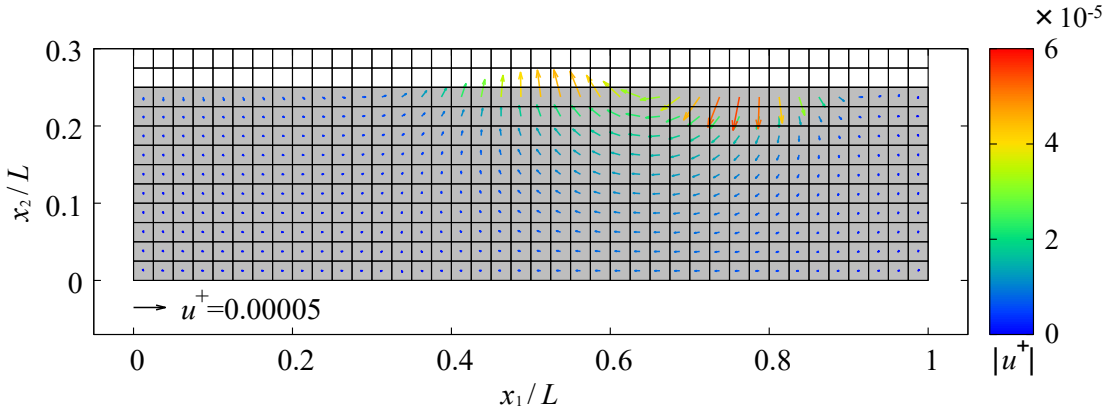

Figure 3.21 Computed velocity vector of flow in Darcy domain.

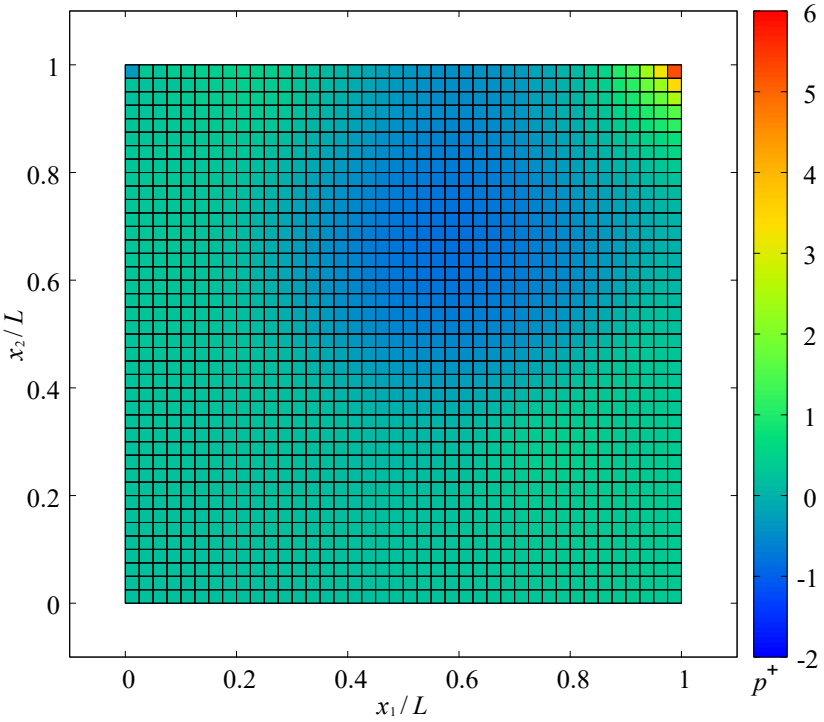

Figure 3.22 Pressure distribution at steady state.

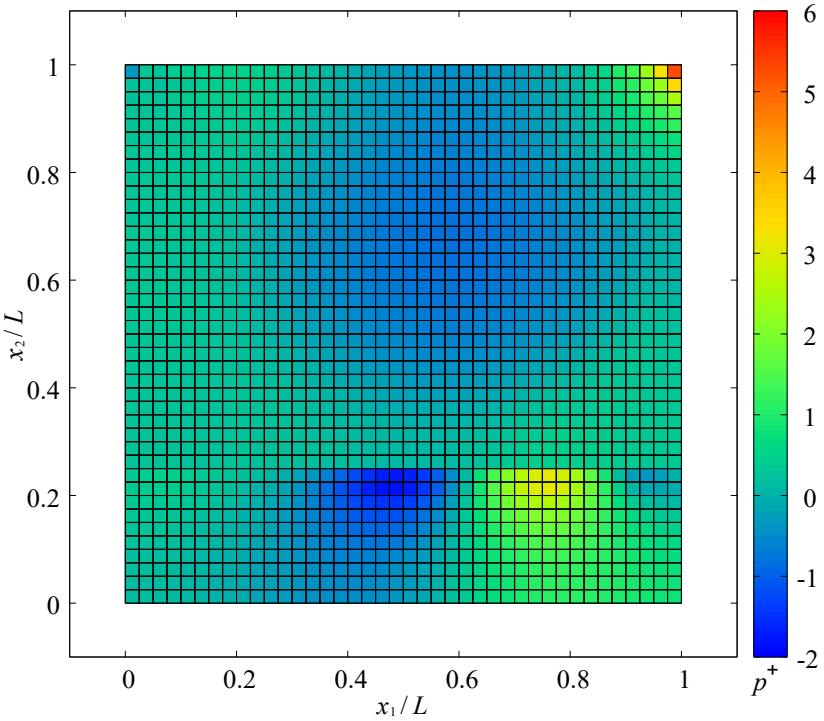

Figure 3.23 Pressure distribution at steady state (Linear interpolation of velocity).

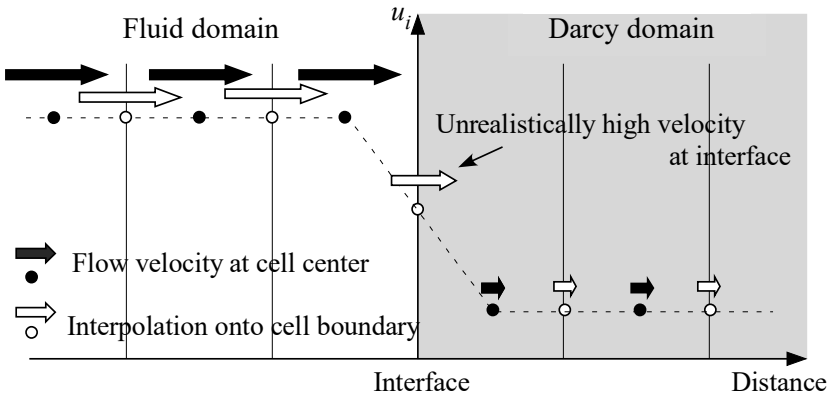

Figure 3.24 Linear interpolation of flow velocity around interface between fluid and Darcy domains.

3.6 Lid-driven cavity flow around porous media

A problem with complex arrangements of porous media was computed. Figure 3.25 shows the geometry and the boundary conditions. It looks like the problem that was presented in the previous section, but the arrangement of the porous media is different. The gray domain in Figure 3.25 is porous media. It was installed around the centroid where the vortex appears in the regular lid-driven cavity flow. The porous media consist of two squares which have different sizes. Accordingly, the influence of the size of the porous media on the flow around the porous media is also investigated in this problem. The Darcy number and the porosity were set to 1.0×10^{-8} and 0.4, respectively; they are the same values as those used for the problem presented in the previous section.

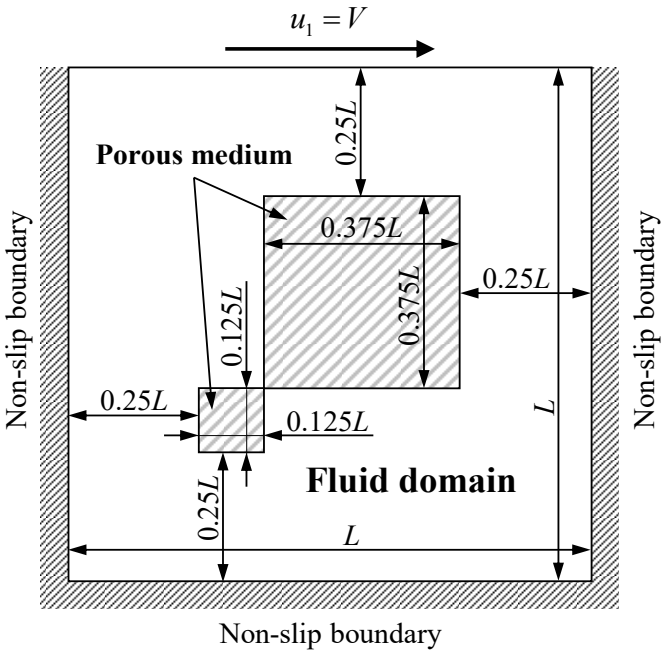

Figure 3.25 Geometry and boundary conditions of cavity flow with Darcy domain at center.

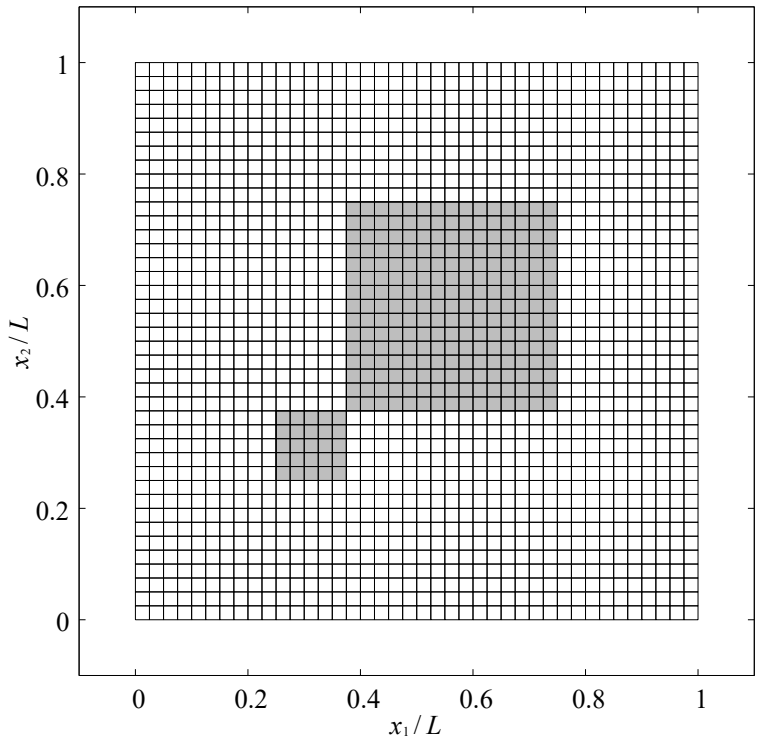

Figure 3.26 Finite volume cells for cavity flow with Darcy domain at center.

Figure 3.27 shows the flow velocity at each state. In the early state, the flow exhibits the vortex in the top right corner of the fluid domain. Afterwards, the vortex disappears progressively. Finally, a flow which goes around the Darcy domain is formed. The velocity in the Darcy domain is very much smaller than the velocity in the fluid domain. Figure 3.28 shows the flow velocity in the Darcy domain. The figure indicates that the seepage water flows into the large Darcy domain from the top of the right surface and flows out from the top surface of the Darcy domain. This is because the water flows towards the right surface of the large Darcy domain in the fluid domain. The flow velocity in the joints of the two Darcy domains becomes relatively large. We have identified that the water might flow easily through the narrow area of the Darcy domain. The velocity of the flow in the smaller Darcy domain is relatively higher than that in the larger Darcy domain, and we have identified that this is due to the same reason. These results indicate that the shape of the Darcy domain has a strong influence not only on the flow in the fluid domain, but also on the seepage flow in the Darcy domain.

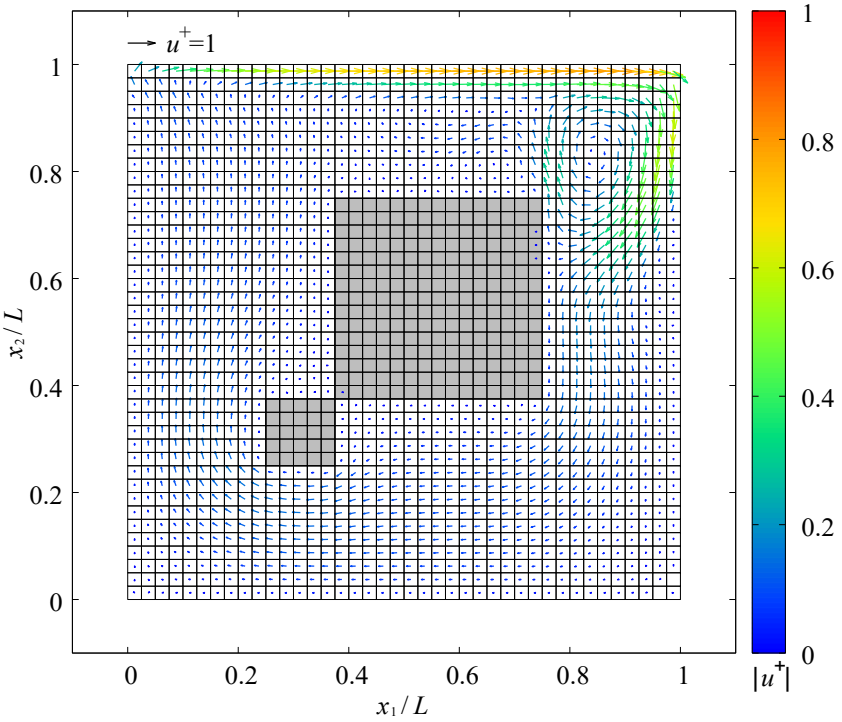

(a) t^+=10

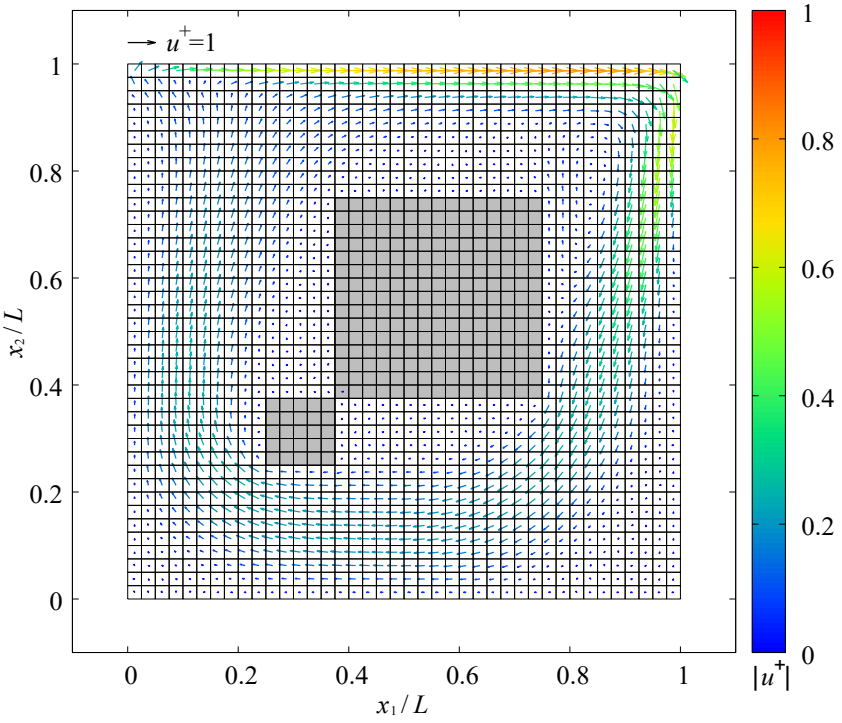

(b) t^+=10

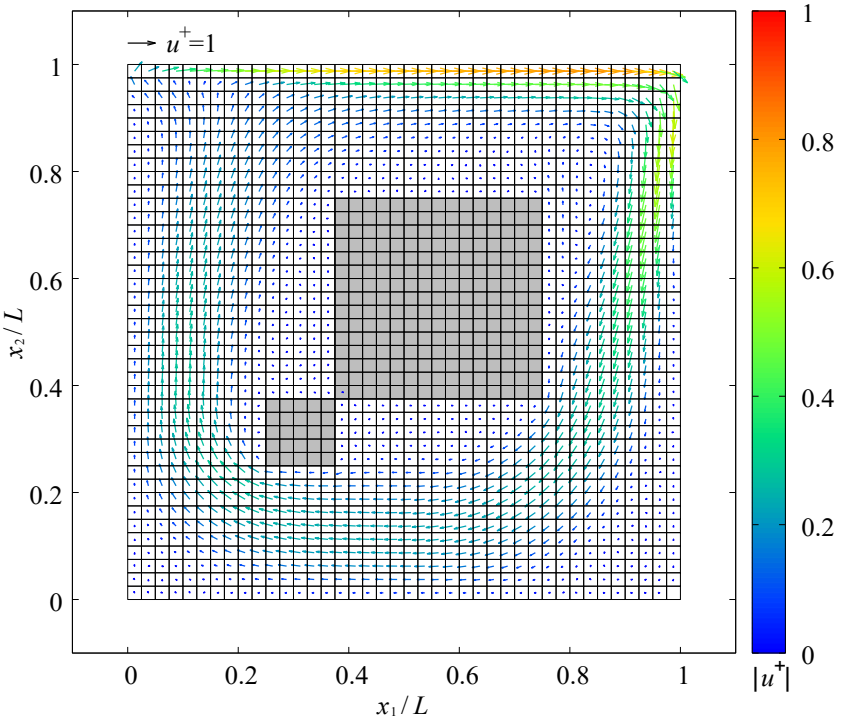

(c) t^+=25

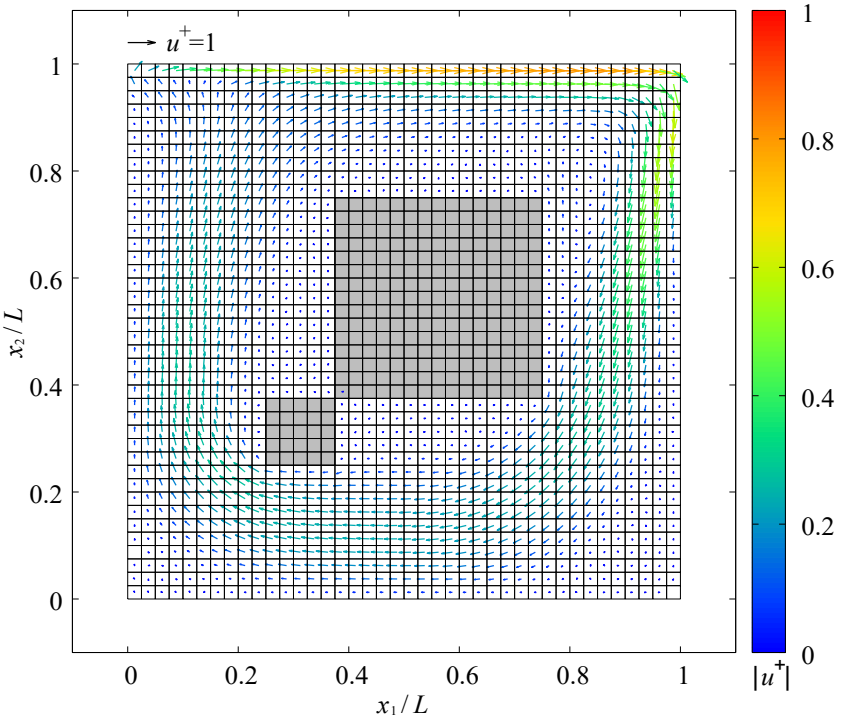

(d) t^+=50

Figure 3.27 Computed velocity vector of flow.

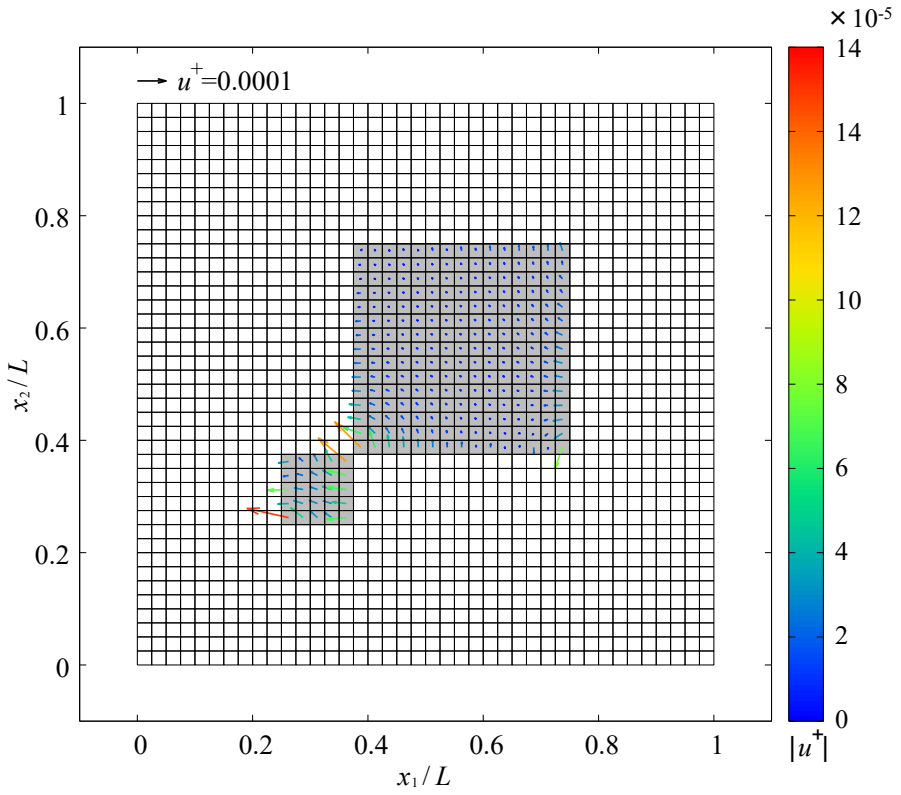

Figure 3.28 Computed velocity vector of flow in Darcy domain.

3.7 Conclusions

In this chapter, several problems were computed to validate the proposed numerical method. The obtained numerical results have shown that the method can produce stable and physically realistic numerical solutions. The results are summarized as follows.

1. The flow velocity in the lid-driven cavity flow and the reattachment point in the backward-facing step flow are in good agreement with the results of previous studies. The proposed numerical method can simulate the Navier-Stokes flow in the fluid domain when λ =1.0 and Da^{-1}=0 are given.

2. The computed pressure in the one-dimensional uniform flow problem is in good agreement with the analytical solutions calculated from Darcy's law, and the flow velocity is kept at a constant value for the inflow velocity along the channel.

3. Using the proposed interpolation of pressure by Equation (2.29), the oscillation of velocity can be avoided. If the pressure is linearly interpolated at the interface, the oscillation appears at the interfaces located on the left- and right-hand sides of the porous media and is amplified with the time steps.

4 Backward-facing step flow with porous step

Chapter 3 described how stable velocity and pressure can be obtained using the numerical method presented in **Chapter 2**. This indicates that the interpolations of velocity and pressure work well. In this chapter, the influence of the Reynolds and the Darcy numbers on the flow will be investigated.

4.1 Introduction

The backward-facing step flow is a well-known problem in computational fluid dynamics. The step is introduced in the water channel, as shown in Figure 4.1, and the separation of the step flow from the left side and its reattachment to the bottom wall on the right side of the step are observed. The first experimental study on the backward-facing step flow goes back to Armaly et al. (1983). Through an experiment in which the Reynolds number was changed from within the range of the laminar flow to the turbulent flow, they showed that the position of the reattachment point depends on the Reynolds number. Several other numerical studies have also been carried out (e.g., Kim and Moin, 1985; Keskar, 1999; Kim and Choi, 2000; Erturk, 2008). In Section 3.3, the proposed numerical method for the coupled analysis of the Navier-Stokes and the Darcy flows was validated by comparing it with the results of Kim and Moin.

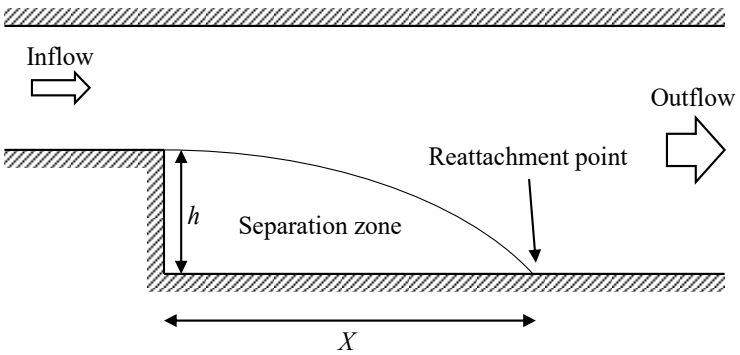

Figure 4.1 Backward-facing step flow.

Now, the influence of the seepage flow in the Darcy domain on the regular water flow in the fluid domain will be investigated. Therefore, a backward-facing step flow whose step is constructed with porous media is computed. In a regular backward-facing step flow, the horizontal flow velocity above the step is distributed like a parabola, known as the Hagen-Poiseuille flow, because the non-slip condition is given to the top and bottom walls including the upper surface of the step. However, if the wall of the water channel is porous media, the flow velocity on the surface of the porous media does not become zero. The wall constructed with porous media behaves like the slip condition. By varying the hydraulic conductivity of the porous media and the inflow rate, it can be seen how the regular water flow changes with the Reynolds number and the Darcy number. The position of the reattachment point is evaluated by the change in the regular water flow, and the reattachment point is defined as the point where the velocity along the bottom wall changes from a positive value to a negative one. The distance from the step to the reattachment point is normalized by the following equation:

$$\overline{X} = \frac{X}{h} \tag{4.1}$$

where $\overline{X}$ denotes the normalized distance between the step and the reattachment point, X denotes the distance between the step and the reattachment point, and h denotes the height of the step (See Figure 4.1).

4.2 Geometry and initial / boundary conditions

The geometry and the boundary conditions of the problem are shown in Figure 4.2. The porous media are installed as the backward-facing step and are located at the bottom left of the computational domain. The parabolic distribution of the flow velocity is given on the left boundary of the fluid domain, and the right side has the free outflow condition where the pressure and the gradient of the velocity are zero. The non-slip condition is imposed onto the top and bottom sides. The flow velocity and the pressure are initially set to zero in all of the computational domain. The finite volume cells are shown in Figure 4.3. A total of 16,000 finite volume cells are used. The computation is carried out until the flow field becomes steady.

By varying the hydraulic conductivity of the porous media and the inflow rate, how the reattachment point changes with the Reynolds number and the Darcy number is investigated. In this problem, the Reynolds number, Re, is defined as follows:

$$\mathrm{Re} = \frac{U_{\mathrm{ave}} L}{\nu} \tag{4.2}$$

where U_{ave} is the bulk velocity in the fluid domain and L is the height of the channel (See Figure 4.2).

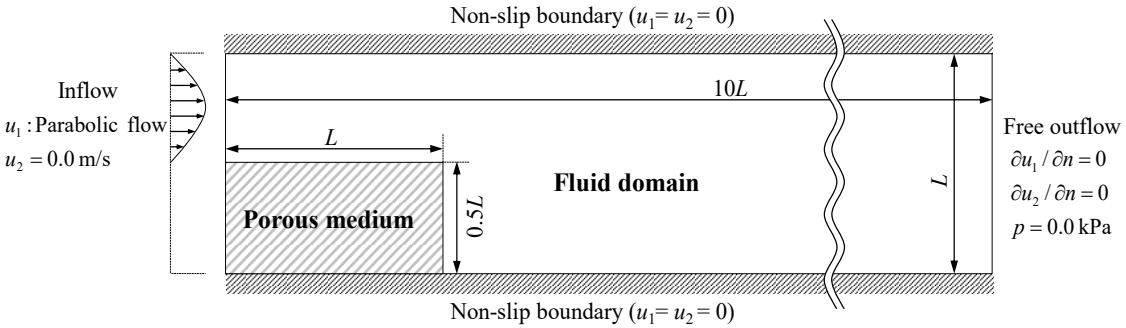

Figure 4.2 Geometry and boundary conditions.

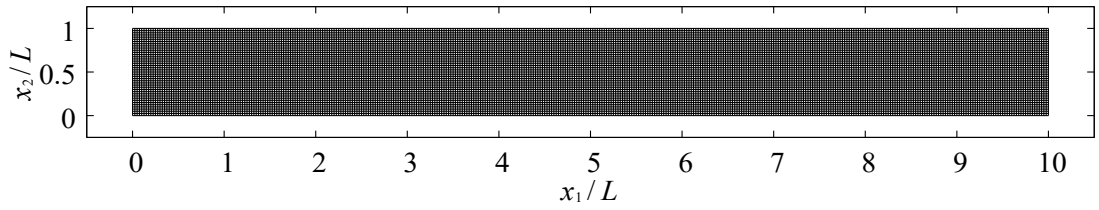

Figure 4.3 Computational finite volume cells for backward-facing step flow.

4.3 Results and discussion

4.3.1 Influence of Reynolds number

Three different Reynolds numbers, namely, 264, 396, and 528, are computed to investigate how the reattachment point changes with the Reynolds number when porous media are installed as the backward-facing step. These values are placed in the range of the previous studies for the backward-facing step flow (e.g., Kim and Moin, 1985; Kim and Choi, 2000), where the Darcy number of the porous media as the backward-facing step is fixed at 1.0×10^{-3} in all cases.

The velocity distributions at the steady state for the all the Reynolds numbers are shown in Figure 4.4. The flows in all cases exhibit separation bubbles after the porous steps as is usually seen in the backward-facing step flow, as shown in Figure 4.5. Then, the separated flow reattaches to the bottom wall around the center of the computational domain. The flow along the top wall also separates from the wall and then reattaches. This is because the width of the duct has expanded to the lower side. After the reattachment to the top and bottom walls, the flow goes along the top and bottom walls. Finally, the distribution of horizontal velocity forms a parabola at the outflow boundary.

Figure 4.6 shows the seepage flow velocity in the porous step in all cases. The flow velocity around the upper surface is greater than the velocity at the bottom of the porous step because the seepage water is accelerated by the Navier-Stokes flow around the upper surface. Thus, the velocity increases with the approaching upper surface of the step. And the flow velocity around the upper surface increases with an increase in the Reynolds number, as shown in Figure 4.7, because the flow velocity in the fluid domain is high.

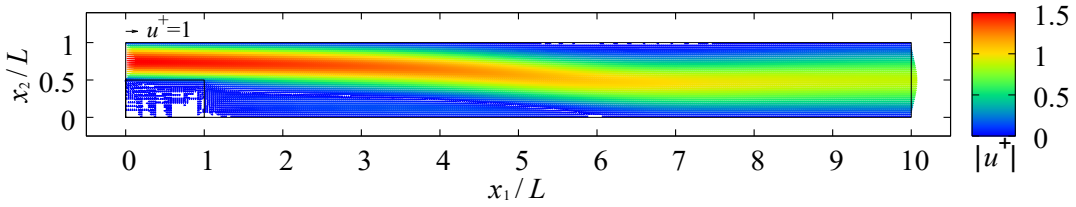

(a) Re=528

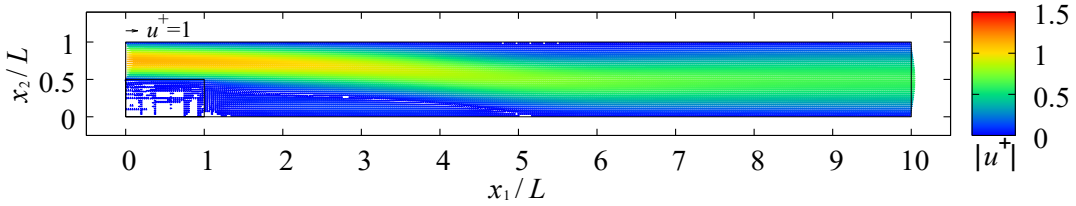

(b) Re=396

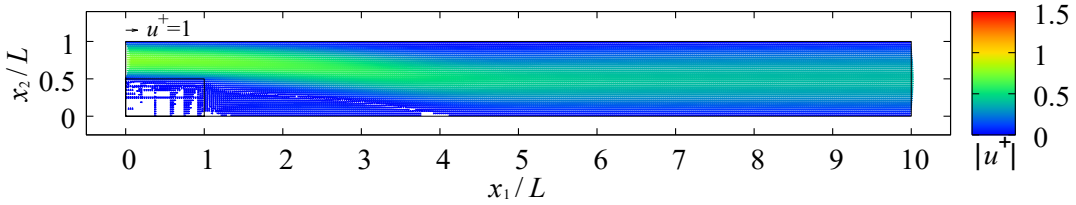

(c) Re=264

Figure 4.4 Computed velocity vector of flow (Da=1.0×10^{-3}).

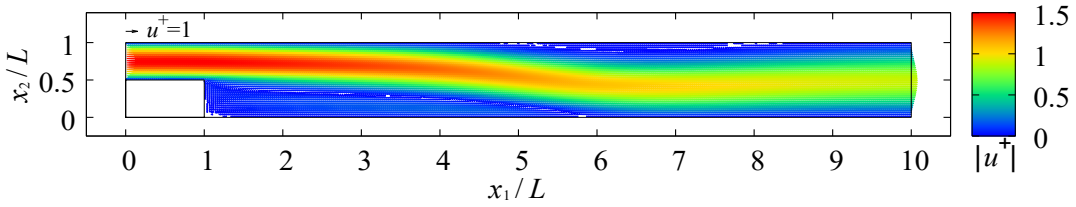

(a) Re=528

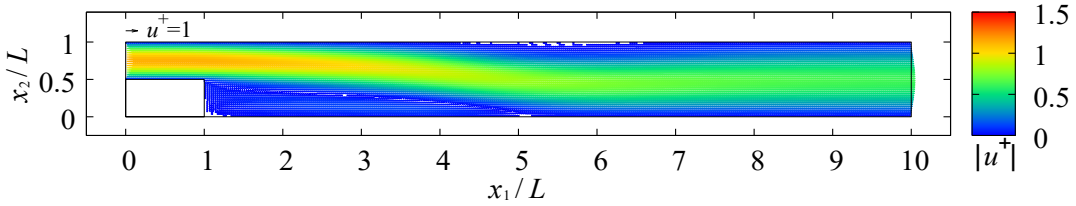

(b) Re=396

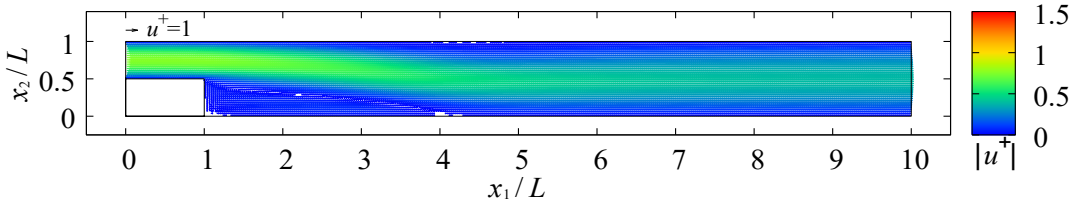

(c) Re=264

Figure 4.5 Computed velocity vector of flow (without porous step).

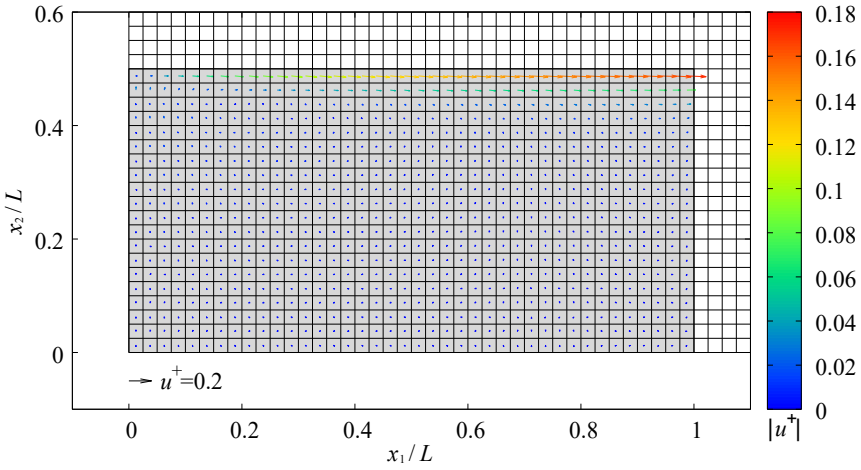

(a) Re=528

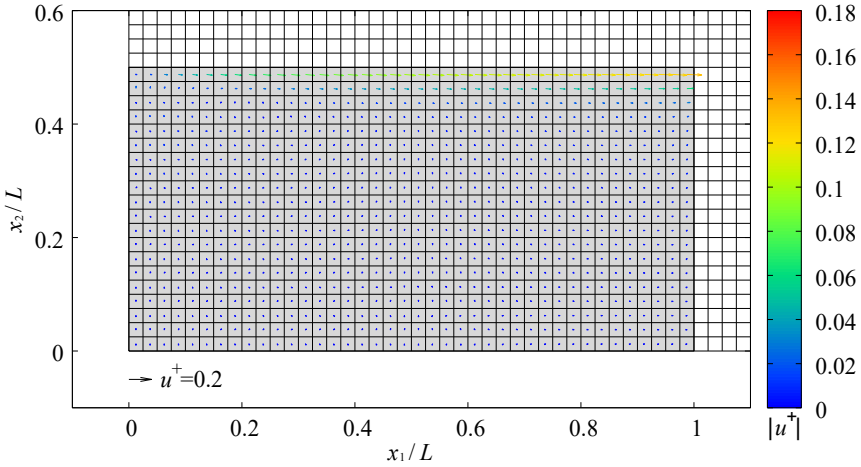

(b) Re=396

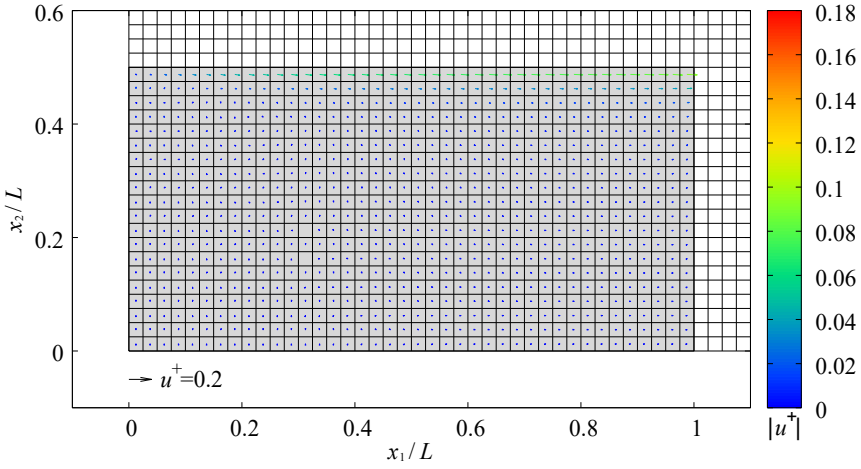

(c) Re=264

Figure 4.6 Computed velocity vector of flow in porous step (Da=1.0×10^{-3}).

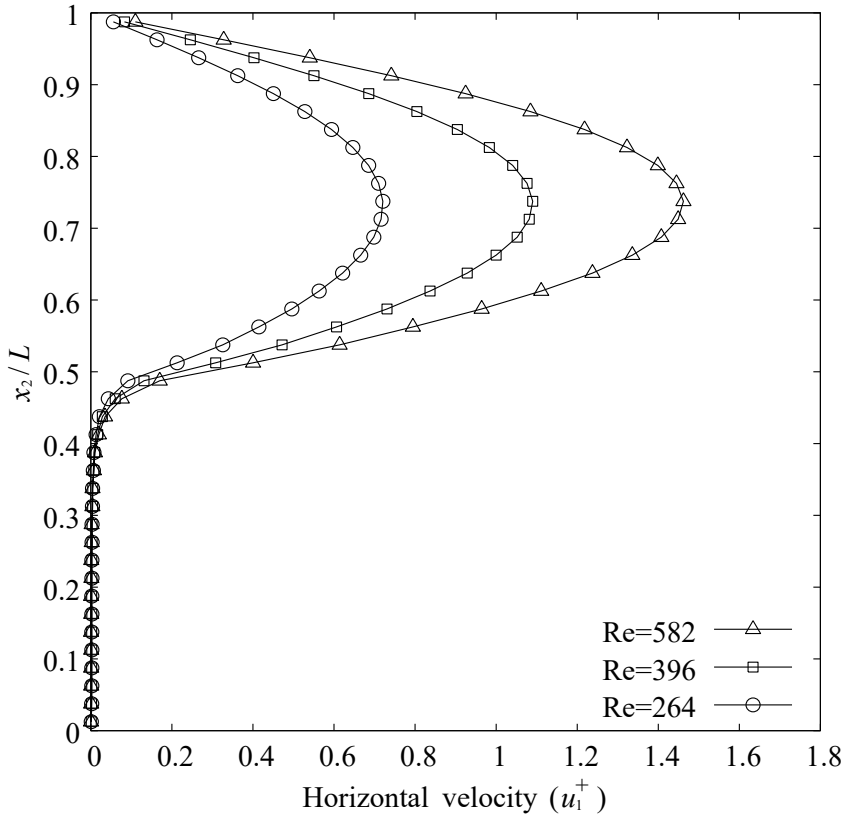

Figure 4.7 Distribution of velocity at vertical lines of x_1/L=1.0 (Da=1.0×10^{-3}).

Figure 4.8 shows the relationship between the Reynolds number and the position of the reattachment point in two cases; one has the porous step (Da=1.0×10^{-3}) and the other is the regular backward-facing step flow with an impermeable step. The reattachment points computed in the two cases become closer to the step as the Reynolds number decreases, and the results are consistent with Kim and Moin (1985). The surface of the porous media behaves like the wall given the non-slip condition, because the seepage flow velocity around the upper surface is small. These results indicate that the influence of the porous media as the backward-facing step on the position of the reattachment point is small, because the Reynolds number has a dominant influence on the flow in the fluid domain.

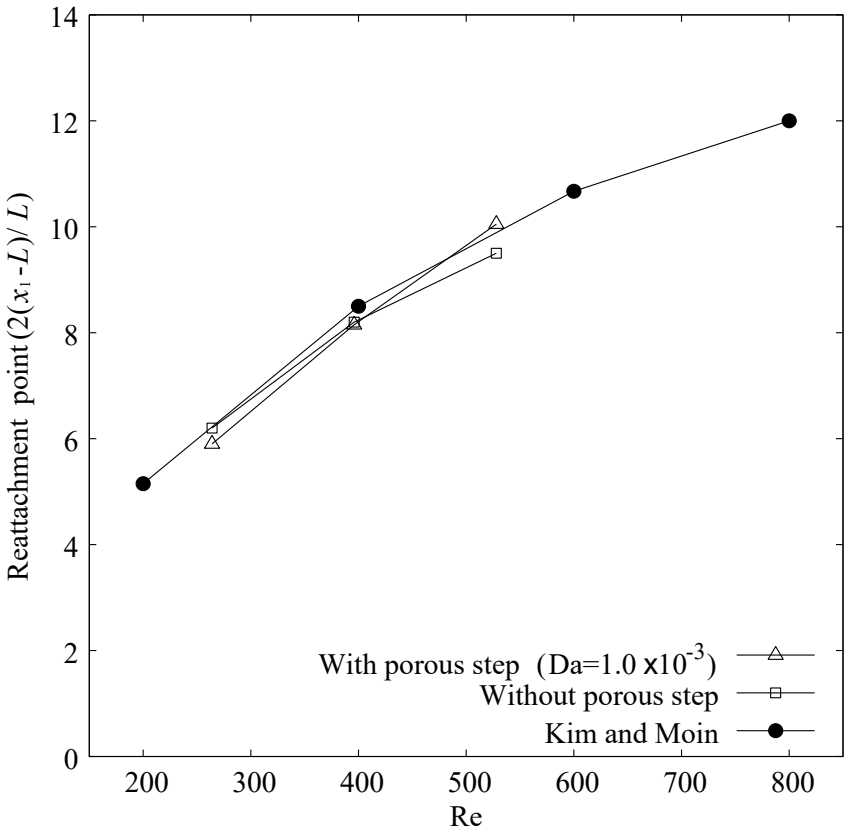

Figure 4.8 Plot of reattachment point using Reynolds number.

4.3.2 Influence of Darcy number

Three different Darcy numbers, namely, 1.0×10^{-11}, 1.0×10^{-7}, and 1.0×10^{-3}, are computed to investigate how the reattachment point changes with the Darcy number for the porous media as the backward-facing step. The Reynolds number is fixed at 528 in all cases.

The velocity distributions at the steady state are shown in Figure 4.9 (a)-(c). The flows in the figures exhibit separation bubbles after the porous steps as is usually seen in the backward-facing step flow, as shown in Figure 4.5(a). The patterns for the Navier-Stokes flow do not change when the Darcy number changes.

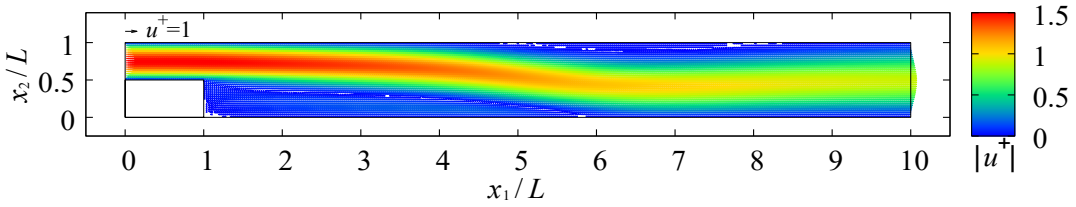

(a) Da=1.0×10^{-11}

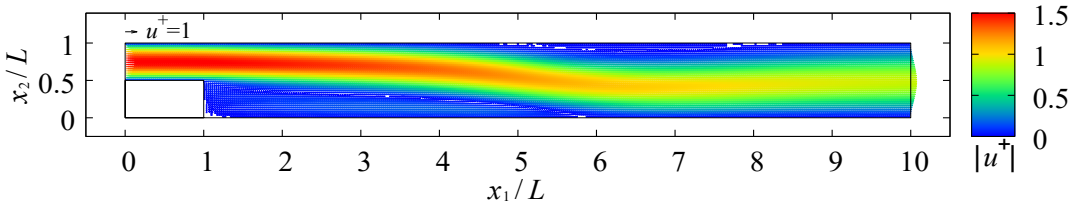

(b) Da=1.0×10^{-7}

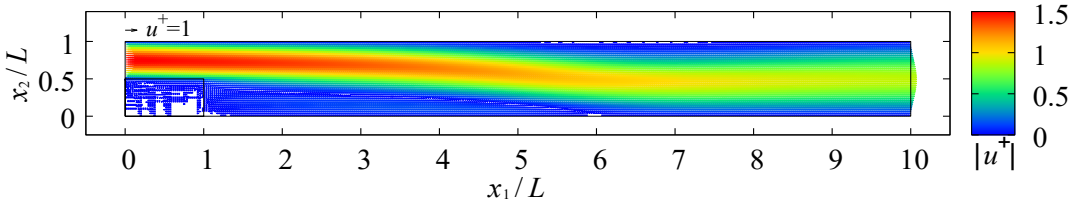

(c) Da=1.0×10^{-3}

Figure 4.9 Computed velocity vector of flow (Re=528).

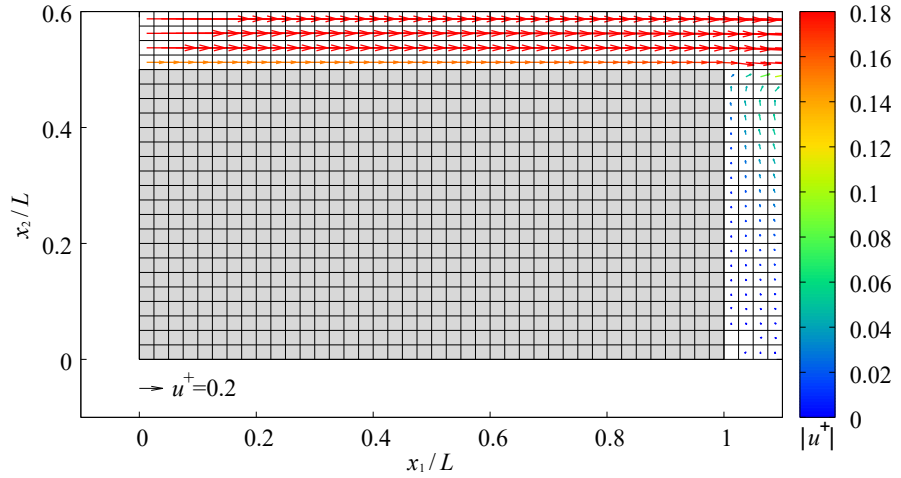

(a) Da=1.0×10^{-11}

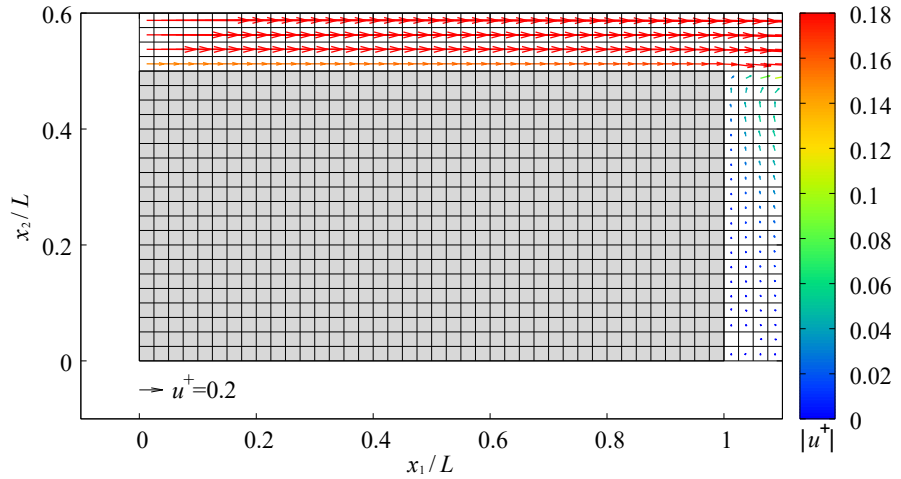

(b) Da=1.0×10^{-7}

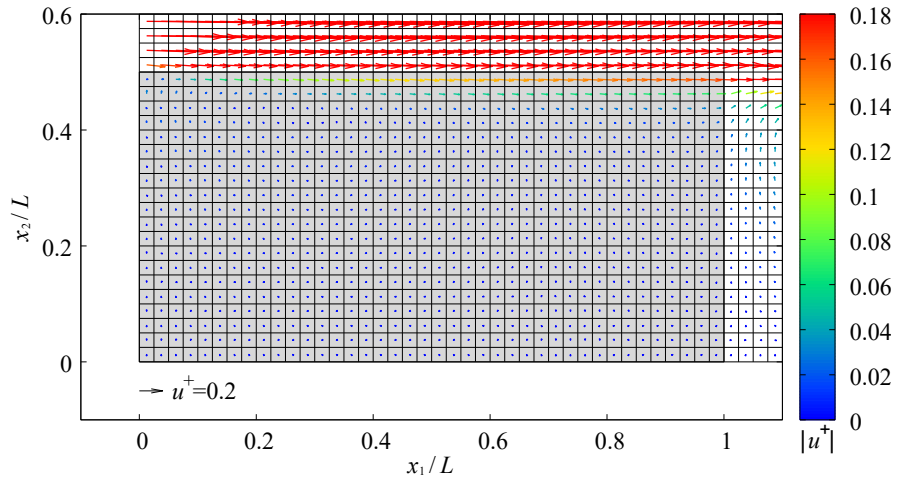

(c) Da=1.0×10^{-3}

Figure 4.10 Computed velocity vector of flow in porous step (Re=528).

Figure 4.11 shows the relationship between the Darcy number and the position of reattachment point. In this figure, the reattachment points do not significantly change even if the Darcy number varies from 1.0×10^{-11} to 1.0×10^{-3}. This is because the velocity in the porous medium is even smaller than that in the fluid domain, as shown in Figure 4.12. However, in the case of $Da=1.0\times10^{-3}$, the profile for the flow velocity at the edge of the step diverts from the Hagen-Poiseuille flow (See Figure 4.12), and the reattachment point moves slightly further from the step.

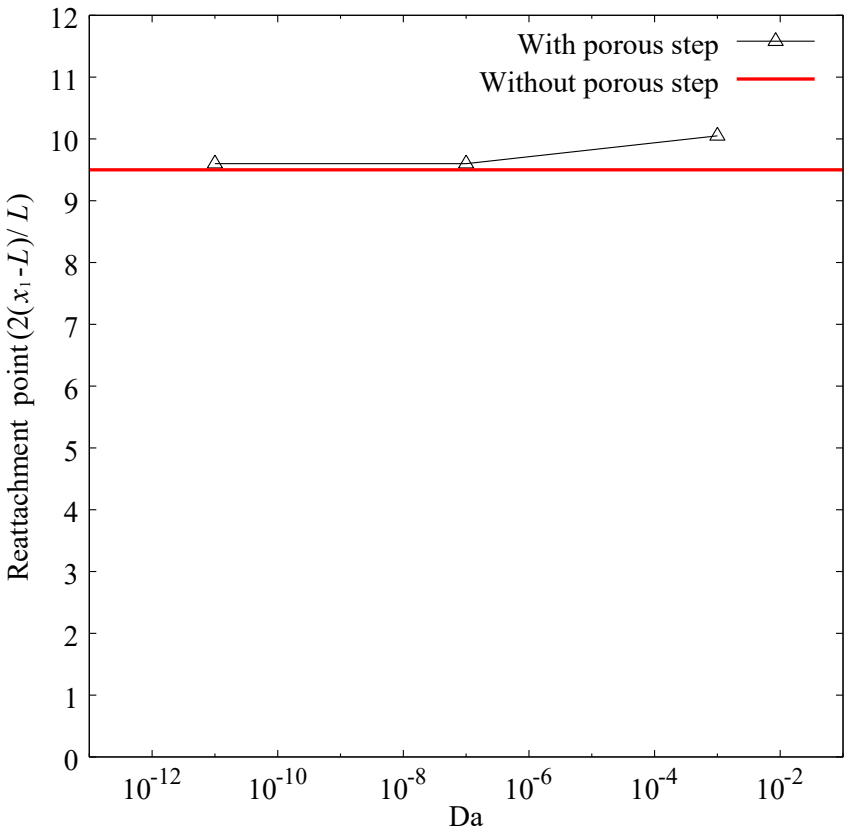

Figure 4.11 Plot of reattachment point using Darcy number (Re=528).

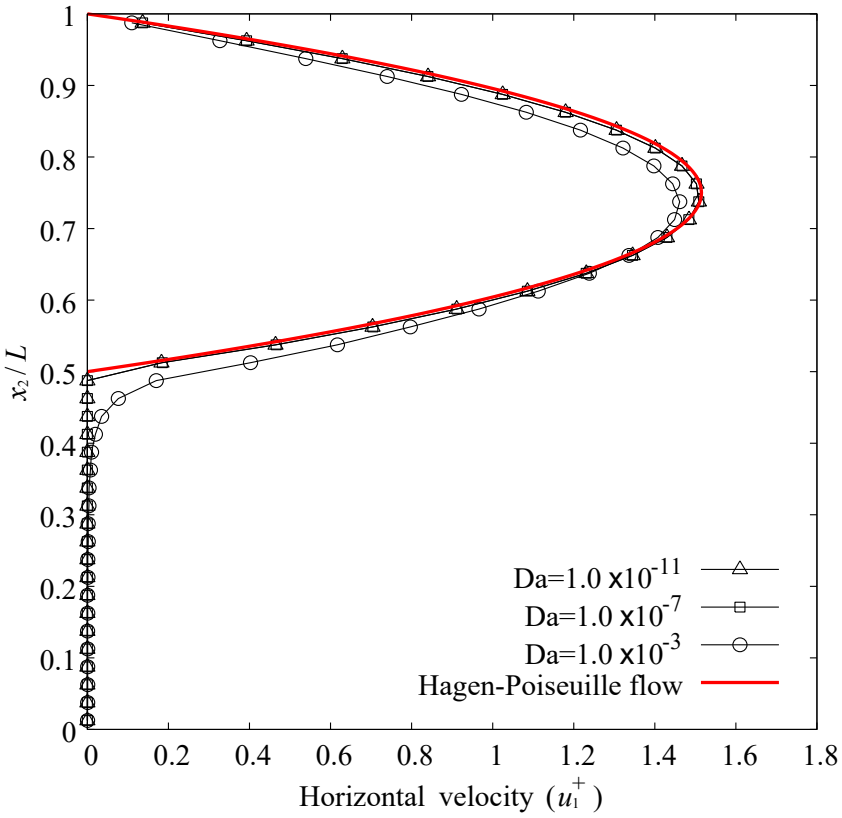

Figure 4.12 Distribution of velocity at vertical lines of x_1/L=1.0 (Re=528).

4.4 Conclusions

The numerical method presented in **Chapter 2** was applied to the backward-facing step flow with a porous step. And the influence of the Reynolds and the Darcy numbers on the position of the reattachment point has been investigated. The results are summarized as follows.

1. The flows in all cases exhibit separation bubbles after the porous step as is usually seen in the backward-facing step flow.

2. The reattachment point gets closer to the step as the Reynolds number decreases, and the results are consistent with those of Kim and Moin (1985).

3. The reattachment point does not significantly change even if the Darcy number changes. However, the reattachment point moves slightly away from the step in the case of $Da=1.0\times10^{-3}$, because the profile for the flow velocity at the edge of the step diverts from the Hagen-Poiseuille flow.

5 Seepage flow within and around closed void

A uniform velocity field is obtained in the rectangular domain filled with porous media when there is a gap in pressure on both sides of the domain. However, the velocity field does not become uniform if the void in the domain is only filled with water. The flow in the void described by the Navier-Stokes equations is different from the flow in porous media, and both flows influence each other. In this chapter, the influence of the void shape on the flow in the Reynolds and the Darcy domains is investigated.

5.1 Introduction

Seepage water flows from the high pressure point to the low pressure point when there is a gap in pressure at different points in the porous media. This is the well-known Darcy's law. A rectangular domain filled with porous media, called the Darcy domain, is assumed. The top and bottom walls are under free slip boundary conditions. When higher pressure than the right side is given to the left side, the seepage water flows from the left side to the right side. Then, the velocity is distributed at a constant value all over the domain, and the pressure decreases linearly from the left side to the right side. As this problem was constructed only with porous media, the flow in the Darcy domain depends on the inflow velocity and the permeability of the porous media. Next, a domain which has a void filled only with water is assumed. The water flows into or out of the void through the interface between the void and the Darcy domain. The behavior of the water in the void is described by the Navier-Stokes equations. The flow of water through the void depends on the shape of the void and the inflow/outflow on the boundary.

The flow in a domain which has a void depends on the velocity on the inflow boundary, the permeability of the porous media, and the shape of the void. In this chapter, the Darcy domain which has a void is computed with various Reynolds numbers, Darcy numbers, and void shapes in order to investigate the influence of these factors on the flow in the domain. The Reynolds and the Darcy numbers are controlled by the inflow velocity and the permeability of the porous media, respectively.

5.2 Geometry and initial / boundary conditions

Figure 5.1 shows the geometry and the boundary conditions of this problem. The computation was carried out in the rectangular domain. The domain was assumed to be filled with porous media, such as soil, and the void is located around the center of the computational domain. Three different void sizes are prepared, as seen in Table 5.1. Several cases for different values of the Reynolds and the Darcy numbers are computed. The porosity is assumed to be 0.40. Uniform inflow velocity is given to the left side of the computational domain, while the free outflow boundary condition is given to the right side of it. The Reynolds and the Darcy numbers are controlled by the inflow velocity from the left side and the hydraulic conductivity of the porous media. The Reynolds number is selected from the range wherein laminar flows can be achieved in the void. The Reynolds number is defined as follows:

$$\mathrm{Re} = \frac{U_{\mathrm{in}} L}{\nu} \tag{5.1}$$

where U_{in} is the velocity on the inflow boundary and L is the representative length of the domain (See Figure 5.1). Both the upper and the lower sides have the free-slip boundary condition. Assuming the flow velocity and the pressure to be zero as the initial conditions, the numerical computation is carried out until the flow field reaches the steady state. The finite volume cells used in the numerical computation are shown in Figure 5.2.

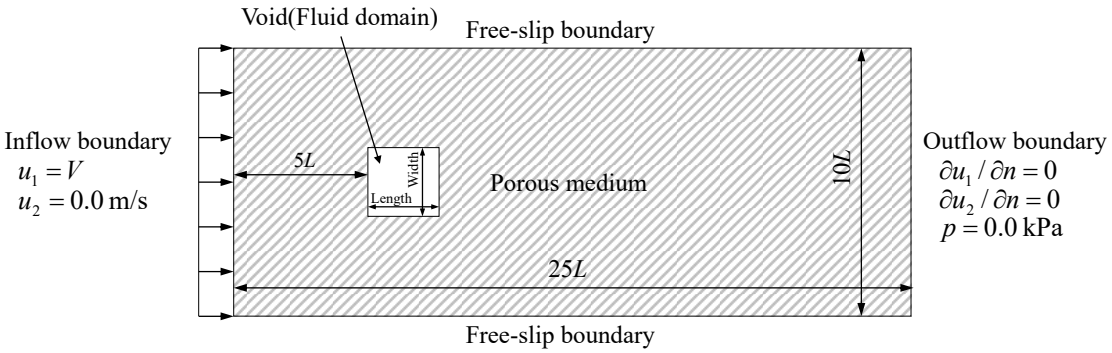

Figure 5.1 Geometry and boundary conditions.

Table 5.1 Size and aspect ratios of voids.

Length	Width	Aspect ratio (=Length/Width)
4*L*	*L*	4.0
2*L*	2*L*	1.0
L	4*L*	0.25

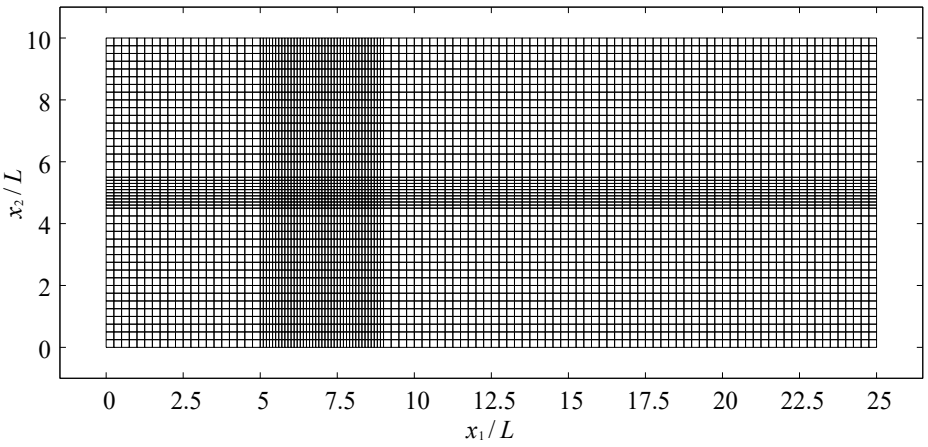

(a) Aspect ratio=4.0

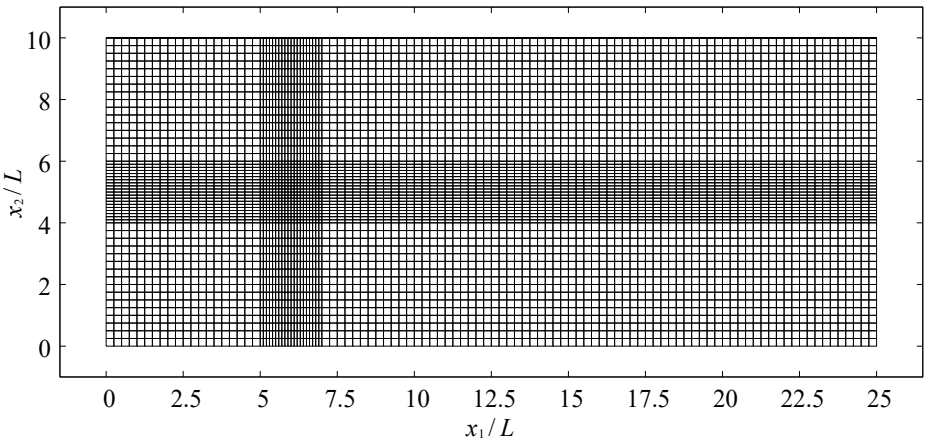

(b) Aspect ratio=1.0

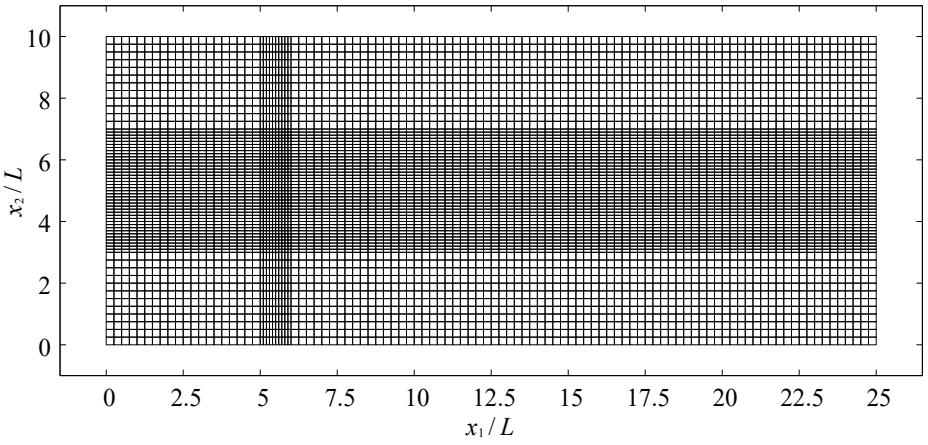

(c) Aspect ratio=0.25

Figure 5.2 Computational finite volume cells.

5.3 Results and discussion

5.3.1 Influence of shape of void on flow

Three different void shapes, seen in Table 5.1, are computed to investigate how the flow in and around the void changes with the shape of the void. Figure 5.3 shows the flow velocity at the steady state. Water accumulates in the void and passes through it. When the aspect ratio is 1.0 or 0.25, seepage water comes into the void from the corners of its left side, and forms two major streams along the upper and lower sides. On the other hand, when the aspect ratio is 4.0, the two streams on the left side of the void immediately combine and form one main steam.

Figure 5.4 shows the distribution of pressure. The span of the pressure contour line means the gradient of pressure. The gradient of pressure is large when the span of the pressure contour line is narrow. The gradient of pressure is small in the void and large on the left and right sides of the void in all three cases. And, it becomes small in the void and large on the left and right sides of the void with increments in the aspect ratio. The pressure decreases linearly from the left side to the right side of the computational domain, and the gradient of pressure becomes uniform in the computational domain if there is no void. However, the gradient of pressure does not become uniform in this problem due to the void.

The gradient of pressure is generally small in the void because there is no resistance to the flow. Moreover, the period during which the gradient of pressure is small expands with increments in the aspect ratio. On the other hand, the gaps in pressure between the inflow and the outflow boundary are the same because the inflow velocities are fixed in all three cases. Thus, the gradient of pressure becomes large on the left and right sides of the void in order to keep the pressure in balance at the inflow and outflow boundaries.

The pressure contour line and the upper and lower surfaces of the void cross at an almost right angle when the aspect ratio is 0.25; however, they cross diagonally when the aspect ratio is 4.0. According to Darcy's law, seepage water flows from high pressure to low pressure. This means that the seepage water flows at a right angle for the pressure contour line. Thus, Figure 5.4 indicates that the seepage water around the upper and lower surfaces of the void flows along the surface when the aspect ratio is 0.25 and the

inflow/outflow through the upper and lower surfaces of the void increases when the aspect ratio is 4.0. These tendencies in the flow are in good agreement with the flow velocity vector, shown in Figure 5.3, and indicate that the shape of the void has a strong influence on the flow in the fluid and the Darcy domains.

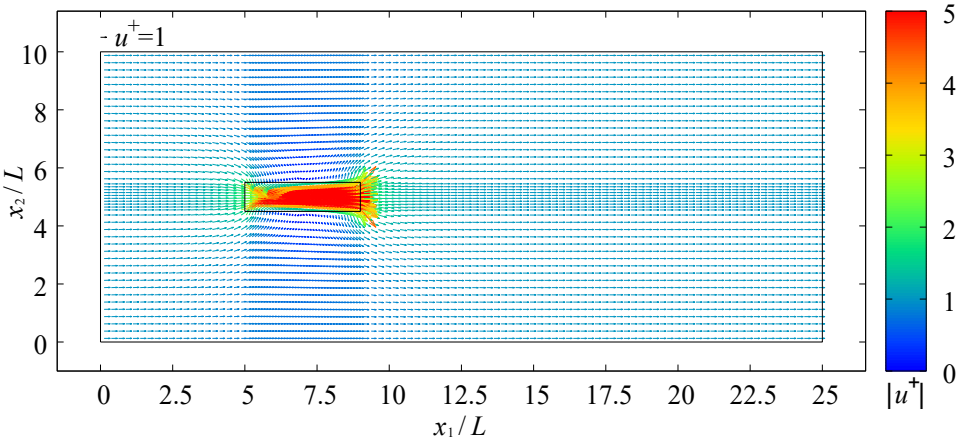

(a) Aspect ratio=4.0

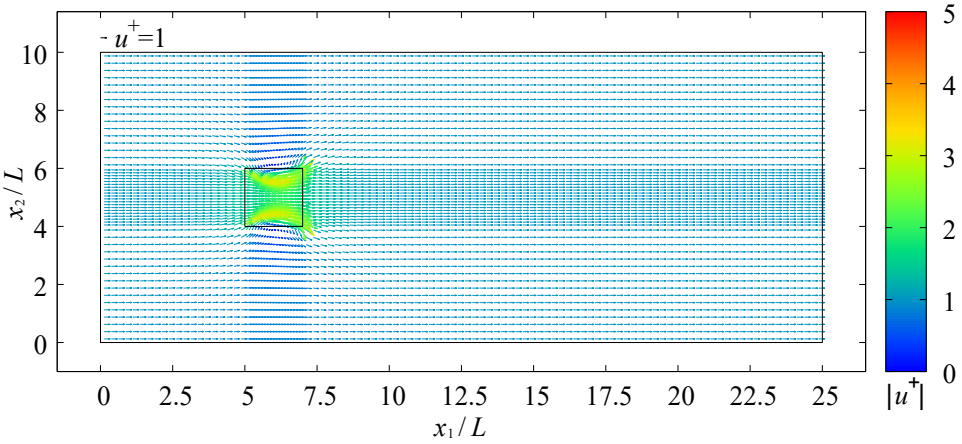

(b) Aspect ratio=1.0

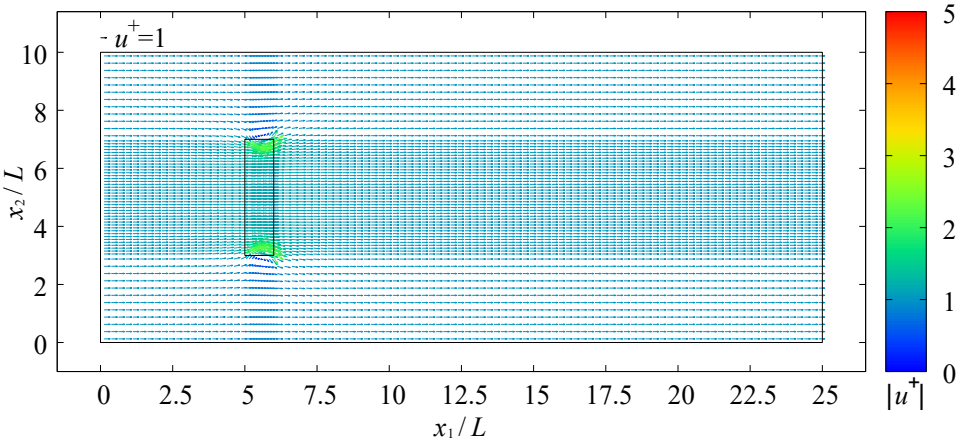

(c) Aspect ratio=0.25

Figure 5.3 Computed velocity vector of flow (Re=30, Da=2.5×10^{-8}).

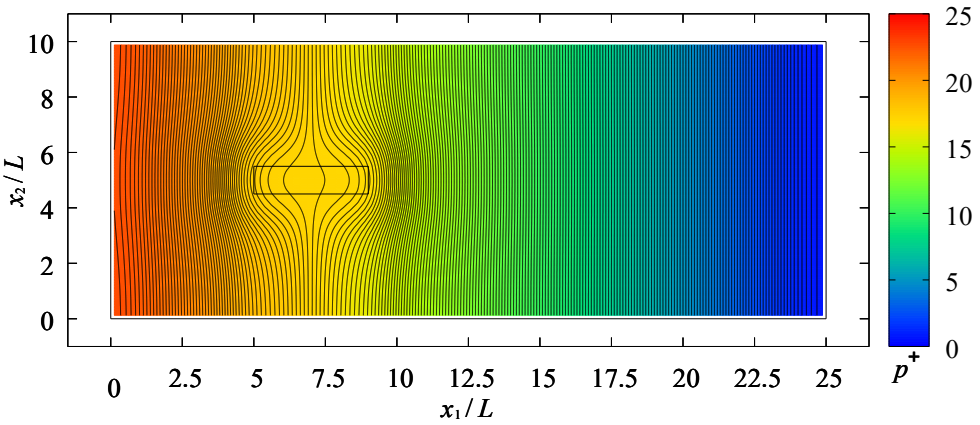

(a) Aspect ratio=4.0

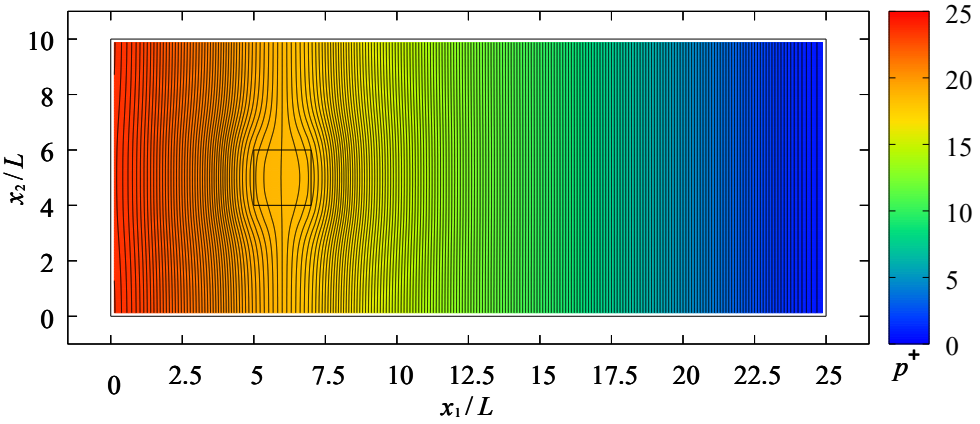

(b) Aspect ratio=1.0

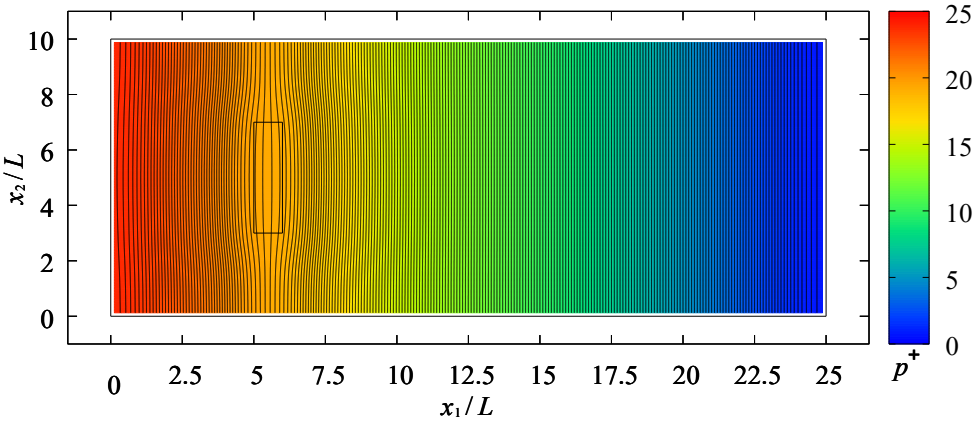

(c) Aspect ratio=0.25

Figure 5.4 Distribution of pressure (Re=30, Da=2.5×10^{-8}).

Figure 5.5 shows the distribution of horizontal flow velocity at the central cross section of the void. The velocity distribution for an aspect ratio of 4.0 is almost parabolic. Moreover, the tangential velocity at the interface between the porous media and the void become small in all three cases, because the pressure in the void does not change significantly and the interface behaves as a constant pressure line.

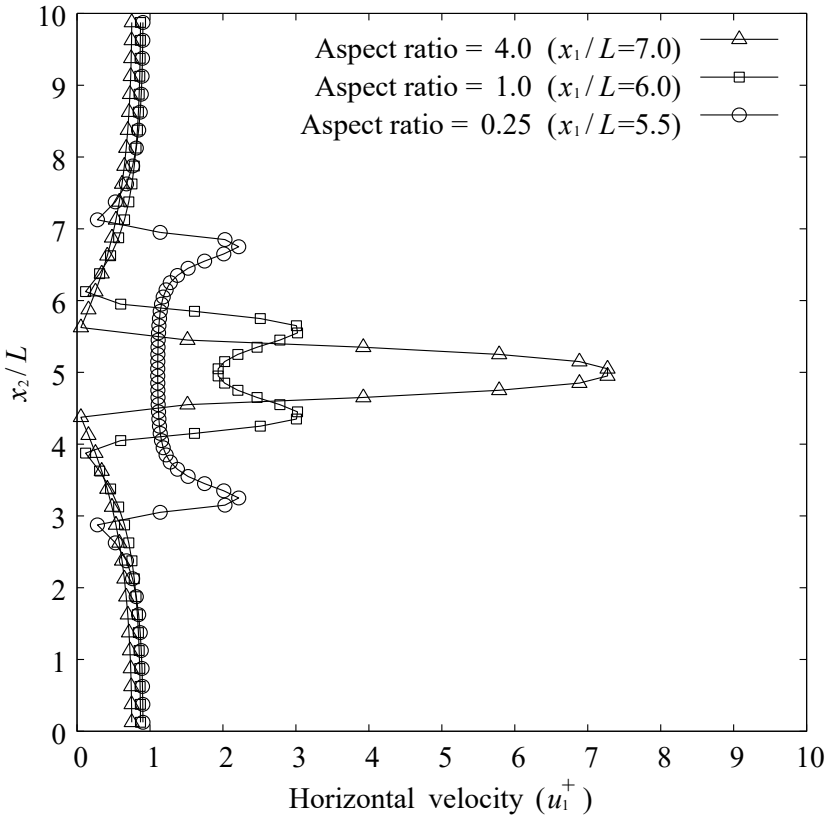

Figure 5.5 Distribution of horizontal velocity at center of void (Re=30, Da=2.5×10^{-8}).

Figure 5.6 shows the distribution of horizontal velocity at the different cross sections of the void when the aspect ratio is 4.0. It can be seen that the velocity quickly approaches a parabolic shape, although it is not parabolic at all on the left side of the void.

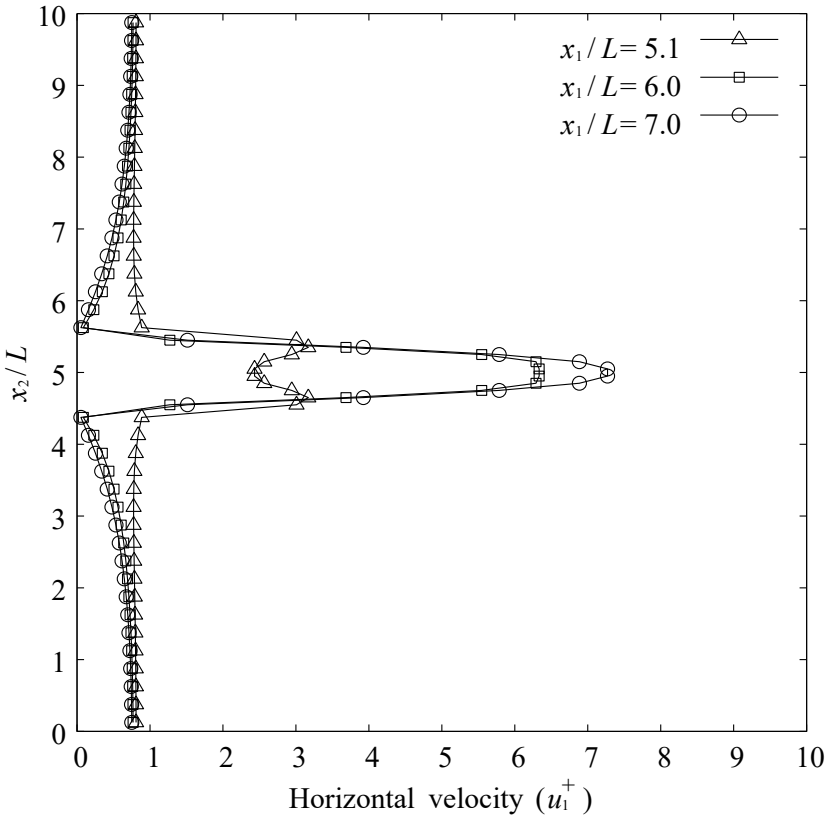

Figure 5.6 Distribution of horizontal velocity at x_1/L=5.1, 6.0, and 7.0 (Aspect ratio=4.0, Re=30, Da=2.5×10^{-8}).

Figure 5.7 shows the relationship between the maximum velocity in the void and the aspect ratio. The maximum velocity increases with an increase in the aspect ratio. The shape of a void in porous media has a strong influence on the flow through it. When the shape of the void is short and wide in the flow direction, the seepage water comes into the void from the corners of its upstream side, and forms two major streams along the upper and lower sides. On the other hand, when the shape is long and narrow in the flow direction, the two streams in the upstream side combine immediately and develop into one main stream.

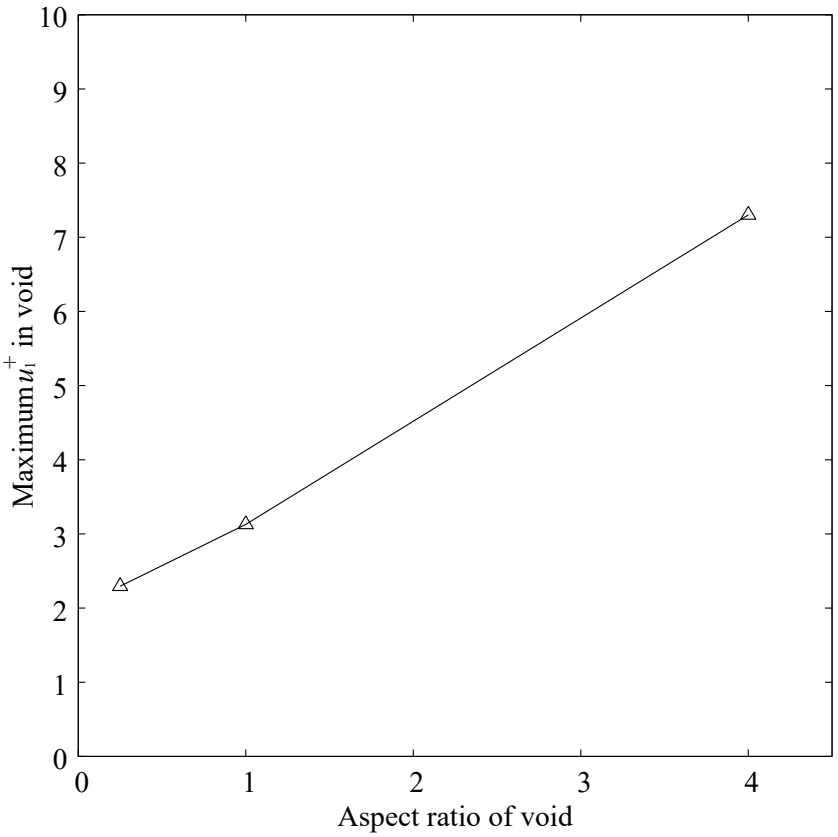

Figure 5.7 Plot of maximum velocity using aspect ratio (Re=30, Da=2.5×10^{-8}).

5.3.2 Influence of Reynolds number

Three different Reynolds numbers, namely, 10, 20, and 30, were computed to investigate the influence of the Reynolds number on the flow within and around the void. The Darcy number was fixed at 2.5×10^{-8} in all cases.

The velocity distributions at the steady state are shown in Figures 5.8 to 5.10. The velocities in the Darcy domain decrease with a reduction in the Reynolds number with all aspect ratios. In this problem, the Reynolds number is controlled by the inflow velocity; therefore, a reduction in the Reynolds number decreases the inflow velocity. The velocities in the void also decrease in the same way as the velocities in the Darcy domain because the velocities around the void decrease due to the reduction in the Reynolds number. One major stream is formed in the void for all Reynolds numbers when the aspect ratio is 4.0, and two major streams along the upper and lower sides are formed for all Reynolds numbers when the aspect ratio is 1.0 or 0.25. The patterns of the flow in the void do not change even if the Reynolds number is changed.

Figures 5.11 to 5.13 show the distribution of pressure. None of the patterns for any of the contour lines of the Reynolds numbers change even if the Reynolds number is changed. This means that the stream line does not change because the flow of seepage water is at a right angle of the pressure contour line. These results match the velocity distribution shown in Figures 5.8 to 5.10.

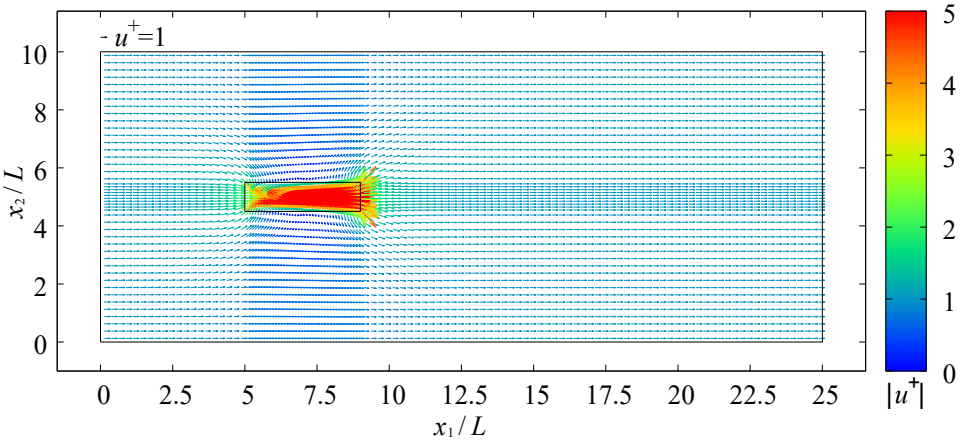

(a) Re=30

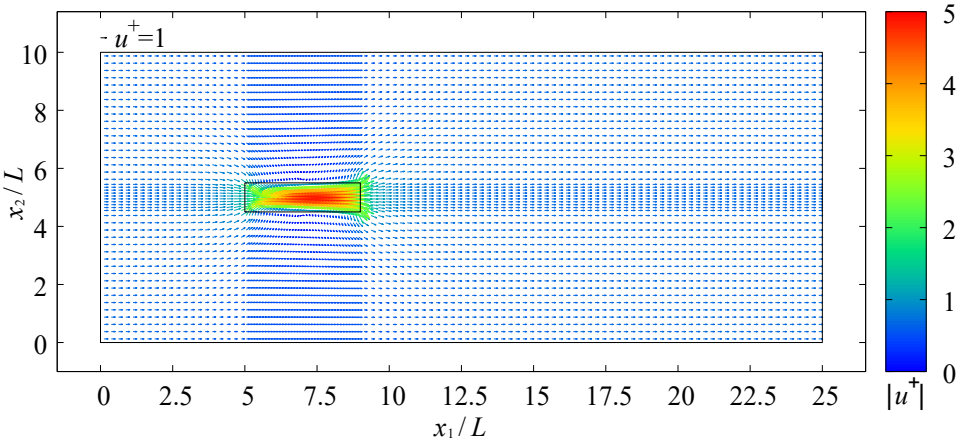

(b) Re=20

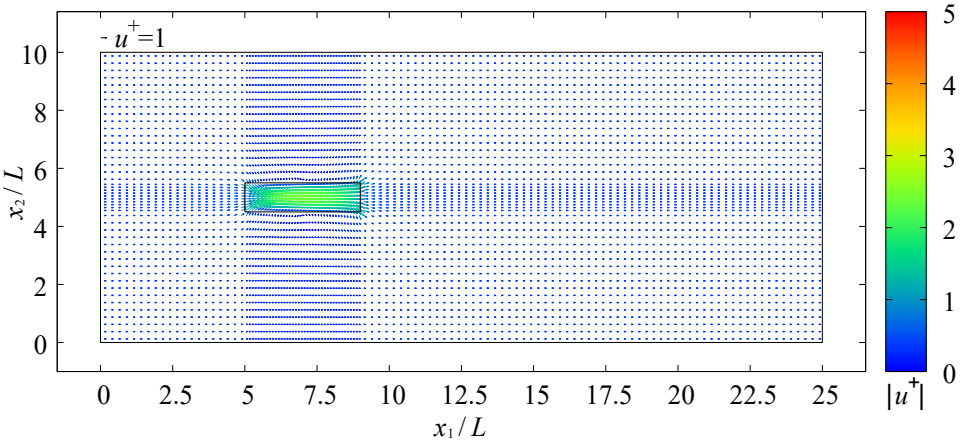

(c) Re=10

Figure 5.8 Computed velocity vector of flow (Aspect ratio=4.0, Da=2.5×10^{-8}).

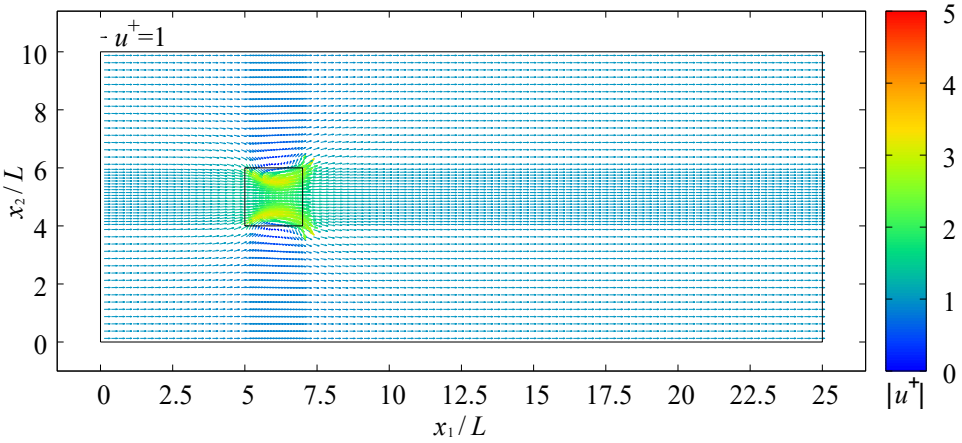

(a) Re=30

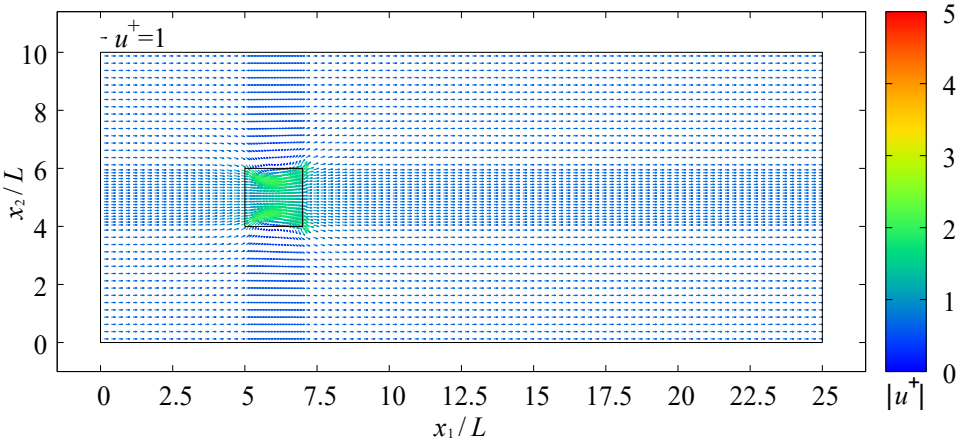

(b) Re=20

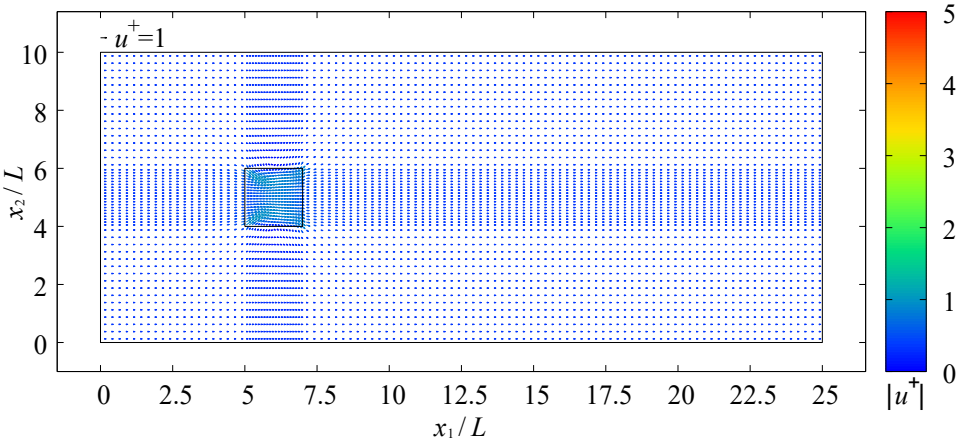

(c) Re=10

Figure 5.9 Computed velocity vector of flow (Aspect ratio=1.0, Da=2.5×10^{-8}).

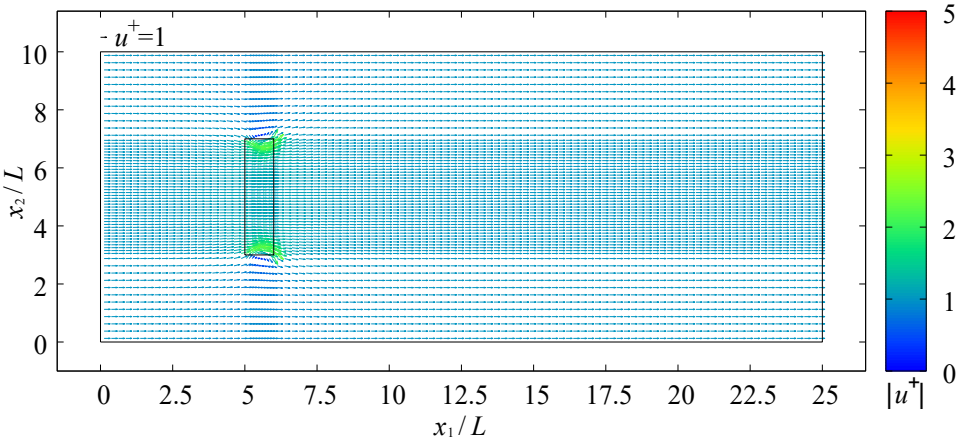

(a) Re=30

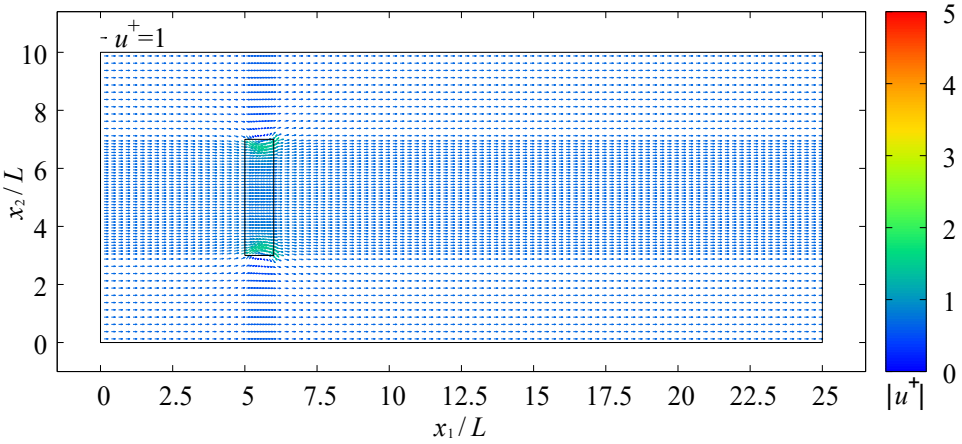

(b) Re=20

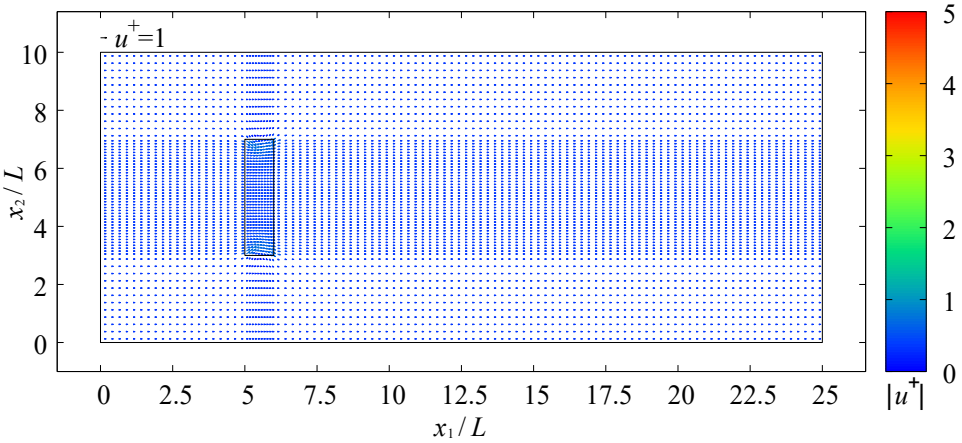

(c) Re=10

Figure 5.10 Computed velocity vector of flow (Aspect ratio=0.25, Da=2.5×10^{-8}).

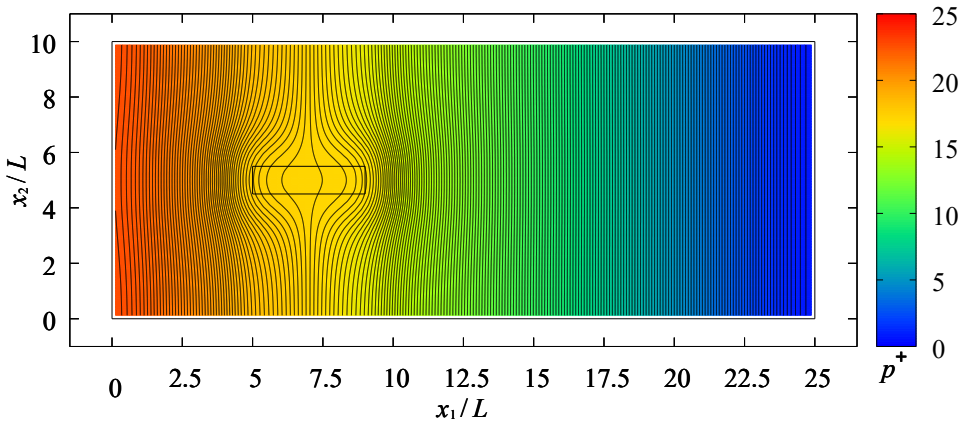

(a) Re=30

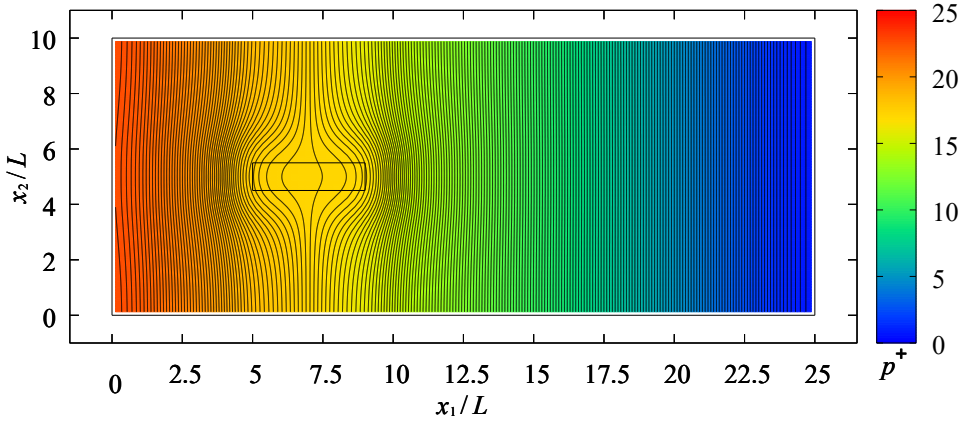

(b) Re=20

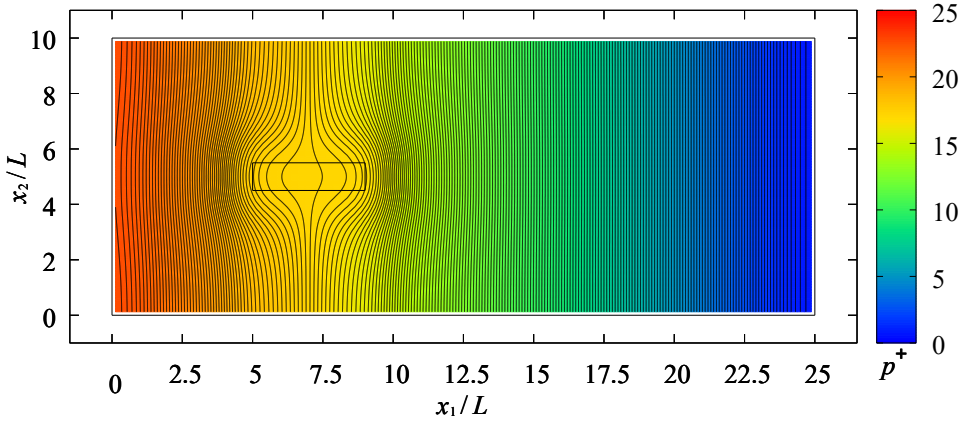

(c) Re=10

Figure 5.11 Distribution of pressure (Aspect ratio=4.0, Da=2.5×10^{-8}).

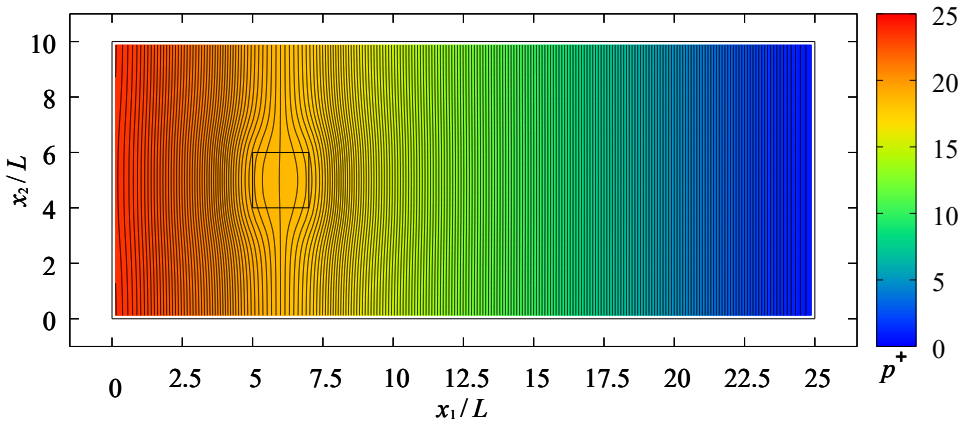

(a) Re=30

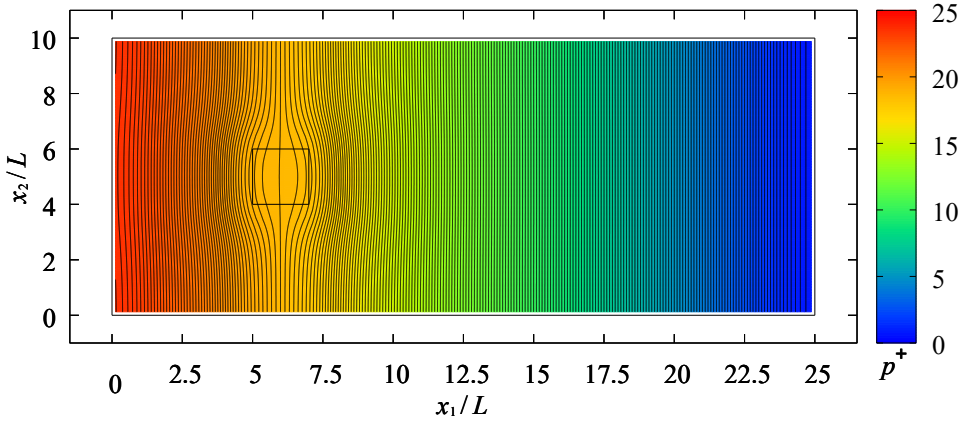

(b) Re=20

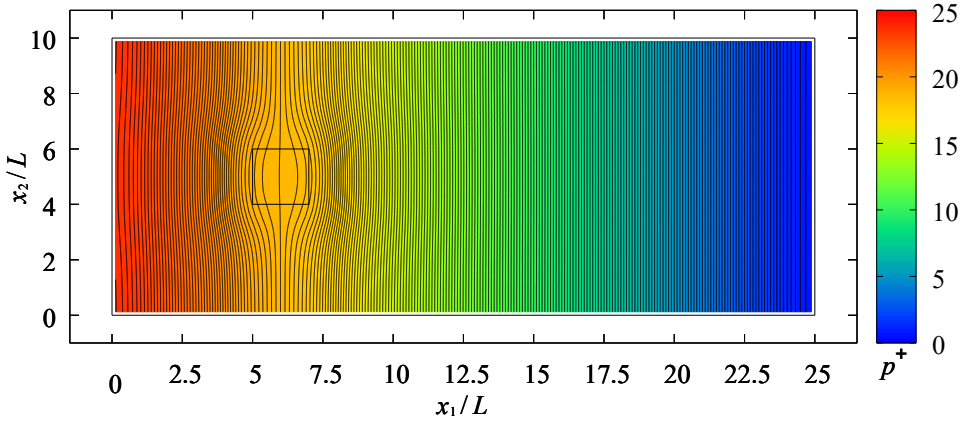

(c) Re=10

Figure 5.12 Distribution of pressure (Aspect ratio=1.0, Da=2.5×10^{-8}).

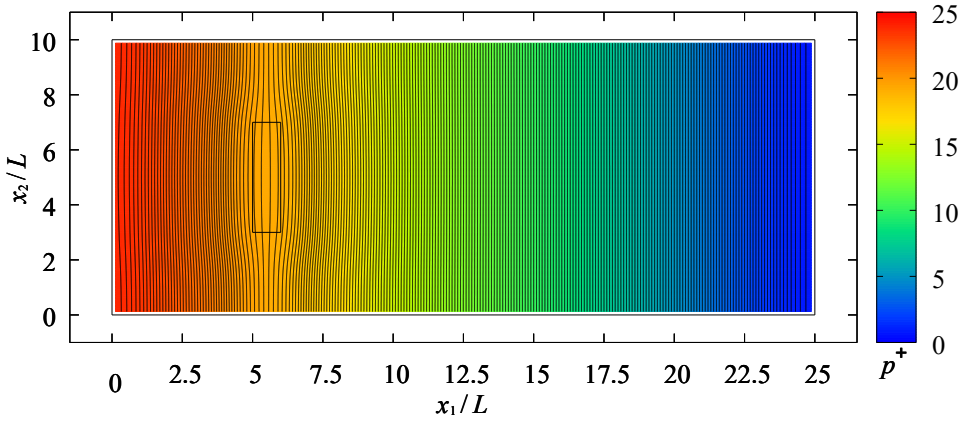

(a) Re=30

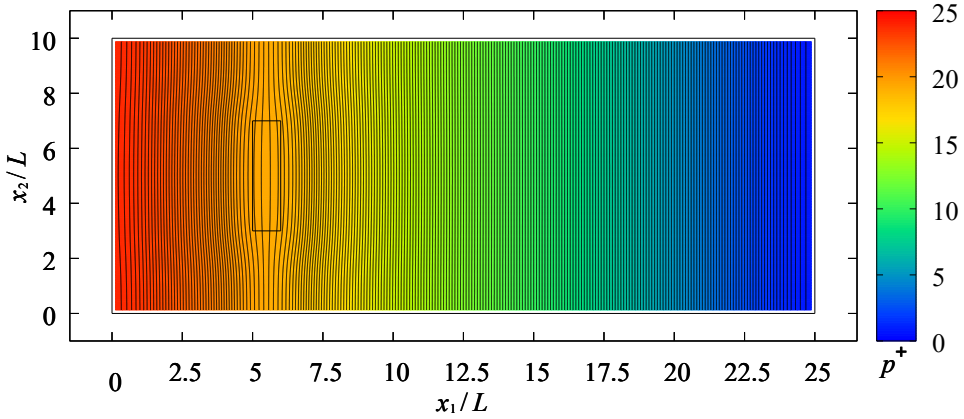

(b) Re=20

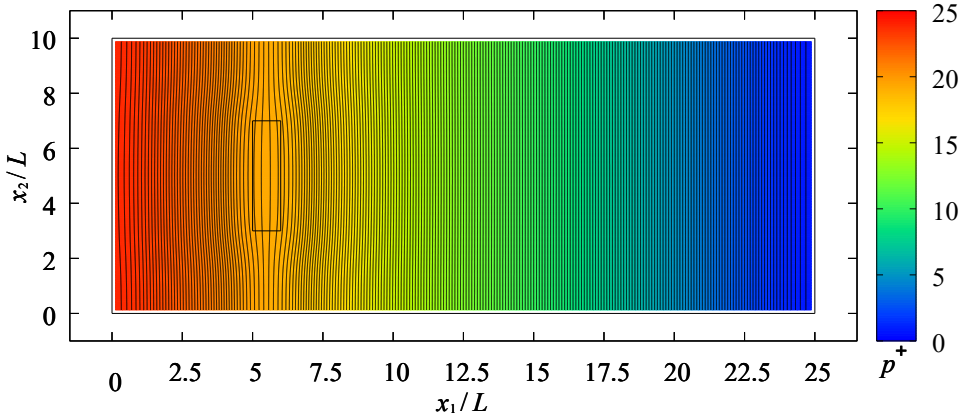

(c) Re=10

Figure 5.13 Distribution of pressure (Aspect ratio=0.25, Da=2.5×10^{-8}).

Figure 5.14 shows the relationship between the Reynolds number and the maximum velocity in the case of Da=2.5×10^{-8}. The maximum velocities increase linearly with an increase in the Reynolds number, because the Reynolds number is controlled by the inflow velocity and the patterns of flow in the void do not change.

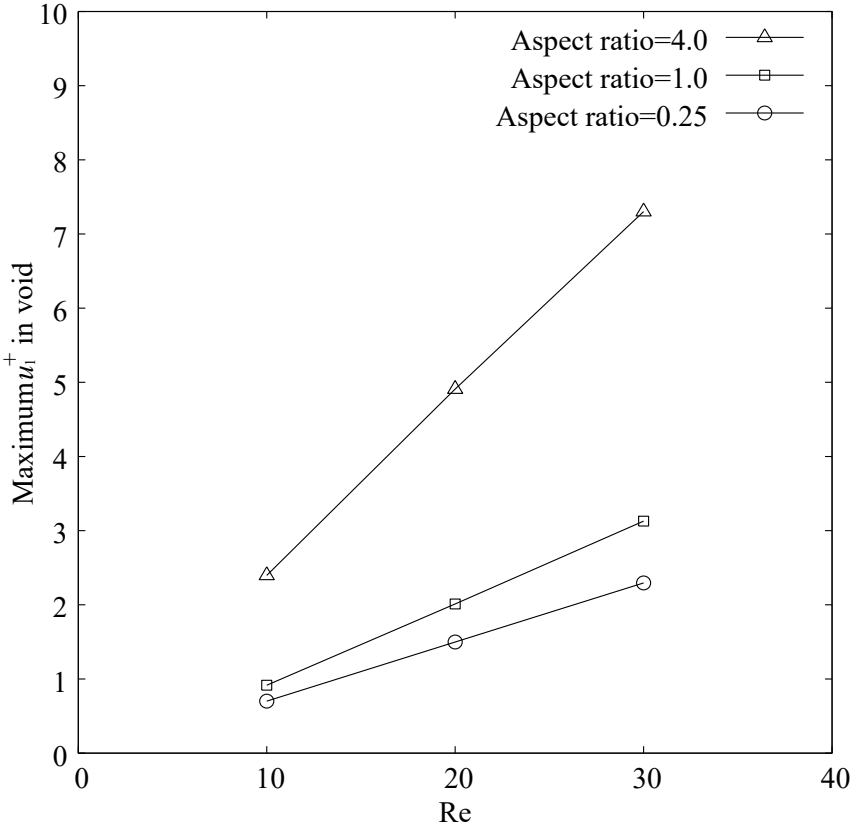

Figure 5.14 Plot of maximum velocity using Reynolds number (Da=2.5×10^{-8}).

5.3.3 Influence of Darcy number

Two different Darcy numbers, 2.5×10^{-8} and 2.5×10^{-4}, were computed to investigate the influence of the Darcy number on the flow within and around the void. The Reynolds number was fixed at 30 in all cases.

The velocity distributions at the steady state are shown in Figures 5.15 to 5.17. The flow velocities only change slightly even if the Darcy number is changed. The inflow velocities are the same in all cases. This is because the Reynolds number, which is controlled by the inflow velocity, is fixed. Therefore, the bulk velocities in the computational domain do not change. Figures 5.15 to 5.17 also exhibit the concentration of seepage water on the left side of the void and the diffusion of it on the right side of the void in all cases. These tendencies are maintained even if the Darcy number is changed. For all Darcy numbers, one major stream is formed in the void when the aspect ratio is 4.0 and two major streams are formed along the upper and lower surfaces of the void when the aspect ratio is 1.0 or 0.25. The flow in the void does not change for any aspect ratios even if the Darcy number is changed. The Darcy number does not have any direct influence on the flow in the void because there is no porous media in the void.

Figures 5.18 to 5.20 show the distribution of pressure at the steady state. The tendency for the gradient of pressure to be large on the left and right sides of the void, and small in the void, is maintained for all aspect ratios. These results indicate that the influence that the Darcy number gives to the flow within and around the void in porous media is small.

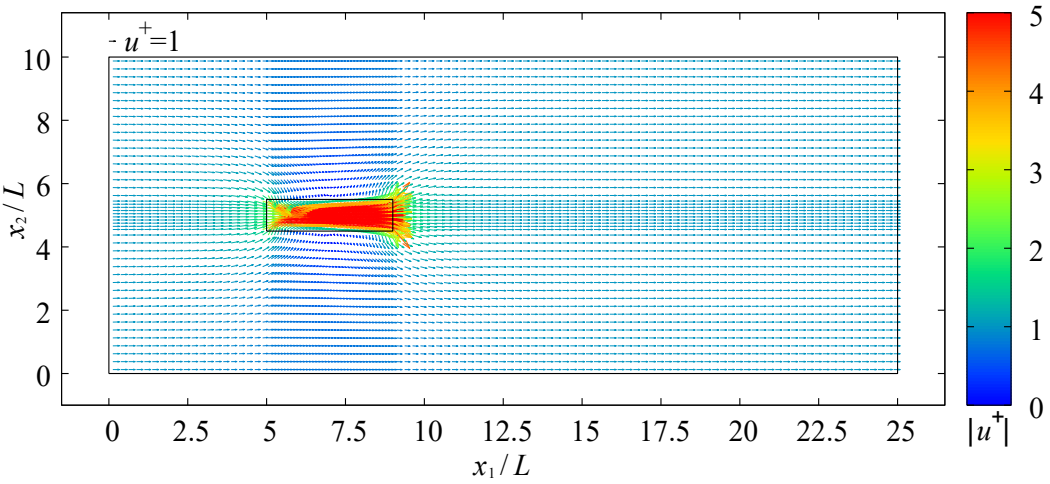

(a) Da=2.5×10^{-8}

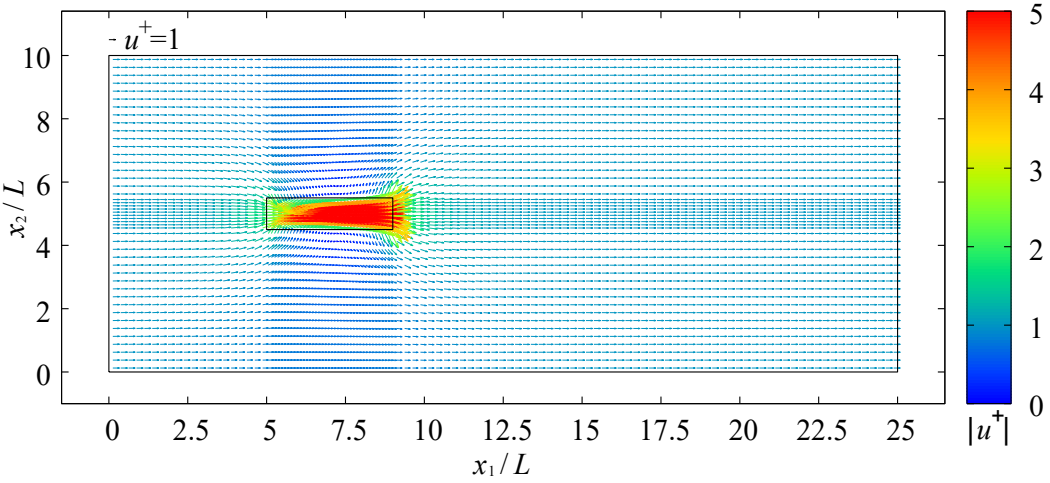

(b) Da=2.5×10^{-4}

Figure 5.15 Computed velocity vector of flow (Aspect ratio=4.0, Re=30).

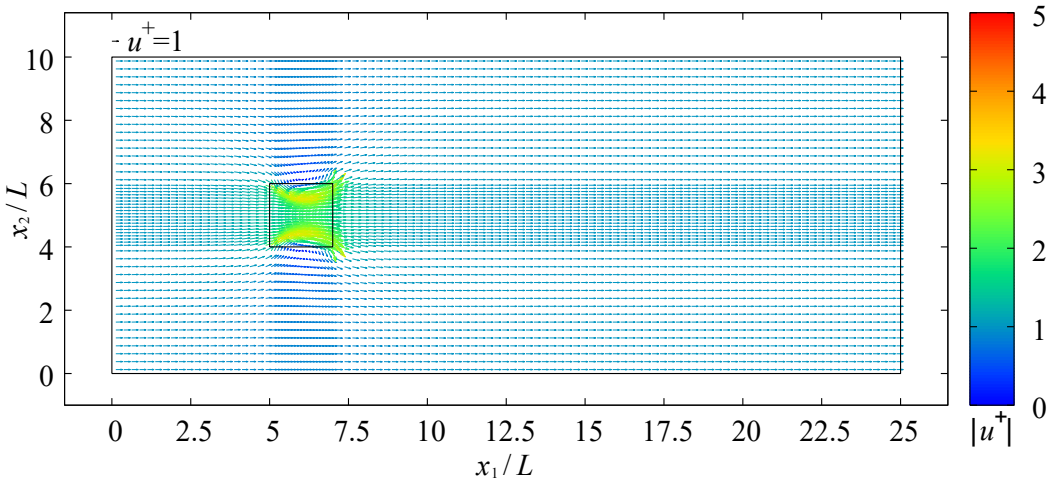

(a) Da=2.5×10^{-8}

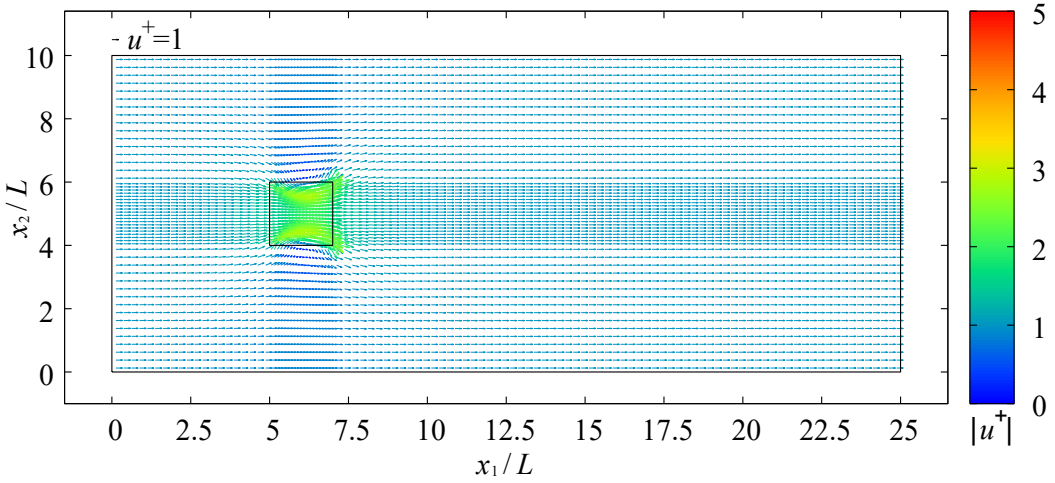

(b) Da=2.5×10^{-4}

Figure 5.16 Computed velocity vector of flow (Aspect ratio=1.0, Re=30).

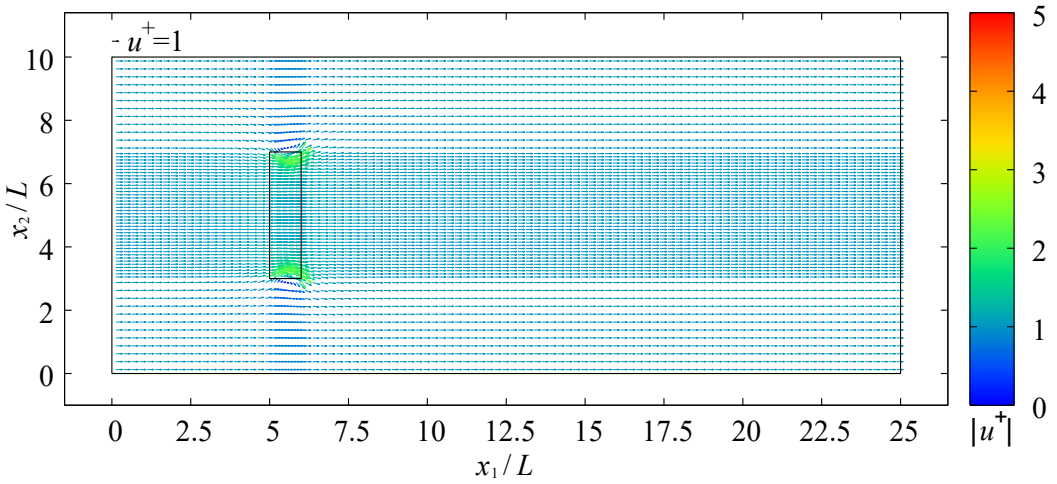

(a) Da=2.5×10^{-8}

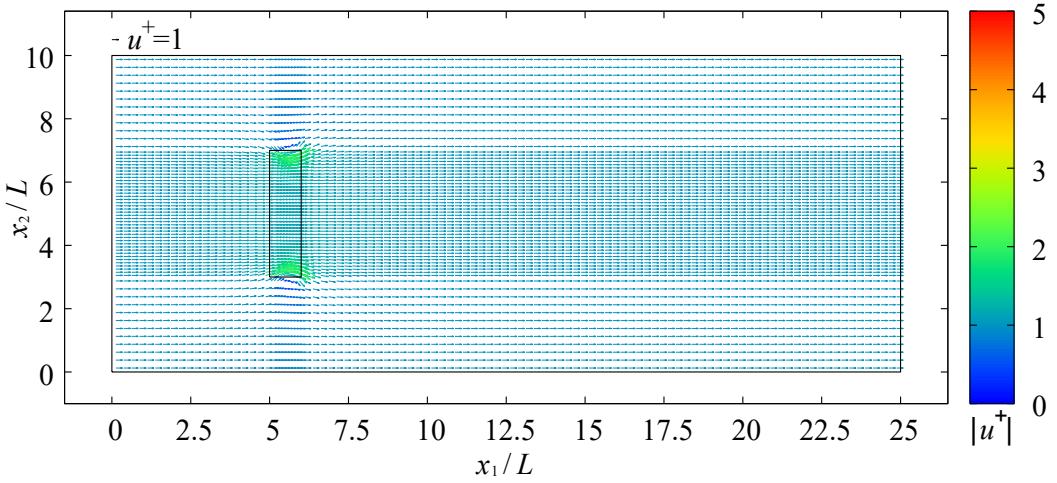

(b) Da=2.5×10^{-4}

Figure 5.17 Computed velocity vector of flow (Aspect ratio=0.25, Re=30).

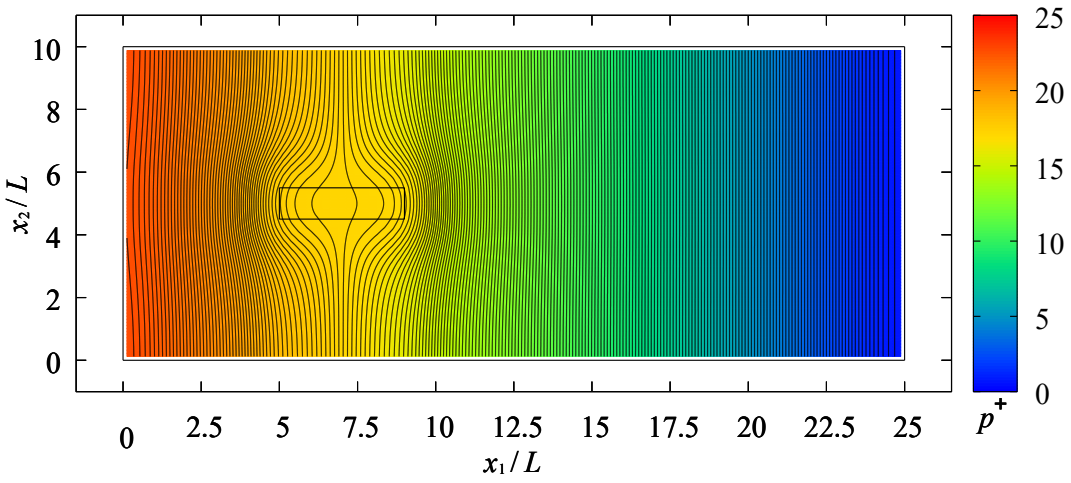

(a) Da=2.5×10^{-8}

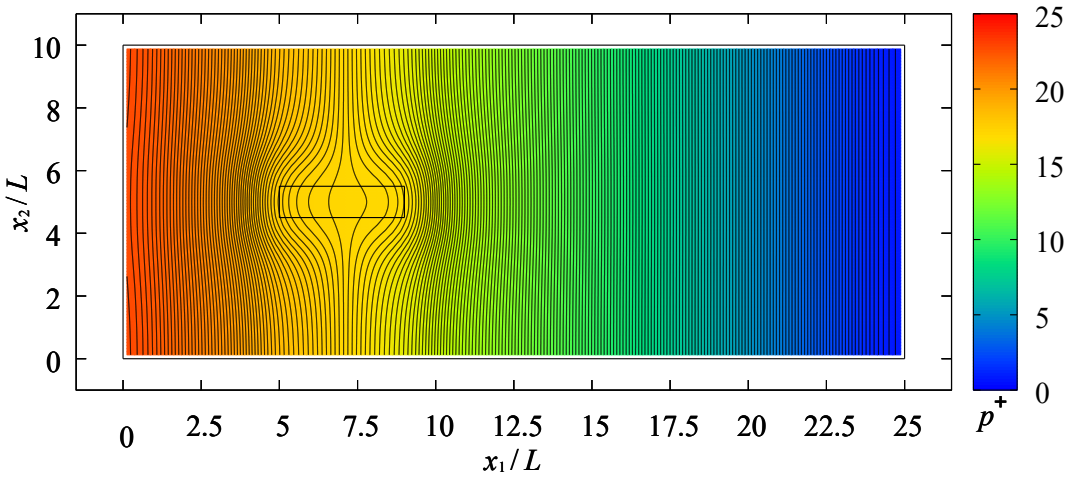

(b) Da=2.5×10^{-4}

Figure 5.18 Distribution of pressure (Aspect ratio=4.0, Re=30).

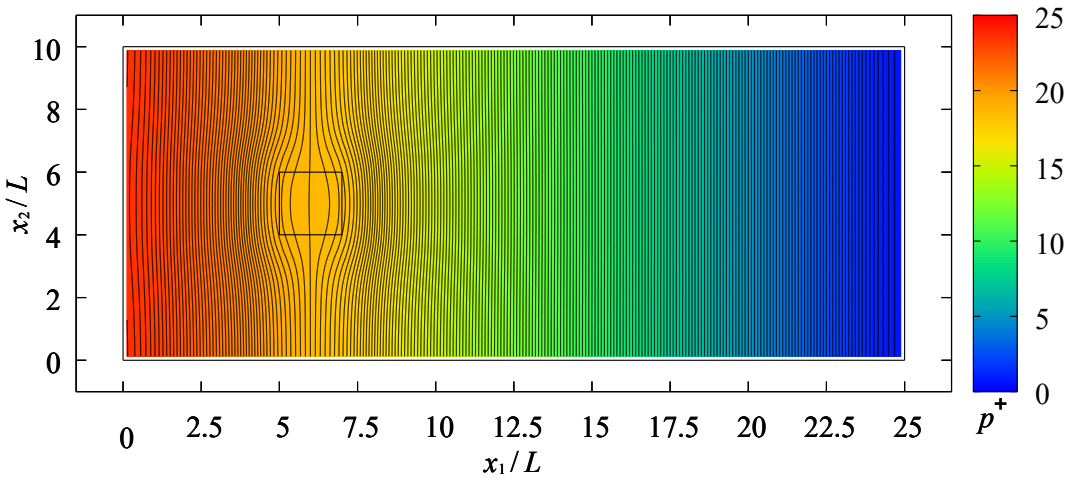

(a) Da=2.5×10^{-8}

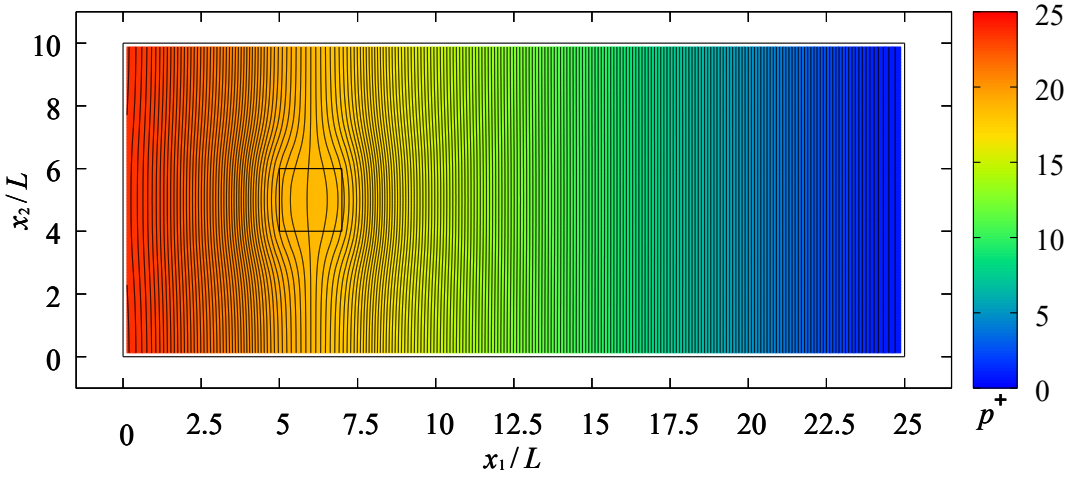

(b) Da=2.5×10^{-4}

Figure 5.19 Distribution of pressure (Aspect ratio=1.0, Re=30).

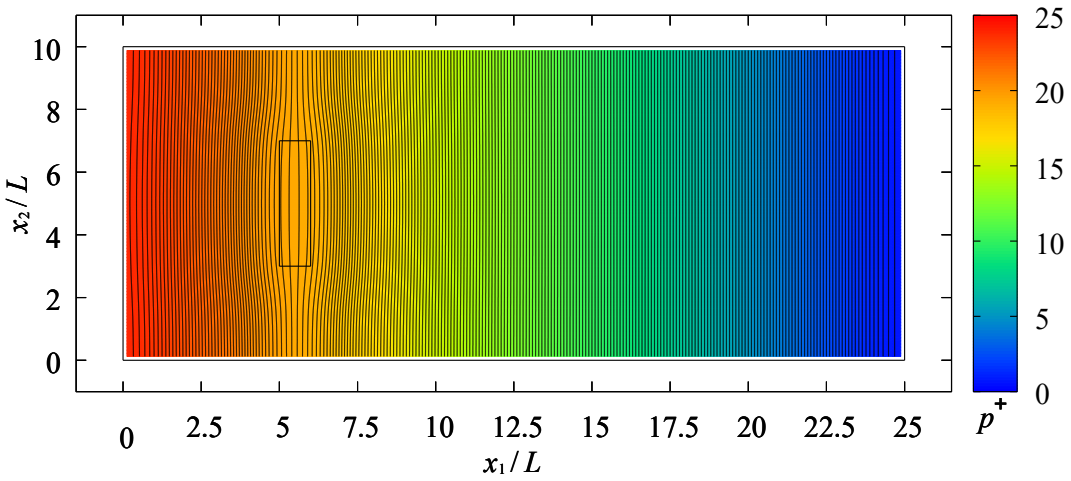

(a) Da=2.5×10^{-8}

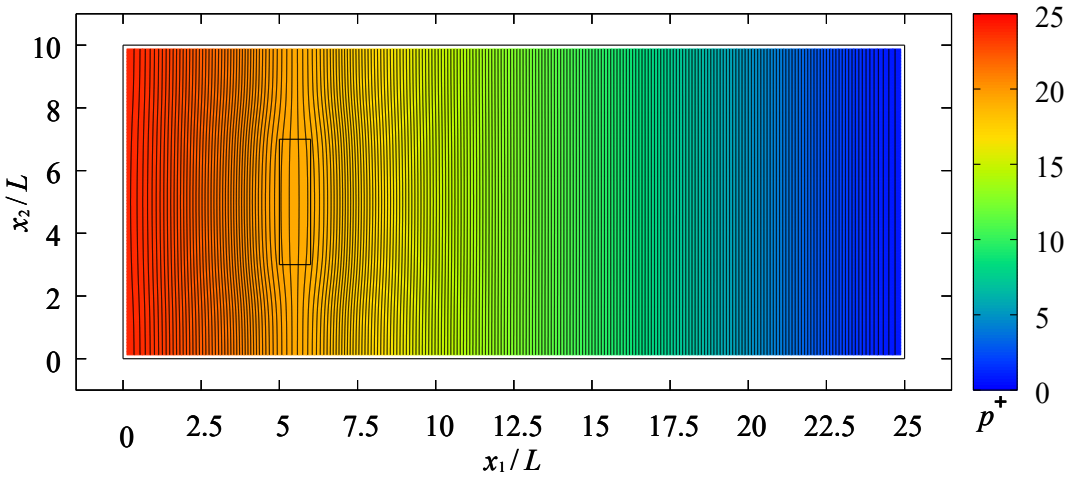

(b) Da=2.5×10^{-4}

Figure 5.20 Distribution of pressure (Aspect ratio=0.25, Re=30).

Figure 5.21 shows the influence of the Darcy number on the maximum velocity. The maximum velocity depends on the Darcy number because the inflow/outflow velocity on the interface between the porous media and the fluid domain changes, as shown in Figure 5.22. U denotes the flux of Equation (2.13) at the left and upper sides, as exhibited in the figure, where the positive and negative values for U mean the inflow into the void and the outflow from the void, respectively. The inflow velocity of Da=2.5×10^{-8} at the corners of the left side is greater than that of Da=2.5×10^{-4}, while the velocity of Da=2.5×10^{-8} on the upper side is smaller than that of Da=2.5×10^{-4}. Thus, in the case of Da=2.5×10^{-8}, the main stream in the void accelerates and reaches the maximum velocity around the center of the void. On the other hand, the acceleration of the main stream of Da=2.5×10^{-4} is slower, because the inflow from the upper and lower sides decelerates the main stream (see Figure 5.23).

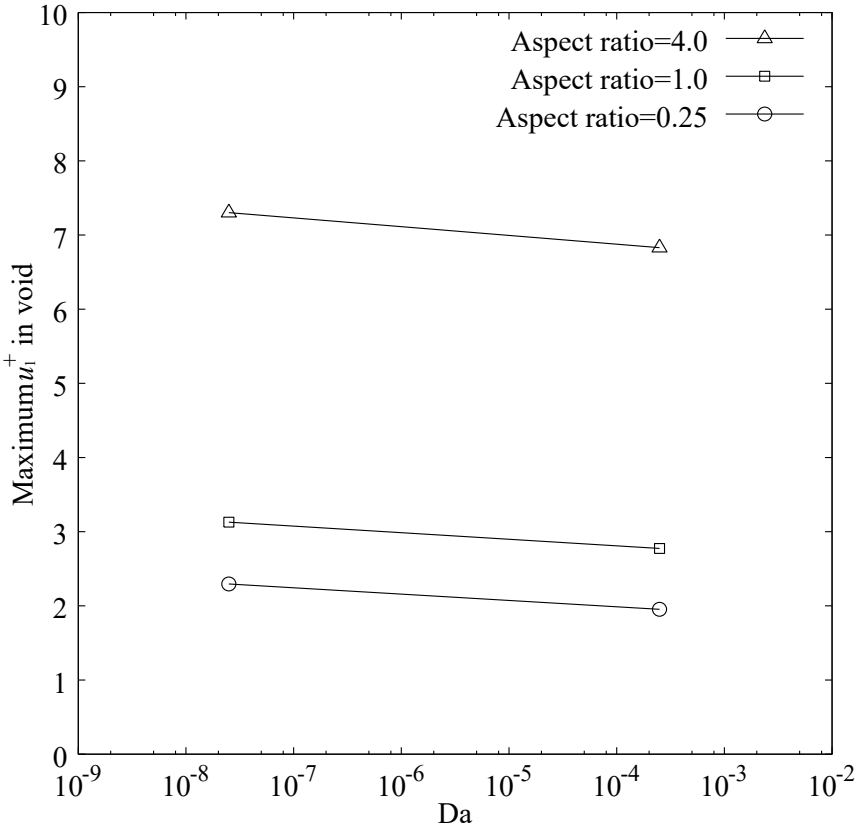

Figure 5.21 Plot of maximum velocity using Darcy number (Re=30).

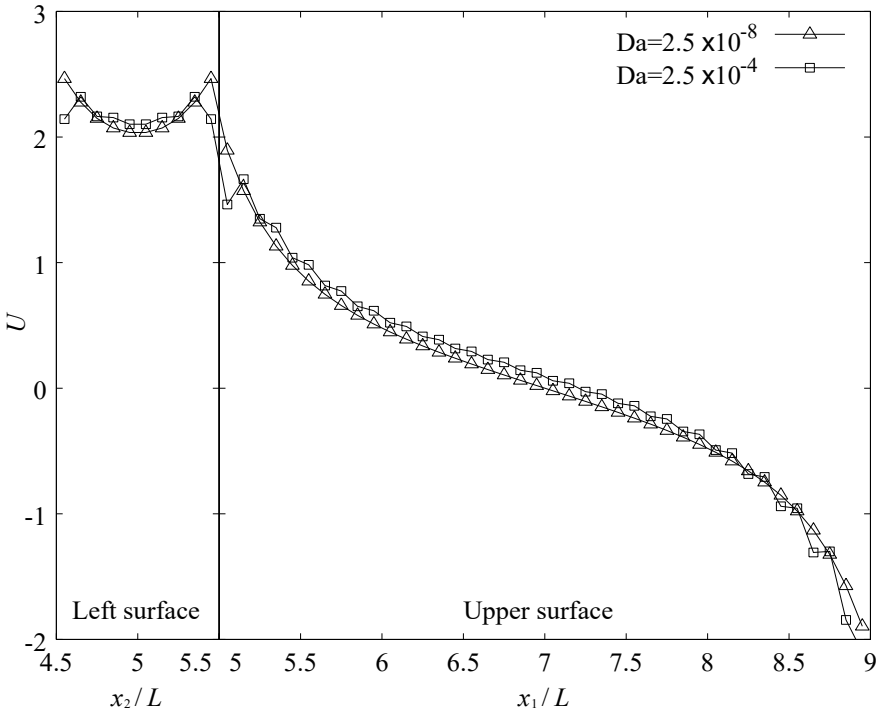

Figure 5.22 Inflow/outflow velocity on surface between void and porous medium (Aspect ratio=4.0, Re=30).

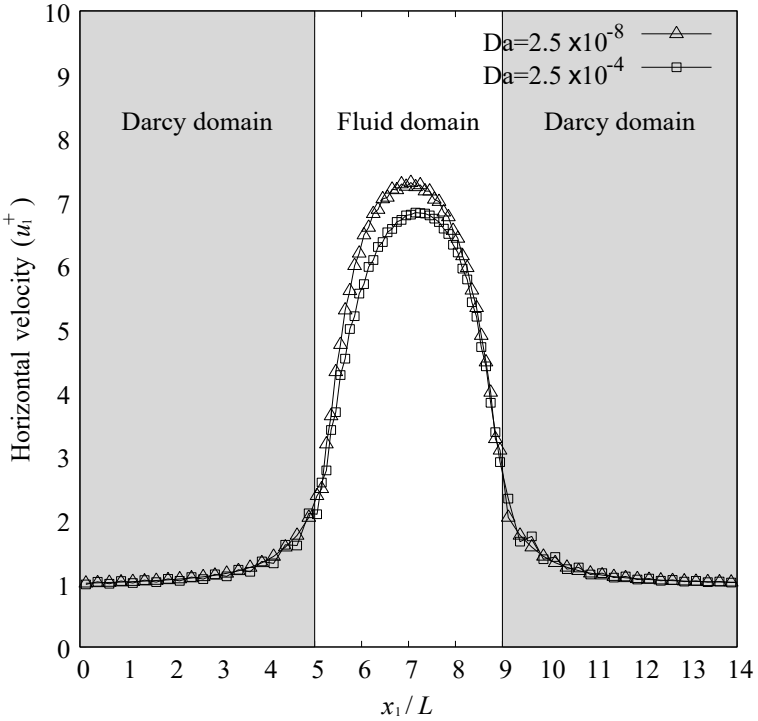

Figure 5.23 Distribution of horizontal velocity at x_2/L=5.15 (Aspect ratio=4.0, Re=30).

5.4 Conclusions

The numerical method presented in **Chapter 2** was applied to a problem which has a void in the porous media. The influence of the void shape on the flow in the Reynolds and the Darcy numbers was investigated. The results are summarized as follows.

1. The shape of the void in porous media has a strong influence on the flow in it. When the shape of the void is short and wide in the flow direction, the seepage water comes into the void from the corners of its upstream side, and forms two major streams along the upper and lower sides. On the other hand, when the shape is long and narrow in the flow direction, the two streams in the upstream side combine immediately and develop into one main stream.

2. The maximum velocities increase linearly with an increasing Reynolds number, because the Reynolds number is controlled by the inflow velocity and the patterns of the flow in the void do not change.

3. The Darcy number influences the flow velocity in the void because of the inflow and the outflow through the interface between the fluid domain and the porous media.

6 Concluding remarks and future prospects

In this study, we have proposed a numerical method for the coupled analysis of the Darcy flow and the Navier-Stokes flow. Several problems were computed using the proposed numerical method. The conclusions of each chapter are summarized as follows.

In **Chapter 2**, a numerical method for achieving a simultaneous analysis of the Darcy and the Navier-Stokes flows, using the Darcy-Brinkman equations as the governing equations, was proposed. It was shown that the governing equations nondimensionalized with the Reynolds and the Darcy numbers can be transformed to Darcy's law when the hydraulic conductivity is sufficiently small and the inverse of the Darcy number is even larger than the Reynolds number. The pressure gradient in the Darcy domain is usually even greater than that in the fluid domain, such that the linear interpolation of the pressure induces an unrealistically high gradient for the water pressure in the fluid domain neighboring the interface. The flow velocity in the fluid domain is usually even greater than that in the Darcy domain, such that the linear interpolation of the velocity overestimates the inward or the outward flux at the interface.

In **Chapter 3**, several problems were computed to validate the proposed numerical method. The obtained numerical results showed that the method can produce stable and physically realistic numerical solutions. The flow velocity in the lid-driven cavity flow and the reattachment point in the backward-facing step flow were found to be in good agreement with the results of previous studies. The proposed numerical method was able to simulate the Navier-Stokes flow in the fluid domain when λ =1.0 and Da^{-1}=0 were given. The computed pressure in the one-dimensional uniform flow problem was in good agreement with the analytical solutions calculated from Darcy's law, and the flow velocity was kept at a constant value of the inflow velocity along the channel. It was proven that use of the proposed interpolation of pressure by Equation (2.29) enables the avoidance of the oscillation of velocity. If the pressure is linearly interpolated at the interface, the oscillation appears at the interfaces located at the left- and right-hand sides of the porous media and is amplified with the time steps.

In **Chapter 4**, the numerical method presented in **Chapter 2** was applied to the backward-facing step flow with a porous step. The influence of the Reynolds and the Darcy numbers on the position of the reattachment point was investigated. The flows in all cases exhibited separation bubbles after the porous steps as is usually seen in the backward-facing step flow. The reattachment point was seen to move closer to the step as the Reynolds number decreased, and the results were consistent with those of Kim and Moin (1985). The reattachment point did not change significantly even if the Darcy number changed. However, the reattachment point moved slightly away from the step in the case of $Da=1.0\times10^{-3}$, because the profile of the flow velocity at the edge of the step diverted from the Hagen-Poiseuille flow.

In **Chapter 5**, the numerical method presented in **Chapter 2** was applied to a problem which had a void in the porous media. The influence of the void shape on the flow in the Reynolds and the Darcy domains was investigated. The shape of the void in the porous media was seen to have a strong influence on the flow in the media. When the shape of the void is short and wide in the flow direction, the seepage water comes into the void from the corners of its upstream side and forms two major streams along the upper and lower sides. On the other hand, when the shape is long and narrow in the flow direction, the two streams in the upstream side combine immediately and form one main stream. The maximum velocities were found to increase linearly with an increasing Reynolds number, because the Reynolds number is controlled by the inflow velocity and the patterns of the flow in the void do not change. The Darcy number influences the flow velocity in the void because of the inflow and the outflow through the interface between the fluid domain and the porous media.

A numerical method to simulate the Navier-Stokes and the Darcy flows was proposed in this thesis. Several problems were computed by the proposed numerical method, and the obtained results indicate that the proposed interpolation methods for water pressure and flow velocity are effective for avoiding the oscillation of water pressure and flow velocity. In order to apply the method to more practical problems, the proposed numerical method should be further developed. In addition, the problems shown in this thesis remain within the laminar flow. The numerical method needs to be expanded to the turbulent flow in order to deal with more practical problems. The interface between

the fluid and the Darcy domains can be moved easily during the computation because the proposed numerical method does not need the boundary condition at the interface between the fluid and the Darcy domains. Thus, it is expected that the proposed numerical method can be applied when problems are encountered in which the interface between the fluid and the Darcy domains moves during the progress of the computation, i.e., the erosion of soil with seepage water.

References

Anderson T. and Jackson R.: A fluid mechanical description of fluidized beds, *Industrial and Engineering Chemistry Fundamentals*, 1967, 6(4), 527–539.

Armaly B.F., Durst F., Pereira J.C.F. and Schonung B.: Experimental and theoretical investigation of backward-facing step flow, *Journal of Fluid Mechanics*, 1983, 127, 473-496.

Badea L., Discacciati M. and Quarteroni A.: Numerical analysis of the Navier–Stokes/Darcy coupling, *Numerische Mathematik*, 2010, 115, 195-227.

Bars M.L. and Worster M.G.: Interfacial conditions between a pure fluid and a porous medium: implications for binary alloy solidification, *Journal of Fluid Mechanics*, 2006, 550, 149-173.

Beavers G.S. and Joseph D.D.: Boundary conditions at a naturally permeable wall, *Journal of Fluid Mechanics*, 1967, 30(1), 197-207.

Brinkman H.C.: A calculation of the viscous force exerted by a flowing fluid on a dense swarm of particles, *Journal of Applied Sciences Research*, 1947, A1, 27-34.

Cai M., Mu M. and Xu J.: Numerical solution to a mixed Navier–Stokes/Darcy model by the two-grid approach, *SIAM Journal on Numerical Analysis*, 2009, 47(5), 3325-3338.

Cesmelioglu A., Girault V. and Rivière B.: Time-dependent coupling of Navier-Stokes and Darcy flows, *Mathematical Modelling and Numerical Analysis*, 2013, 47, 539-554.

Chan T.F., Gallopoulos E., Simoncini V., Szeto T. and Tong C.H.: A quasi-minimal residual variant of the Bi-CGStab algorithm for nonsymmetric systems, *SIAM Journal on Scientific Computing*, 1994, 15(2), 338-347.

Chandesris M. and Jamet D.: Boundary conditions at a planar fluid-porous interface for a Poiseuille flow, *International Journal of Heat and Mass Transfer*, 2006, 49, 2137-

2150.

Choi H. and Moin P.: Effects of the computational time step on numerical solutions of turbulent flow, *Journal of Computational Physics*, 1994, 113, 1-4.

Chidyagwai P. and Rivière B.: On the solution of the coupled Navier-Stokes and Darcy equations, *Computer Methods in Applied Mechanics and Engineering*, 2009, 198, 3806-3820.

Chidyagwai P. and Rivière B.: A two-grid method for coupled free flow with porous media flow, *Advances in Water Resources*, 2011, 34, 1113-1123.

Çeşmelioğlu A. and Rivière B.: Existence of a weak solution for the fully coupled Navier–Stokes/Darcy-transport problem, *Journal of Differential Equations*, 2012, 252, 4138-4175.

Davidson L.: A pressure correction method for unstructured meshes with arbitrary control volumes, *International Journal for Numerical Methods in Fluids*, 1996, 22, 265-281.

Dukhan N.: Analysis of Brinkman-extended Darcy flow in porous media and experimental verification using metal foam, *Journal of Fluids Engineering*, 2012, 134(7), 071201, doi:10.1115/1.4005678.

Ergun S.: Fluid flow through packed columns, *Chemical Engineering Progress*, 1952, 43(2), 89-94.

Erturk E.: Numerical solutions of 2-D steady incompressible flow over a backward-facing step, Part I: High Reynolds number solutions, *Computers & Fluids*, 2008, 37, 633-655.

Forchheimer P.: Wasserbewegung durch Boden, *Forschtlft ver. D. Ing.*, 1901, 45, 1782-1788. (In German)

Fujisawa K., Arimoto S. and Murakami A.: Simultaneous computation of incompressible and Darcy flows solving the Darcy-Brinkman equations, Irrigation, *Drainage and Rural Engineering Journal*, 2013, 287, 35-44. (In Japanese)

Ghia U., Ghia K. N. and Shin C. T.: High-Re solutions for incompressible flow using the

Navier-Stokes equations and a multigrid method, *Journal of Computational Physics*, 1982, 48, 387-411.

Girault V. and Rivière B.: DG approximation of coupled Navier-Stokes and Darcy equations by Beaver-Joseph-Saffman interface condition, *SIAM Journal on Numerical Analysis*, 2009, 47(3), 2052-2089.

Howes F.A. and Whitaker S.: The spatial averaging theorem revisited, *Chemical Engineering Science*, 1985, 40(8), 1387-1392.

Hwang Y.H.: Calculations of incompressible flow on a staggered triangular grid, Part I: Mathematical formulation, *Numerical Heat Transfer* Part B, 1995, 27, 323-336.

Hwang Y.H.: Stability and accuracy analyses for the incompressible Navier-Stokes equations on the staggered triangular grid, *Numerical Heat Transfer* Part B, 1997, 32, 321-349.

Jue TC.: Numerical analysis of vortex shedding behind a porous cylinder, *International Journal of Numerical Methods for Heat and Fluid Flow*, 2004, 14, 649-663.

Keskar J.: Computations of a laminar backward-facing step flow at *Re*=800 with a spectral domain decomposition method, *International Journal for Numerical Methods in Fluids*, 1999, 29, 411-427.

Kim D. and Choi H.: A second-order time-accurate finite volume method for unsteady incompressible flow on hybrid unstructured grids, *Journal of Computational Physics*, 2000, 162, 411-428.

Kim J. and Moin P.: Application of a fractional-step method to incompressible Navier–Stokes equations, *Journal of Computational Physics*, 1985, 59, 308-323.

Kobayashi M.H., Pereira J.M.C. and Pereira J.C.F.: A conservative finite-volume second-order-accurate projection method on hybrid unstructured grids, *Journal of Computational Physics*, 1999, 150, 40-75.

Lai Y.G.: An unstructured grid method for a pressure-based flow and heat transfer solver, *Numerical Heat Transfer* Part B, 1997, 32, 267-281.

Le H. and Moin P.: An improvement of fractional step methods for the incompressible

Navier-Stokes equations, *Journal of Computational Physics*, 1991, 92, 369-379.

Liu H., Patil P.R. and Narusawa U.: On Darcy–Brinkman equation: viscous flow between two parallel plates packed with regular square arrays of cylinders, *Entropy*, 2007, 9(3), 118-131.

Mathur R. and Murthy J.Y.: A pressure-based method for unstructured meshes, *Numerical Heat Transfer* Part B, 1997, 31, 195-215.

Mercier J., Weisman C., Firdaouss M. and Quéré PL.: Heat transfer associated to natural convection flow in a partly porous cavity, *Journal of Heat Transfer*, 2002, 124, 130-143.

Mu M. and Xu J.: A two-grid method of a mixed Stokes-Darcy model for coupling fluid flow with porous media flow, *SIAM Journal on Numerical Analysis*, 2007, 45(5), 1801-1813.

Neale G. and Nader W.: Practical significance of Brinkman's extension of Darcy's law: Coupled parallel flows within a channel and a bounding porous medium, *The Canadian Journal of Chemical Engineering*, 1974, 52, 475-478.

Ochoa-Tapia J. and Whitaker S.: Momentum transfer at the boundary between a porous medium and a homogeneous fluid: I. Theoretical development, *International Journal of Heat and Mass Transfer*, 1995a, 38, 2635-2646.

Ochoa-Tapia J. and Whitaker S.: Momentum transfer at the boundary between a porous medium and a homogeneous fluid: II. Comparison with experiment, *International Journal of Heat and Mass Transfer*, 1995b, 38, 2647-2655.

Saffman P.G.: On the boundary condition at the surface of a porous medium, *Studies in Applied Mathematics*, 1971, 50, 93-101.

Salinger A.G., Aris R. and Derby J.J.: Finite element formulations for large-scale coupled flows in adjacent porous and open fluid domains, *International Journal for Numerical Methods in Fluids*, 1994, 18, 1185-1209.

Si Z., Wang Y. and Li S.: Decoupled modified characteristics finite element method for the time dependent Navier–Stokes/Darcy problem, *Mathematical Methods in the*

Applied Sciences, 2014, 37, 1392-1404.

Taniguchi N. and Kobayashi T.: Finite volume method on the unstructured grid system, *Computers & Fluids*, 1991, 19, 287-295.

Thomadakis M. and Leschziner M.: A pressure-correction method for the solution of incompressible viscous flows on unstructured grids, *International Journal for Numerical Methods in Fluids*, 1996, 22, 581-601.

Urquiza J.M., N'Dri D., Garon A. and Delfour M.C.: Coupling Stokes and Darcy equations, *Applied Numerical Mathematics*, 2008, 58, 525-538.

Vafai K. and Kim S.J.: Fluid mechanics of the interface region between a porous medium and a fluid layer - an exact solution, *International Journal of Heat and Fluid Flow*, 1990, 11(3), 254-356.

Whitaker S.: *The method of volume averaging*, Kluwer, 1999.